Wan-Hui Wang

Xiujuan Feng

Ming Bao

Transformation of Carbon Dioxide to Formic Acid and Methanol

Springer

SpringerBriefs in Molecular Science

Green Chemistry for Sustainability

Series editor

Sanjay K. Sharma, Jaipur, India

Wan-Hui Wang · Xiujuan Feng
Ming Bao

Transformation of Carbon Dioxide to Formic Acid and Methanol

Wan-Hui Wang
School of Petroleum and Chemical
  Engineering
Dalian University of Technology
Panjin, Liaoning
China

Ming Bao
Dalian University of Technology
Dalian, Liaoning
China

Xiujuan Feng
Dalian University of Technology
Dalian, Liaoning
China

Contents

Chapter 1
Introduction

Abstract Huge amount of carbon dioxide emission poses a serious threat to our environmental and biological systems. Development of sustainable energy system based on CO_2 is highly desired. This chapter briefly introduces the approaches of CO_2 activation and transformation, and emphasizes CO_2 reduction to formic acid and methanol, which are currently considered as promising energy carriers and alternative fuels.

Keywords CO_2 emission · CO_2 activation · CO_2 reduction · Alternative fuels Hydrogen economy · Methanol economy

In nature, plants use carbon dioxide (CO_2) to produce hydrocarbon and oxygen via photosynthesis, whereas the respiration consumes oxygen and releases CO_2. The levels of CO_2 concentration were almost constant and fluctuated minutely before the beginning of the industrial revolution. However, the balance in nature was broken since the start of the industrial revolution. Human activities, including deforestation, cement manufacture, and consumption of fossil fuels, caused the dramatic increase of CO_2 atmospheric concentration. This concentration has exceeded 400 ppm milestone in 2015 and will no longer decrease [1]. CO_2 is known as one of the important greenhouse gases. Global warming is the direct effect of increased atmospheric CO_2 concentration. The average global surface temperature has increased by 1 °C than in the 1960s [1]. The period from 2011 to 2015 has been the hottest 5-year period on record. Global warming leads to severe decline of Arctic sea ice and land ice, thus resulting in the sea level rise of 200 mm from 1870 to 2000. Another consequence of anthropogenic CO_2 emission is ocean acidification. This phenomenon causes major damage to the ocean ecosystems [2]. These combined effects have a strong influence on the biological and ecological systems worldwide.

Another major concern of our society is the depletion of fossil fuels, a nonrenewable energy resource. Since the modern society mainly relies on fossil resources to provide either energy or basic chemical resource, building a sustainable energy or chemical industry system before the depletion of fossil resources is of much
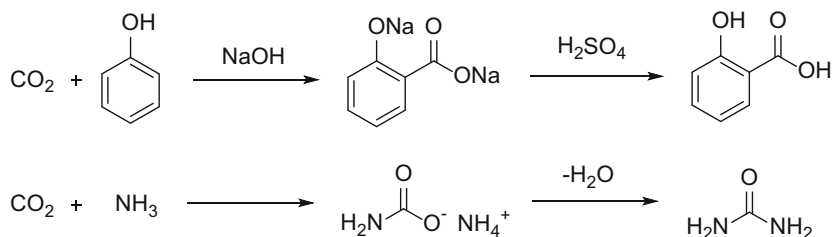
Fig. 1.1 Industrial production of salicylic acid and urea with CO_2

importance. Therefore, capture and utilization of CO_2 as fuels and chemicals is becoming an important scientific project. The use of CO_2 as an economical and abundant C1 building block to construct various chemicals and fuels has attracted increasing attention [3–8]. However, CO_2 is a thermodynamic stable molecule. Converting CO_2 into value-added chemicals and fuels is a challenging task. In the industry, CO_2 is only used to produce limited products including urea, organic carbonates, and salicylic acid (Fig. 1.1). A total of 150 million tons of urea is produced annually. This process utilizes 109.5 million tons of CO_2, which accounts for 94% of CO_2 consumption [9]. However, urea production makes no contribution to carbon sequestration because urea emits equal amounts of CO_2 when applied to the soil as a fertilizer. Moreover, the production of the co-reactant, ammonia, from fossil resources releases more CO_2.

The great challenge of CO_2 transformation is ascribed to the thermodynamic stability and kinetic inertness of CO_2 molecule. The length of the C=O double bond in CO_2 is 116 pm, which is shorter than that of C=O in carbonyl compounds (123 pm); therefore, the C=O double bond of CO_2 is extremely stable.

To overcome the high energy barrier of CO_2 activation, catalysts are required. In the linear CO_2 molecule, the carbon atom is electron deficient and thus acts a Lewis acid, whereas the oxygen atom is a Lewis base. Transition metal as a Lewis base is demonstrated to be efficient in activating the weak electrophilic CO_2 molecule. The three possible coordination modes are illustrated in Fig. 1.2a. η^1 C-bound structure is the most common mode. Besides metals in a low oxidation state, other electron-rich species, such as base and hydride, are prone to attack C by forming a σ bond. Transfer of electron to the C atom results in a bent CO_2^- anion. This process can be facilitated by the interaction of the O atom with the electrophilic atoms through the outer coordination sphere. π coordination of one C=O bond to the metal center leads to a η^2-CO bonding mode. In this mode, the electron transfers from CO_2 to the metal center and weakens the C=O bonds. Transition metals such as electron-poor species with a high oxidation state attack the O atom. η^1 O-bound mode is observed, but difficult to form. η^2-OO mode is usually found in interaction with alkali metals. In addition, organocatalysts, such as frustrated Lewis pairs (FLPs), have recently achieved great progress in CO_2 activation [10, 11]. FLPs are a combination of bulky Lewis acid and Lewis base that do not form classical adducts because of the steric or geometric constraints. FLPs are ambiphilic and thus can activate CO_2 by adduct formation (Fig. 1.2b).

(a)

η^1–C η^2–CO η^1–O η^2–OO

(b)
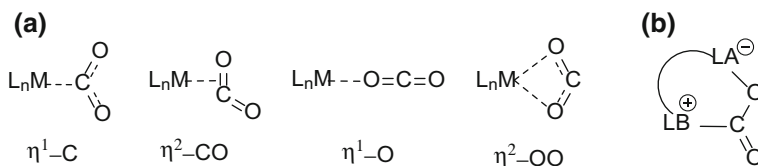
Fig. 1.2 **a** Coordination modes of CO_2 with transition metal complex. **b** Ambiphilic activation of CO_2 with FLPs

Besides using catalysts to decrease the energy barrier, using reactants of high intrinsic energy can render CO_2 transformation thermodynamically feasible. Three-membered heterocycles, especially epoxides, is typically used to incorporate the entire CO_2 molecule into products. The production of cyclic carbonate ethylene, propylene carbonate, and polycarbonate has been industrialized [7]. Nevertheless, no formal reduction is involved in this process. CO_2 is the end product of hydrocarbon combustion with the highest oxidation state. To fulfill the energy storage and convert CO_2 to fuels, CO_2 reduction is a prerequisite. CO_2 is reduced by photochemical, electrochemical, and thermal hydrogenation methods [12–14]. Photo- and electrochemical CO_2 reduction are of great interest, but this topic is beyond the scope of this book. As shown in Fig. 1.3, CO_2 can be reduced to various compounds, including aldehydes, acids, amides, alcohols, amines, and hydrocarbon.

Among these products, formic acid (FA) is recently recognized as a promising hydrogen storage material [15, 16]. Moreover, it can be directly used in the formic
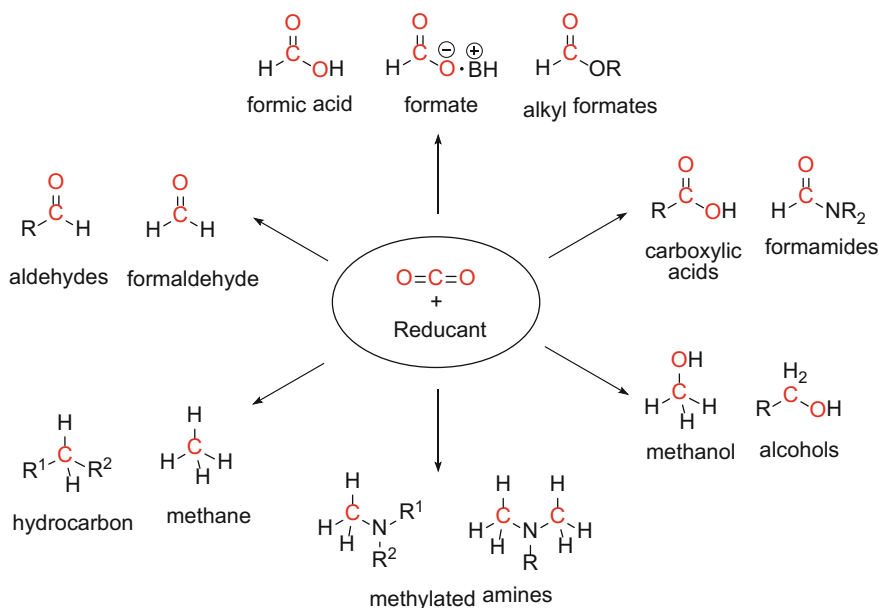
Fig. 1.3 Various chemicals and fuels from CO_2 reduction

acid fuel cell to produce electricity. Production of FA from CO_2 contributes greatly to the proposed "hydrogen economy" [17]. The hydrogenation of CO_2 into formic acid (Eq. 1.1) in the gas phase is endergonic ($\Delta G°_{298} = +33$ kJ mol^{-1}). When the reaction is carried out in the aqueous phase ($\Delta G°_{298} = -4$ kJ mol^{-1}) or with the addition of a base such as ammonia (Eq. 1.2, $\Delta G°_{298} = -9.5$ kJ mol^{-1} in the gas phase), the CO_2 hydrogenation becomes exergonic and feasible. If base is added to the aqueous solution, the reaction is more favorable (Eq. 1.2, $\Delta G°_{298} = -35$ kJ mol^{-1} in the aqueous phase) [18]. The solvent effects of water and deprotonation of FA with base are important for CO_2 hydrogenation. The acid/base equilibrium of CO_2 in water (Eq. 1.3) makes the reaction quite complicated. Although "hydrogenation of CO_2" is frequently used in this book and elsewhere, in basic aqueous solutions, the substrates used are HCO_3^- and CO_3^{2-} besides CO_2, depending on the pH of the solution. The hydrogenation of bicarbonate into formate in water 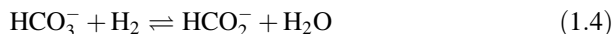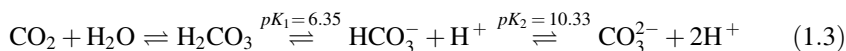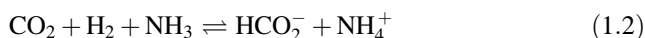(Eq. 1.4) is also known to be exergonic on the basis of the theoretical calculations ($\Delta G°_{298} = -9.6$ kJ mol^{-1}) [19].

$$CO_2 + H_2 \rightleftharpoons HCO_2H \tag{1.1}$$

$$CO_2 + H_2 + NH_3 \rightleftharpoons HCO_2^- + NH_4^+ \tag{1.2}$$

$$CO_2 + H_2O \rightleftharpoons H_2CO_3 \overset{pK_1 = 6.35}{\rightleftharpoons} HCO_3^- + H^+ \overset{pK_2 = 10.33}{\rightleftharpoons} CO_3^{2-} + 2H^+ \tag{1.3}$$

$$HCO_3^- + H_2 \rightleftharpoons HCO_2^- + H_2O \tag{1.4}$$

Another product methanol is applied as liquid fuel, as well as in MeOH fuel cell. The generation of water makes the CO_2 hydrogenation to MeOH thermodynamically favorable (Eq. 1.5, $\Delta G°_{298} = -9.5$ kJ mol^{-1}) in the gas phase [20]. The thermodynamics is more favorable for this reaction in an aqueous solution (Eq. 1.5, $\Delta G°_{298} = -79$ kJ mol^{-1}) [18]. The concept of "methanol economy" has recently been put forward by Olah and co-workers [21–24].

$$CO_2 + H_2 \rightleftharpoons CH_3OH + H_2O \tag{1.5}$$
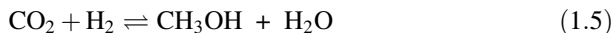
Both in hydrogen economy and methanol economy, fossil fuels are replaced with hydrogen or methanol as a means of energy storage. In methanol economy, methanol can be regenerated from chemical recycling of CO_2. Therefore, carbon neutral process is achieved. In hydrogen economy, if H_2 is totally produced from photocatalytic water splitting, CO_2 emission is completely avoided. Both economy forms have specific advantages and disadvantages; they provide promising alternatives to the current economy based on fossil fuels. A number of previous books and reviews described the CO_2 transformation [9, 18, 25–31]. Whereas our main focus is the development of an alternative and sustainable economy involving CO_2 conversion [32]. This book discusses the transformation of CO_2 to FA and MeOH utilizing either homogenous or heterogeneous catalysts. This book covers the most recent advances in both transformations, including the design of catalysts and

catalytic mechanism. Hence, this book will help and serve as motivation for studying mechanism of CO_2 transformation and developing renewable energy sources.

References

1. NASA Climate Official Site. https://climate.nasa.gov/. Accessed July, 2017
2. Hofmann GE, Barry JP, Edmunds PJ, Gates RD, Hutchins DA, Klinger T, Sewell MA (2010) The effect of ocean acidification on calcifying organisms in marine ecosystems: An organism-to-ecosystem perspective. Annu Rev Ecol Evol Syst 41:127–147. doi:10.1146/annurev.ecolsys.110308.120227
3. Sakakura T, Choi JC, Yasuda H (2007) Transformation of carbon dioxide. Chem Rev 107 (6):2365–2387. doi:10.1021/cr068357u
4. Omae I (2012) Recent developments in carbon dioxide utilization for the production of organic chemicals. Coord Chem Rev 256(13–14):1384–1405. doi:10.1016/j.ccr.2012.03.017
5. Liu X, He LN (2017) Synthesis of lactones and other heterocycles. Top Curr Chem 375(2):21. doi:10.1007/s41061-017-0108-9
6. Cokoja M, Bruckmeier C, Rieger B, Herrmann WA, Kuhn FE (2011) Transformation of carbon dioxide with homogeneous transition-metal catalysts: a molecular solution to a global challenge? Angew Chem Int Ed 50(37):8510–8537. doi:10.1002/anie.201102010
7. Klankermayer J, Wesselbaum S, Beydoun K, Leitner W (2016) Selective catalytic synthesis using the combination of carbon dioxide and hydrogen: catalytic chess at the interface of energy and chemistry. Angew Chem Int Ed 55(26):7296–7343. doi:10.1002/anie.201507458
8. Riduan SN, Zhang Y (2010) Recent developments in carbon dioxide utilization under mild conditions. Dalton Trans 39(14):3347–3357. doi:10.1039/b920163g
9. Otto A, Grube T, Schiebahn S, Stolten D (2015) Closing the loop: captured CO_2 as a feedstock in the chemical industry. Energy Environ Sci 8(11):3283–3297. doi:10.1039/C5EE02591E
10. Fontaine FG, Courtemanche MA, Légaré MA (2014) Transition-metal-free catalytic reduction of carbon dioxide. Chem–Eur J 20(11):2990–2996. doi:10.1002/chem.201304376
11. Fontaine F-G, Stephan DW (2017) Metal-free reduction of CO_2. Curr Opin Green Sustain Chem 3:28–32. doi:10.1016/j.cogsc.2016.11.004
12. Qiao J, Liu Y, Hong F, Zhang J (2014) A review of catalysts for the electro reduction of carbon dioxide to produce low-carbon fuels. Chem Soc Rev 43(2):631–675. doi:10.1039/c3cs60323g
13. Kondratenko EV, Mul G, Baltrusaitis J, Larrazabal GO, Perez-Ramirez J (2013) Status and perspectives of CO_2 conversion into fuels and chemicals by catalytic, photocatalytic and electrocatalytic processes. Energy Environ Sci 6(11):3112–3135. doi:10.1039/c3ee41272e
14. Izumi Y (2013) Recent advances in the photocatalytic conversion of carbon dioxide to fuels with water and/or hydrogen using solar energy and beyond. Coord Chem Rev 257(1):171–186. doi:10.1016/j.ccr.2012.04.018
15. Grasemann M, Laurenczy G (2012) Formic acid as a hydrogen source—recent developments and future trends. Energy Environ Sci 5(8):8171–8181. doi:10.1039/c2ee21928j
16. Dalebrook AF, Gan W, Grasemann M, Moret S, Laurenczy G (2013) Hydrogen storage: beyond conventional methods. Chem Commun 49(78):8735–8751. doi:10.1039/c3cc43836h
17. Crabtree GW, Dresselhaus MS, Buchanan MV (2004) The hydrogen economy. Phys Today 57(12):39–44. doi:10.1063/1.1878333
18. Jessop PG, Ikariya T, Noyori R (1995) Homogeneous hydrogenation of carbon dioxide. Chem Rev 95(2):259–272. doi:10.1021/cr00034a001

19. Kovacs G, Schubert G, Joó F, Papai I (2006) Theoretical investigation of catalytic HCO_3^- hydrogenation in aqueous solutions. Catal Today 115(1–4):53–60. doi:10.1016/j.cattod.2006.02.018
20. Yadav M, Xu Q (2012) Liquid-phase chemical hydrogen storage materials. Energy Environ Sci 5(12):9698–9725. doi:10.1039/c2ee22937d
21. Olah GA (2005) Beyond oil and gas: the methanol economy. Angew Chem Int Ed 44 (18):2636–2639. doi:10.1002/anie.200462121
22. Olah GA (2013) Towards oil independence through renewable methanol chemistry. Angew Chem Int Ed 52(1):104–107. doi:10.1002/anie.201204995
23. Goeppert A, Czaun M, Jones JP, Surya Prakash GK, Olah GA (2014) Recycling of carbon dioxide to methanol and derived products—closing the loop. Chem Soc Rev 43(23):7995–8048. doi:10.1039/c4cs00122b
24. Olah GA, Goeppert A, Prakash GKS (2009) Chemical recycling of carbon dioxide to methanol and dimethyl ether: from greenhouse gas to renewable, environmentally carbon neutral fuels and synthetic hydrocarbons. J Org Chem 74(2):487–498. doi:10.1021/jo801260f
25. Leitner W, Dinjus E, Gassner F (1998) CO_2 Chemistry. In: Cornils B, Herrmann WA (eds) Aqueous-phase organometallic catalysis, concepts and applications. Wiley-VCH, Weinheim, pp 486–498
26. Jessop PG, Joó F, Tai CC (2004) Recent advances in the homogeneous hydrogenation of carbon dioxide. Coord Chem Rev 248(21–24):2425–2442. doi:10.1016/j.ccr.2004.05.019
27. Jessop PG (2007) Homogeneous hydrogenation of carbon dioxide. In: De Vries JG, Elsevier CJ (eds) Handbook of homogeneous hydrogenation, vol 1. Wiley-VCH, Weinheim, pp 489–511
28. Markewitz P, Kuckshinrichs W, Leitner W, Linssen J, Zapp P, Bongartz R, Schreiber A, Mueller TE (2012) Worldwide innovations in the development of carbon capture technologies and the utilization of CO_2. Energy Environ Sci 5(6):7281–7305. doi:10.1039/c2ee03403d
29. Aresta M, Dibenedetto A, Angelini A (2014) Catalysis for the valorization of exhaust carbon: from CO_2 to chemicals, materials, and fuels. Technological use of CO_2. Chem Rev 114 (3):1709–1742. doi:10.1021/cr4002758
30. Bhanage BM, Arai M (2014) Transformation and utilization of carbon dioxide. Green chemistry and sustainable technology, 1 Edn. Springer-Verlag Berlin Heidelberg. doi:10.1007/978-3-642-44988-8
31. Dong K, Razzaq R, Hu Y, Ding K (2017) Homogeneous reduction of carbon dioxide with hydrogen. Top Curr Chem 375(2):23. doi:10.1007/s41061-017-0107-x
32. Wang WH, Himeda Y, Muckerman JT, Manbeck GF, Fujita E (2015) CO_2 hydrogenation to formate and methanol as an alternative to photo- and electrochemical CO_2 reduction. Chem Rev 115(23):12936–12973. doi:10.1021/acs.chemrev.5b00197

Chapter 2
Transformation of CO_2 to Formic Acid or Formate with Homogeneous Catalysts

Abstract Homogeneous hydrogenation of carbon dioxide to formic acid or formate has attracted much attention due to its high performance. Various metals including noble metals and nonprecious metals combined with different ligands have been investigated. The catalytic mechanism and catalyst design principle are described in detail. Recently developed CO_2 hydroboration and hydrosilylation to formate are also covered.

Formic acid is widely used as preservative, insecticide, and industrial material for synthetic processes. It can be used directly in FA fuel cells to provide electricity. Most recently, it is recognized as one of the most promising hydrogen storage materials, especially for portable power application, because of its many advantages: (1) nontoxic and biodegradable, (2) liquid at ambient conditions, (3) easy to store and transport, (4) has relatively high hydrogen content (4.4 wt%), and (5) highly sustainable and renewable. The interconversion of H_2/CO_2 and FA/formate occurs highly selectively under relatively mild conditions.

The hydrogenation of CO_2 to formic acid or formate dates back to 1976. The pioneering work by Inoue et al., using triphenylphosphine (PPh_3) complexes of Ru, Rh, and Ir, opened the avenue for homogeneous catalytic hydrogenation of CO_2 to formic acid [1]. However, their research did not attract considerable attention until the 1990s, in which the interest on CO_2 conversion to formate was revived. The catalysts were extended to a variety of transition metals, such as Pd, Ni, and Fe. In addition to phosphorous ligands, *C,N*- and *N,N*-chelated ligands, *N*-heterocyclic carbine (NHC) ligands, and pincer ligands were also developed. The solvent effect has also been widely investigated. Highly polar solvents, such as MeOH, DMSO, and DMF, are demonstrated to be favorable for the transformation [2]. Noyori and Jessop et al. used supercritical carbon dioxide ($scCO_2$) as reactant and solvent and obtained high activity [3, 4]. Recently, water has achieved great success in a wide variety of applications [5].

Carbon dioxide is a cheap, safe, and abundant C1 building block [6]. Hydrogenation of CO_2 to formate/formic acid provides a sustainable method for

producing basic chemicals and fuels. Homogeneous hydrogenation of CO_2 to formate or formic acid has attracted increasing attention, and a number of reviews have summarized significant progress in the last two decades [6–11]. Table 2.1 lists the most efficient systems for this transformation. In this chapter, we will introduce the most recent development of CO_2 hydrogenation to FA/formate and highlight the most efficient catalytic systems and catalyst design principle.

2.1 CO_2 Hydrogenation Using Noble Metals

The work by Inoue et al. on homogeneous CO_2 hydrogenation to formic acid used a series of metal complexes with Ru, Rh, and Ir [1]. Following their work, a variety of noble metal complexes have been developed and exhibited remarkable activity.

2.1.1   Ruthenium Complexes
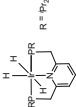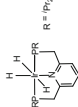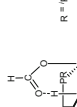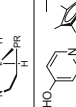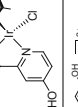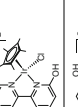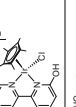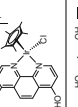
2.1.1.1   Ru Complexes with Phosphine Ligands

In 1994, Noyori and Jessop et al. explored a $scCO_2$ system for CO_2 hydrogenation with serval merits [3]. $scCO_2$ can act as solvent and reactant, and hydrogen has high solubility in $scCO_2$. Therefore, $scCO_2$ is favorable for mass transport and heat transfer. $RuH_2(PMe_3)_4$ (**1**) and $RuCl_2(PMe_3)_4$ (**2**) afforded high initial rates of 1400 and 1040 h^{-1}, respectively, in the presence of Et_3N and MeOH at 50 °C. Subsequently, Jessop et al. utilized appropriate amine and alcohol adducts to accelerate the reaction rate, achieving a high TOF of 95,000 h^{-1} with RuCl(OAc) $(PMe_3)_4$ (**3**) in $scCO_2$ [4, 47].

Joó et al. performed extensive studies using phosphine ruthenium complexes including $[RuCl_2(tppms)_2]_2$ (**4**) (tppms: 3-sulfonatophenyldiphenylphosphine) and $[RuCl_2(PTA)]_2$ (**5**) (PTA: 1,3,5-triaza-7-phosphaadamantane) (Fig. 2.1) in amine-free aqueous solutions [27, 28, 48–50]. A high TOF of 9600 h^{-1} was obtained with catalyst **4** at 9.5 MPa and 80 °C. Subsequently, reaction mechanisms were investigated in detail by Laurenczy and co-workers using ruthenium catalysts **5** [27, 51–53]. Beller and Laurenczy et al. reported moderate catalytic activity (TOF: 1259 h^{-1}) using in situ complex $[RuCl_2(C_6H_6)]_2$/dppm (**6**) (dppm: 1,2-bis (diphenylphosphino)methane) in aqueous $NaHCO_3$ under 8.5 MPa of H_2/CO_2 (5/3.5) at 70 °C [29]. Although this catalyst provided a high initial reaction rate, deactivation was observed after the first few hours.
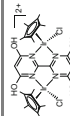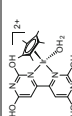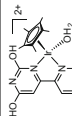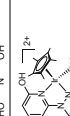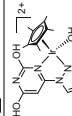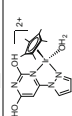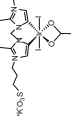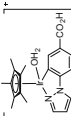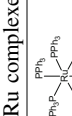
Leitner et al. developed a continuous-flow system for the hydrogenation of $scCO_2$ to produce pure formic acid in a single process unit [38]. They performed the reaction with a ruthenium precursor $[Ru(cod)(methallyl)_2]$ (**7**) (cod: 1,5-cyclooctadiene; methallyl: $CH_2C(CH_3)CH_2-$) and ligand PBu_4tppms, using amine-free or amine-functionalized IL as the stationary phase at 50 °C under 10 MPa of H_2/CO_2 (1/1). Notably, they obtained high TON (1970) and TOF (>295 h^{-1}) values in a continuous-flow system using the amine-free IL EMIM

Table 2.1 Hydrogenation of CO$_2$ to formic acid/formate[a,b]

Catalyst	Solvent	Additive	P(H$_2$/CO$_2$)/MPa	T/°C	Reaction time/h	TON	TOF[c]/h^{-1}	Ref.
Ir complexes								
(structure, R = ^{i}Pr$_2$)	H$_2$O/THF	KOH	4/4	200	2	300,000	150,000	[12, 13]
(structure, R = ^{i}Pr$_2$)	H$_2$O/THF	KOH	4/4	120	48	3,500,000	73,000	[12, 13]
(structure, R = ^{i}Pr$_2$)	H$_2$O	KOH	2.8/2.8	185	24	348,000	14,500	[14]
(structure)	H$_2$O	KOH	3/3	120	57	190,000	(42,000)	[15]
(structure)	H$_2$O	KHCO$_3$	0.5/0.5	120	8	12,500	(25,200)	[16]
(structure)	H$_2$O	NaHCO$_3$	0.05/0.05	25	33	330	(27)	[16]
(structure)	H$_2$O	KOH	3/3	120	48	222,000	(33,000)	[17]
(structure)	H$_2$O	KHCO$_3$	0.05/0.05	25	336	7200	(65)	[18]
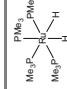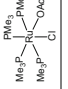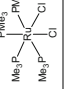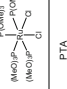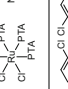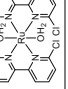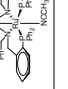
(continued)

Table 2.1 (continued)

Catalyst	Solvent	Additive	P(H$_2$/CO$_2$)/MPa	T/°C	Reaction time/h	TON	TOF^c/h^{-1}	Ref.
	H$_2$O	KHCO$_3$	2.5/2.5	80	2	79,000	(53,800)	[18]
	H$_2$O	KHCO$_3$	1.5/1.5	80	8	34,000	(33,300)	[19]
	H$_2$O	KHCO$_3$	0.05/0.05	25	24	190	65	[19]
	H$_2$O	KHCO$_3$	0.5/0.5	50	1	388	388	[20]
	H$_2$O	KHCO$_3$	0.5/0.5	50	1	440	440	[20]
	H$_2$O	KHCO$_3$	0.5/0.5	50	1	637	637	[20]
	H$_2$O	KOH	3/3	200	75	190,000	2500	[21]
	H$_2$O	K$_2$CO$_3$	1/1	25	15	100	6.8	[22]
Ru complexes								
	C$_6$H$_6$	Et$_3$N/H$_2$O	2.5/2.5	rt	20	87	4	[1]
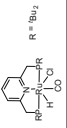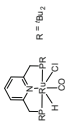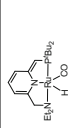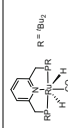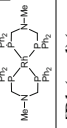
(continued)

Table 2.1 (continued)

Catalyst	Solvent	Additive	P(H$_2$/CO$_2$)/MPa	T/°C	Reaction time/h	TON	TOF^c/h^{-1}	Ref.
(structure)	scCO$_2$	Et$_3$N	8.5/12	50	–	3700	1400	[3]
(structure)	scCO$_2$	Et$_3$N	8.5/12	50	–	7200	1040	[3]
(structure)	scCO$_2$	Et$_3$N/ C$_6$F$_5$OH	7/12	50	0.33	32,000	95,000	[4]
(structure)	scCO$_2$	DBU/ C$_6$F$_5$OH	7/10	100	4	7625	1905	[23]
(structure)	scCO$_2$	DBU/ C$_6$F$_5$OH	7/10	100	4	6630	1660	[23]
(structure)	DMSO	–	5/5	60	–	750		[24]
(structure)	EtOH	Et$_3$N	3/3	150	8	5000	625	[25]
K[RuCl(EDTA-H)]	H$_2$O	–	1.7/8.2	40	0.5	–	3750	[26]
(structure)	H$_2$O	NaHCO$_3$	6/0	80	–	–	345	[27]
[RuCl$_2$(tppms)$_2$]$_2$	H$_2$O	NaHCO$_3$	6/3.5	80	0.03	–	9600	[28]
[RuCl$_2$(C$_6$H$_6$)]/dppm	H$_2$O	NaHCO$_3$	5/3.5	70	2	2520	1260	[29]
(structure)	toluene	DBU	70/70	100	4	1880		[30]
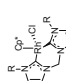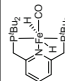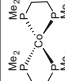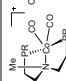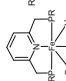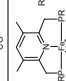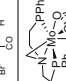
(continued)

Table 2.1 (continued)

Catalyst	Solvent	Additive	$P(H_2/CO_2)/$ MPa	T/°C	Reaction time/h	TON	TOF[c]/h^{-1}	Ref.
R = $^tBu_2$	DMF	DBU	2/2	70	2	38,600	–	[31]
R = $^tBu_2$	DMF	DBU	3/1	120			1,100,000	[31]
	Diglyme	K_2CO_3	3/1	200	48	23,000	2200	[32]
R = $^tBu_2$	H_2O		37/3	70			21,500	[33]
Rh complexes								
[Rh(cod)Cl]$_2$/dppb	DMSO	Et_3N	2/2	rt	22	1150	30–47	[34]
RhCl(tppts)$_3$	H_2O	$NHMe_2$	2/2	81	0.5	–	7300	[9]
RhCl(tppts)$_3$	H_2O	$NHMe_2$	2/2	rt	12	3440	290	[9, 35]
RhCl(PPh$_3$)$_3$	DMSO	Et_3N	2/4	25	20	2500	125	[2]
[RhCl(tppms)$_3$]/tppms	H_2O	HCO_2Na	1/1	50	20	120	–	[36]
	THF	Verkade's base	20/20	21	–	280	920	[37]
[Rh(cod)(methallyl)$_2$]/ PBu$_4$/tppms	scCO$_2$/EMIM NTf$_2$	Et_3N	5/5	50	20	310	630	[38]
[Rh(cod)(methallyl)$_2$]/ PBu$_4$/tppms	scCO$_2$/EMIM NTf$_2$	Et_3N/ EMIMCl	5/5	50	20	545	1090	[38]
			5/5	50	20	1970	>295	[38]

(continued)

Table 2.1 (continued)

Catalyst	Solvent	Additive	$P(H_2/CO_2)$/ MPa	T/°C	Reaction time/h	TON	TOF[c]/h^{-1}	Ref.
[Rh(cod)(methallyl)2]/ PBu4/tppms	scCO2/EMIM HCO2 (flow system)	KHCO3		100	72	3600		[39]
Non-precious metal complexes								
Ni(dppe)2	C6H6	Et3N/H2O	2.5/2.5	rt	20	7	0.35	[1]
Fe(BF4)2/PP3	MeOH	NaHCO3	6/0	80	20	610	30	[40]
Co(BF4)2/PP3	MeOH	NaHCO3	6/0	120	20	3900	200	[41]
(structure)	H2O/THF	NaOH	0.67/0.33	80	5	788	156	[42]
(structure)	THF	Verkade's base	0.05/0.05	21	<1	2000	3400	[43]
(structure)	MeCN		1/1	45	16	29,000	5700	[44]
(structure)	H2O/THF	NaHCO3		25	72	188		[45]
(structure)	EtOH	DBU	1/1	25	72	1032		[45]
(structure)	C6H6	DBU	1/1	100	16	35		[46]

[a]Insignificant digits are rounded. [b]Abbreviations are the following: cod: 1,5-cyclooctadiene, dppb: $Ph_2P(CH_2)_4PPh_2$, tppts: tris(3-sulfontophenyl)phosphine, tppms: 3-sulfonatophenyldiphenylphosphine, PP_3: $P(CH_2CH_2PPh_2)_3$, dppm: 1,1-bis(diphenylphosphino)methane, dppe: 1,2-bis(diphenylphosphino)ethane, N-N': pyridinylazolato, methallyl: $CH_2C(CH_3)CH_2-$. [c]The data in the parenthesis are initial TOFs

(HCO$_2$) (EMIM: 1-ethyl-3-methylimidazolium). The extraction rate of formic acid from the amine-functionalized ionic liquid was found to be the limiting factor under continuous-flow conditions.

A series of ruthenium(II) complexes [(N–N′)RuCl(PMe$_3$)$_3$] (**8**) with PMe$_3$ and pyridinylazolato ligands (N–N′, Fig. 2.1) bearing various electron-withdrawing and -donating substituents was investigated in the hydrogenation of CO$_2$ under supercritical conditions [54]. The triazolato system with an unsubstituted ligand was found to be superior (TON up to 4800) under relatively mild conditions. Under supercritical conditions, Thiel et al. reported that CO$_2$ hydrogenation catalyzed by simple ruthenium complexes with P(OMe)$_3$, P(OEt)$_3$, P(O^{i}Pr)$_3$, and P(OPh)$_3$ in the presence of DBU (1,8-diazabicyclo[5.4.0]undec-7-ene) and C$_6$F$_5$OH [23]. *trans*-[RuCl$_2${P(OMe)$_3$}$_4$] offered high activity (TON = 6630, TOF = 1655 h^{-1}) similar to that of [RuCl$_2$(PMe$_3$)$_4$] (TON = 7625, TOF = 1905 h^{-1}) under the same experimental conditions.

Byers et al. studied the effect of inexpensive additives for CO$_2$ hydrogenation with RuCl$_2$(PPh$_3$)(*p*-cymene) (**9**) in DMSO or MeOH [55]. They suggested that the addition of inorganic additives, such as KHCO$_3$, KOAc, and KNO$_3$, improved catalytic activity by up to 510%. This study promoted the investigation of cheap additives to enhance CO$_2$ transformation.

Recently, Laurenczy et al. reported the direct hydrogenation of CO$_2$ to produce formic acid with [RuCl$_2$(PTA)$_4$] (**10**) in acidic media [24]. When H$_2$O was used as solvent, a formic acid solution of 0.2 M was obtained at pH 2.7 and 60 °C under 20 MPa H$_2$/CO$_2$ (3/1), corresponding to a TON of 74. When DMSO was used, formic acid concentration of 1.9 M was obtained at 60 °C under 10 MPa H$_2$/CO$_2$ (1/1) after 120 h. The catalyst is highly stable and can be recycled and reused multiple times without loss of activity. A total TON of 749 was achieved after the fourth cycle in recyclability tests. The most important merits of this system are direct FA production and without the need for basic additive and the requirement of acidification after reaction.

In 2016, Dang et al. investigated the steric and electronic effects of bidentate phosphine ligands in the Ru complexes **11–13** for the hydrogenation of CO$_2$ to formic acid by DFT calculations [56]. As shown in Scheme 2.1, the reaction undergoes three major steps: *cis-trans* isomerization of ruthenium dihydride complex, CO$_2$ insertion into the Ru–H bond, and H$_2$ insertion into the ruthenium formate ion to release HCOOH. The steric effect of the ligands slightly affected the reaction, and the electronic effect activated *cis-trans* isomerization and H$_2$ insertion.
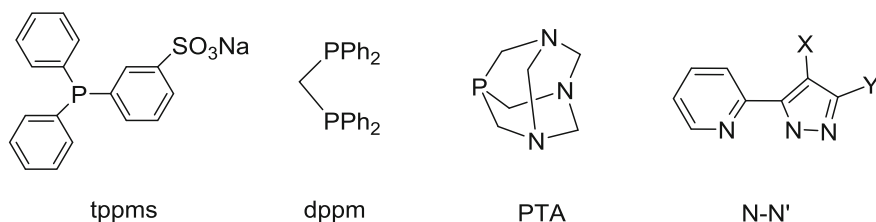
Fig. 2.1 Phosphine and *N,N*-bidentate ligands used in Ru complexes
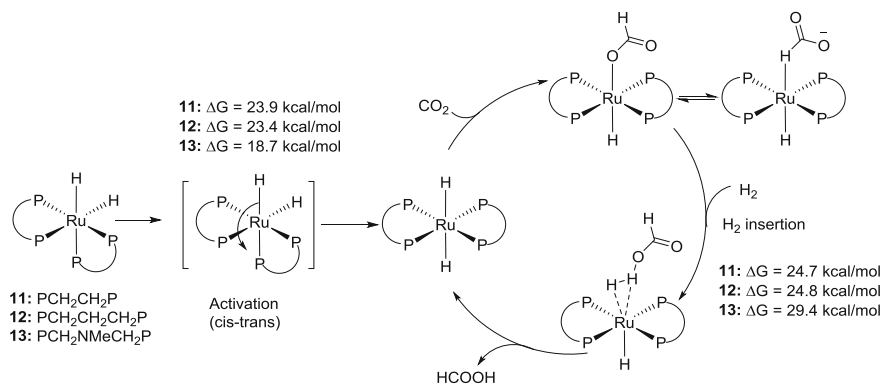
Scheme 2.1 Overall process of Ru-catalyzed CO$_2$ hydrogenation. Redrawn based on Ref. [56]. Copyright (2016) Wiley-VCH GmbH & Co. KGaA, Weinheim

2.1.1.2 Ru Complexes with Pincer Ligands

Pincer complexes are demonstrated to activate small molecules, such as H$_2$ and CO$_2$, through metal–ligand cooperation [57]. The non-innocent nature of pincer ligands is crucial in the activation of CO$_2$ via an aromatization/de-aromatization mechanism [58, 59]. The crystal structures of CO$_2$ adducts **14** and **15** derived from Ru(PNP) complex **16** and Ru(PNN) complex **17** were reported by Milstein and Sanford, respectively (Fig. 2.2) [60, 61]. During hydrogenation, complex **16** reversibly converts to **15**. Complex **17** showed high activity in CO$_2$ hydrogenation and afforded a TON up to 23,000 and a TOF up to 2200 h^{-1} at 200 °C for 48 h under 4 MPa H$_2$/CO$_2$ (3/1) in diglyme in the presence of K$_2$CO$_3$ [32].

In 2013, Pidko et al. reported the catalytic CO$_2$ hydrogenation with Ru–PNP pincer complexes **18–21** in the presence of DBU in THF. Complex **20** gave a high TOF of 14,500 h^{-1} at 70 °C under 40 bar H$_2$/CO$_2$, whereas complex **21** exhibited better performance with a TOF of 21,500 h^{-1} [33]. The authors revealed the effect of metal–ligand cooperation in catalytic CO$_2$ hydrogenation by in situ NMR spectroscopy and DFT calculations. Complex **20** produced from ligand-assisted CO$_2$ activation remained in an inactive state and inhibited the catalytic reaction. The addition of water restored the catalytic activity by providing a pathway toward the formation of active species (Scheme 2.2). Their group further investigated the reversible hydrogenation of CO$_2$ under mild conditions with Ru pincer complex **18** [31]. Using DBU as a base, complex **18** provided an unprecedented TOF as high as 1,100,000 h^{-1} at 120 °C under 4 MPa H$_2$/CO$_2$ (3/1) in DMF. The catalytic mechanism of the Ru–PNP pincer complex in the presence of DBU was subsequently investigated using DFT calculations [62].

In 2016, Olah and Prakash et al. reported an environmentally friendly and direct approach for CO$_2$ capture by amines in aqueous media and in situ conversation to ammonium formate with Ru–PNP complexes **25** and **26** (Scheme 2.3) [63]. The amines in this process had a dual purpose of transforming CO$_2$ to ammonium
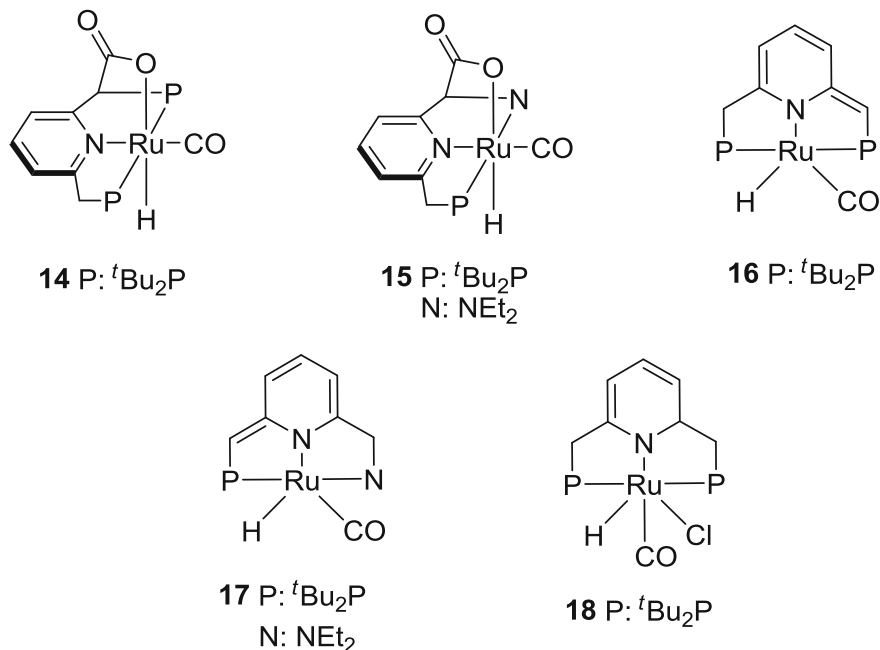
Fig. 2.2 Pincer Ru complexes for CO_2 hydrogenation

carbamate/bicarbonate/carbonate and stabilizing the formate product. Among the various amines tested, tetramethylguanidine (TMG) provided the highest yield of 95% and highest TON of 7375 for 20 h at 50 °C under 50 bar H_2 in the presence of complex **25**, while diazabicyclo[2.2.2]octane (DABCO) afforded the highest TOF ($433 \ h^{-1}$) under the same conditions. Catalyst recycling was also studied in a biphasic system consisting of 2-methyltetrahydrofuran and water. When catalyst **25** was used, an overall TON of >7000 for formate was obtained after five cycles, and the activity of the catalyst exhibited no significant decrease. This study presented an environmentally friendly and straightforward approach to produce formate from captured CO_2.

2.1.2 Rhodium Complexes

For CO_2 hydrogenation, phosphine ligands as σ-donors were demonstrated to be effective and applicable with metals, such as rhodium. In 1992, Tsai and Nicholas reported that a precatalyst [Rh(NBD)(PMe$_2$Ph)$_3$]BF$_4$ (**27**) (NBD: norbornadiene) can be converted to [H$_2$Rh(PMe$_2$Ph)$_3$(OH$_2$)]BF$_4$ (**28**) by the addition of H_2 in wet
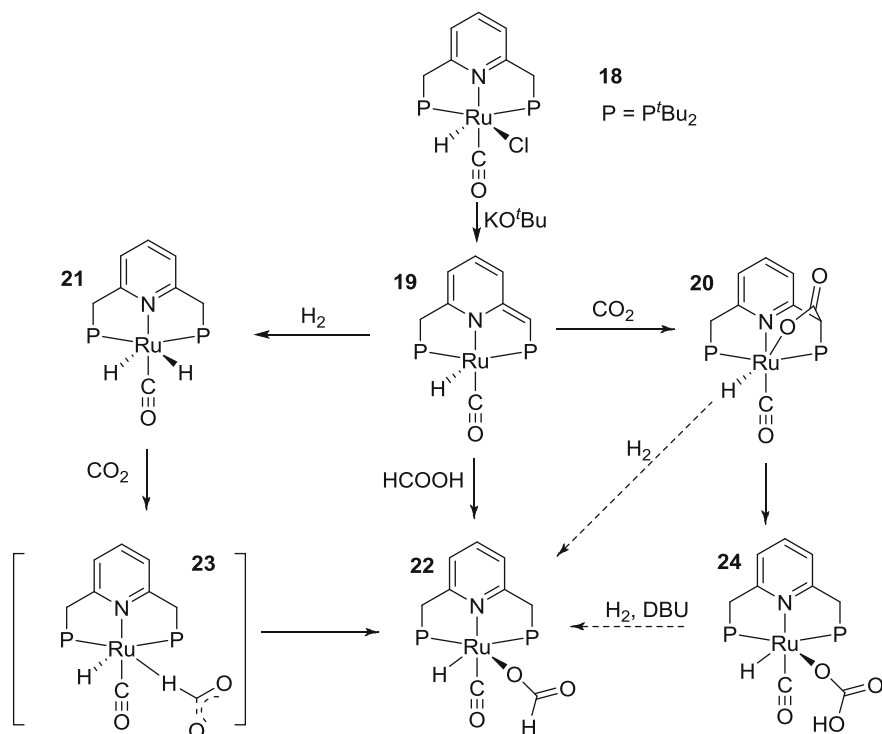
Scheme 2.2 Experimentally observed transformations of Ru–PNP complexes in the presence of H$_2$ and CO$_2$. Redrawn based on Ref. [33]
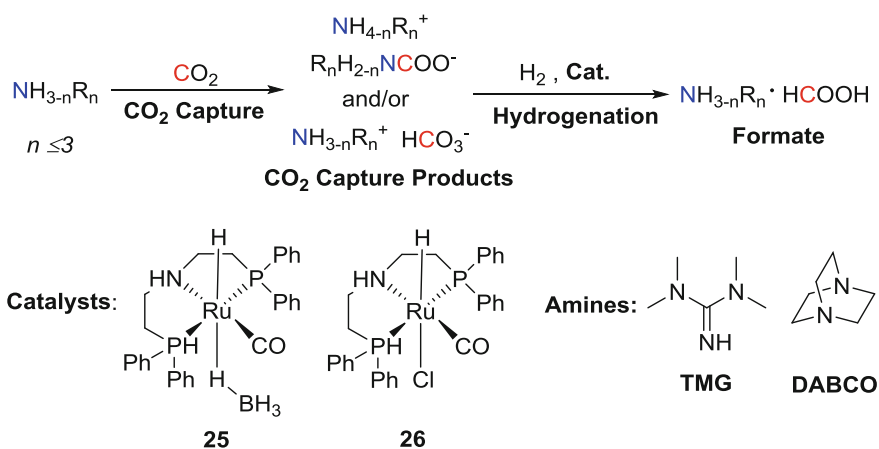
Scheme 2.3 CO$_2$ capture and conversion to ammonium formate

THF (4% H$_2$O) and produced formate more than twice as fast than that in dry THF [64]. The addition of a small amount of water was favorable for the catalytic activity of rhodium complex in CO$_2$ hydrogenation in THF. The authors speculated that H$_2$O molecule bound to a metal center could form a hydrogen bond with the oxygen atom of CO$_2$, improve electrophilicity of the carbon atom, and stabilize the transition state for CO$_2$ insertion. Kolesnichenko et al. studied the hydrogenation reaction catalyzed by Wilkinson's complex RhCl(PPh$_3$)$_3$ (**29**) in polar solvents (e.g., DMSO and MeOH), which afforded a TON of 2500 for 20 h at 25 °C under 6 MPa H$_2$/CO$_2$ (2/4) [2].

Most metal phosphine complexes are lipophilic, while introduction of polar groups, such as sulfonic acid, endows water solubility on the complexes. This improvement satisfied the catalytic CO$_2$ reduction in water. In 1993, a water-soluble rhodium catalyst RhCl(tppts)$_3$ (**30**) (tppts: tris(3-sulfonatophenyl)phosphine) was first reported by Leitner et al. for CO$_2$ hydrogenation in water. It gave a high TON of 3440 under relatively mild conditions (rt, 4 MPa H$_2$/CO$_2$ = 1/1) in the presence of HNMe$_2$ for 12 h [35].

Phosphines are usually "spectator" ligands. Mimicking the active site of [Fe–Fe]-hydrogenase, Kubiak et al. synthesized five [Rh(P$_2$N$_2$)$_2$]$^+$ complexes and the corresponding rhodium hydrides with substituted cyclic diphosphine P$_2$N$_2$ (1,5-diaza-3,7-diphosphacyclooctane) [65]. They found that pendant amines introduced in the second coordination sphere were unable to deprotonate the strongly basic dihydride species. The effect of the P$_2$N$_2$ ligands was attributed to their electron-donating ability, which increased electron density at the metal center. [Rh(depe)$_2$]$^+$ (depe: 1,2-bis(diethylphosphino)ethane) (**31**) was found to be the most active catalyst that gave a TON of 515 under 2 atm H$_2$/CO$_2$ (1/1) and 21 °C in THF in the presence of Verkade's base (2,8,9-triisobutyl-2,5,8,9-tetraaza-1-phosphabicyclo[3.3.3]undecane) for 1 h. The less hindered depe ligand is favorable for accessing the external base to the metal center to promote the oxidative addition of H$_2$.

NHC ligands are also strong electron donors. Very recently, Herrmann and Kühn et al. reported the hydrogenation of bicarbonate to formate using Rh catalyst **32** with water-soluble *bis*-NHC ligand under mild reaction conditions [39]. A high TON of 3600 was obtained with complex **32** under 50 bar H$_2$ in 2 mol/L KHCO$_3$ aqueous solution for 72 h at 100 °C. KHCO$_3$ showed better catalytic performance than NaHCO$_3$ as bicarbonate source because of the lower solubility of NaHCO$_3$ in water. The authors utilized DFT calculations to investigate the mechanism (Scheme 2.4). The mechanism was divided into three steps: first, the chloride ligand was replaced by bicarbonate; subsequently, bicarbonate was reduced to formate by reducing agents; and finally, formate was exchanged by bicarbonate. The rate-limiting step could be the reduction of the carbon atom. The authors suggested the involvement of another catalyst molecule, which provided an external hydride for the reduction of bicarbonate.
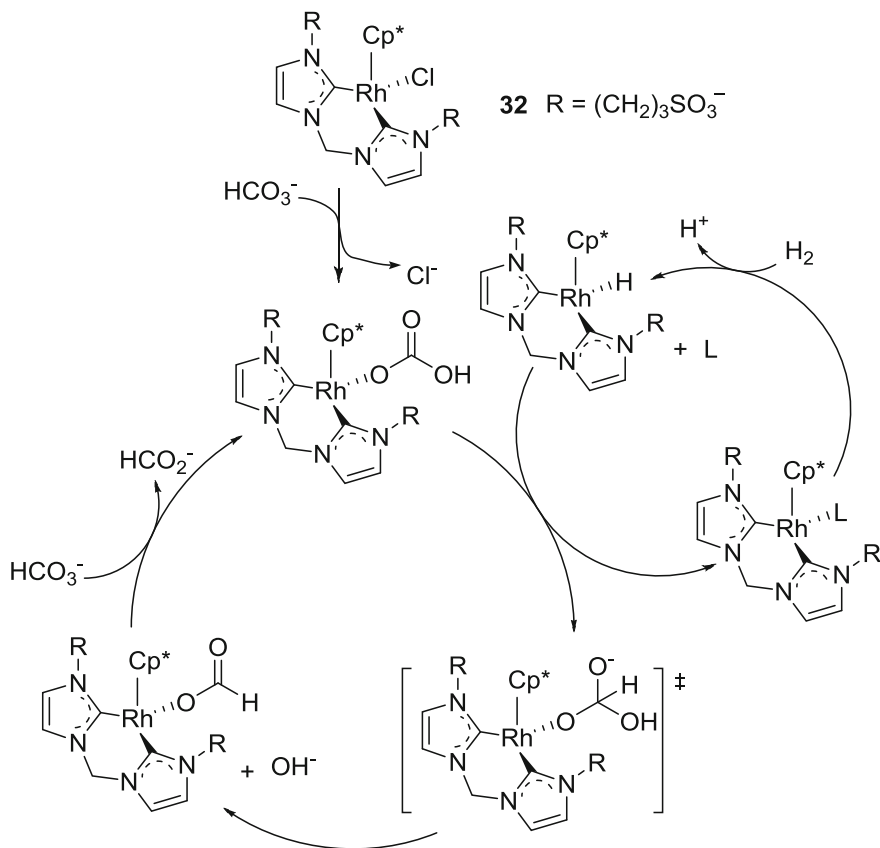
Scheme 2.4 Proposed overall mechanism for the reduction of bicarbonate to formate with sulfonated water-soluble complex **32**. Redrawn based on Ref. [39]. Copyright (2016) Wiley-VCH GmbH & Co. KGaA, Weinheim

2.1.3 Iridium Complexes

Compared with Ru and Rh complexes, Ir complexes have exhibited superior activity and recently attracted considerable attention. They also showed high stability and catalyzed reactions under high temperature, thereby providing higher outcomes.

2.1.3.1 Ir Complexes with Pincer Ligands

In 2009, Nozaki and co-workers developed an Ir trihydride complex IrH$_3$(PNP) (**33**, Scheme 2.5) and achieved the highest activity for CO$_2$ hydrogenation. Given the low water solubility of the PNP complex, they chose THF as a cosolvent for
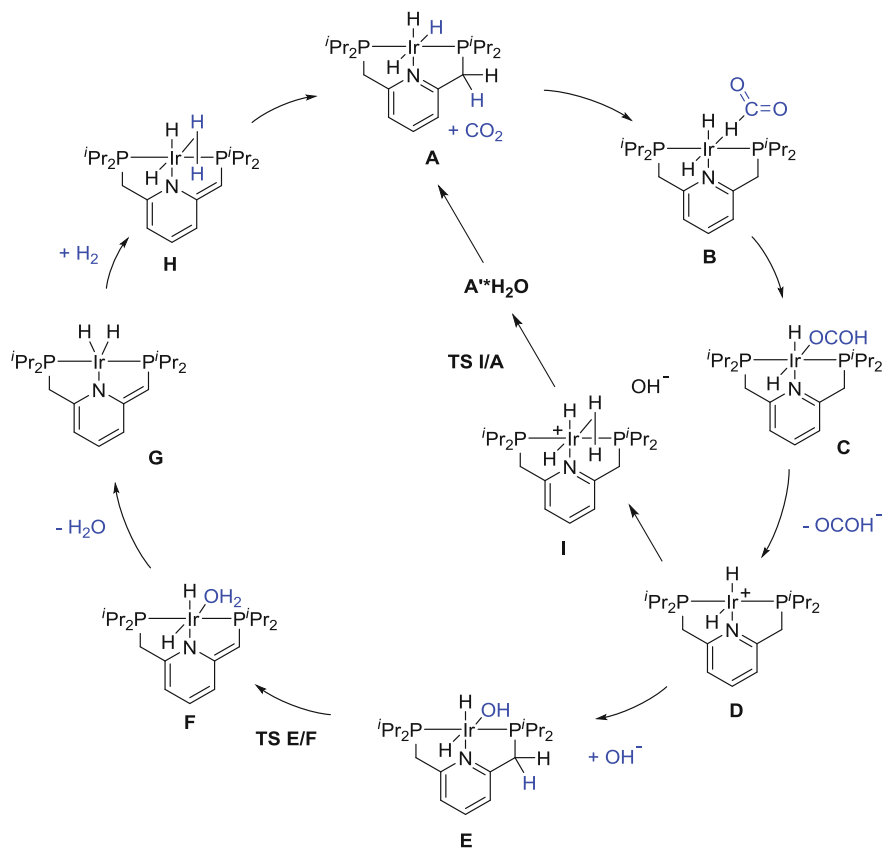
Scheme 2.5 Proposed mechanism for the hydrogenation of CO$_2$ by **33** based on Ref. [13]

homogeneous catalysis. Complex **33** (Fig. 2.3) showed an extraordinarily high TOF of 150,000 h^{-1} at 200 °C and TON of 3,500,000 (48 h) at 120 °C under 8 MPa H$_2$/CO$_2$ (1/1) in H$_2$O/THF (5/1) [12, 13]. Soon after their study, the catalytic mechanisms of the PNP Ir complex were investigated with computational methods [13, 66, 67].
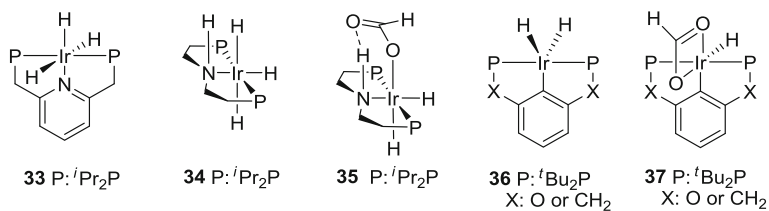
Fig. 2.3 Pincer Ir complexes for CO$_2$ hydrogenation in water
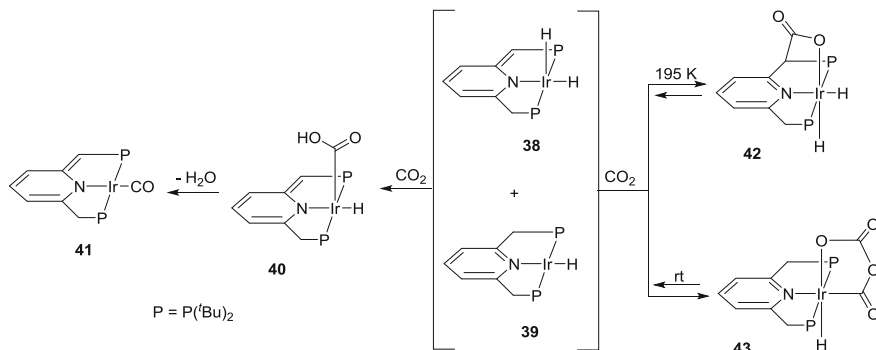
Scheme 2.6 Reaction pathway of complexes **38** and **39** with CO$_2$ to give complexes **40–43**. Reprinted with permission from Ref. [68]. Copyright (2016) American Chemical Society

Nozaki et al. carried out DFT calculations using pincer complex **33** as a catalyst [13]. Two competing reaction pathways were identified, and the rate-determining steps (RDSs) were determined to be deprotonative de-aromatization (via TS E/F) and hydrogenolysis (via TS I/A) (Scheme 2.5). The calculated free energy profiles provided an explanation for the effect of H$_2$ pressure, base, and solvent and were consistent with experimental data.

Feller and Milstein et al. presented a unique mode of stoichiometric CO$_2$ activation and reductive splitting based on metal–ligand cooperation [68]. The Ir pincer complexes **38** and **39** reacted with CO$_2$ to give intermediate **40**, which resulted in de-aromatized complex **41** by intramolecular dehydration with the assistance of H$_2$O molecule. Complexes **42** and **43** were formed reversibly by CO$_2$ binding to the ligand and metal (Scheme 2.6). DFT calculations revealed that thermodynamic products **42** and **43** were side products rather than intermediates. Their study helped us further understand the CO$_2$ activation mode of pincer complex through metal–ligand cooperation.

Scheme 2.7 Proposed mechanism for CO$_2$ hydrogenation using catalyst **34** with the displacement of formate by H$_2$ as the rate-determining step. Redrawn based on Ref. [14]. Copyright (2011) American Chemical Society
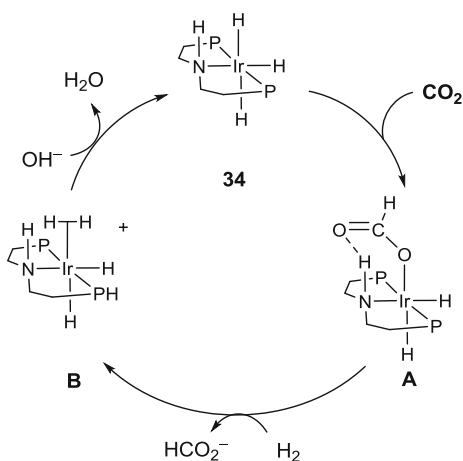
In 2011, Hazari and co-workers developed IrH_3(PNP) complex **34** bearing an N–H group, which formed stable complex **35** with CO_2 (Fig. 2.3) [14]. Their calculations indicated that CO_2 insertion was facilitated by an N–H–O hydrogen bond through an outer sphere interaction (Scheme 2.7). Complex **35** achieved a maximum TON of 348,000 and a high TOF of 18,780 h^{-1}. IrH_2(PCP) pincer complex **36** could form κ^2-formato complex **37** by reaction with CO_2 (Fig. 2.3) [69]. Complexes **36** and **37** are efficient and selective catalysts for electrocatalytic reduction of CO_2 to formate in CH_3CN/H_2O.

2.1.3.2   Ir Complexes with *N,N*-Chelated Ligands

Compared with the widely used phosphine complexes, molecular complexes with *N,N*-chelated ligands have attracted less attention in the context of CO_2 hydrogenation [25, 70–73]. Recently, Himeda et al. have developed a series of *N,N*-chelated complexes $[Cp^*Ir(DHPT)(OH_2)]^{2+}$ (DHPT: 4,7-dihydroxy-1,10-phenanthroline), $[Cp^*Ir(nDHBP)(OH_2)]^{2+}$ (nDHBP: n,n′-dihydroxy-2,2′-bipyridine, n = 3, 4, 5, 6), $[(Cp^*IrCl)_2(THBPM)]^{2+}$ (THBPM: 4,4′,6,6′-tetrahydroxy-2,2′-bipyrimidine), and $[Cp^*Ir(Nn)(OH_2)]^{2+}$ (n = 1–14, Fig. 2.4). Among these complexes, functionalized complex bearing OH group exhibited remarkable activity. The significant effect of the ligands is illustrated as follows:

Electronic effects. The studies by Jessop and Sakaki et al. indicated that complexes bearing strong electron-donating ligands have high activity in CO_2 hydrogenation [4, 74]. Inspired by their studies, Himeda's group developed a series of half-sandwich Ir complexes $[Cp^*Ir(4,4′-R_2-bpy)Cl]^+$ (R = OH, OMe, Me, H) [17, 75–77]. The chloro ligand in these complexes can readily hydrolyze to form the corresponding aqua complexes $[Cp^*Ir(4,4′-R_2-bpy)(OH_2)]^{2+}$ in the presence of water.

Among these catalysts, complexes bearing OH substituents show unique properties. The OH group (σ_p^+ = −0.92) is readily deprotonated to generate a considerably stronger oxyanion electron donor (σ_p^+ = −2.30) when the solution pH increases beyond 5–6 [76]. Tautomerism of the oxyanion form is observed. The conjugation effect makes the ligand highly electron donating (Scheme 2.8). These hydroxy-substituted diamine ligands are classified as "proton-responsive ligands" (Fig. 2.4) [78]. They are pH switchable and tunable in polarity and electron-donating ability, and thus, are capable of adjusting the catalytic activity and water solubility of the complexes.

Hammett constants (σ_p^+) are usually used to characterize the electron-donating ability of the substituents: the more negative the σ_p^+ values, the stronger their electron-donating ability. Figure 2.5 shows the correlation between the initial TOFs and the σ_p^+ values of the substituents for the $[Cp^*Ir(4,4′-R_2-bpy)(OH_2)]SO_4$ complexes. The activity of $[Cp^*Ir(4DHBP)(OH_2)]SO_4$ (4DHBP: 4,4′-dihydroxy-2,2′-bipyridine; Fig. 2.4) is over 1000 times higher than that of the unsubstituted analogue $[Cp^*Ir(bpy)(OH_2)]SO_4$ under the same conditions (80 °C, 1 MPa CO_2/
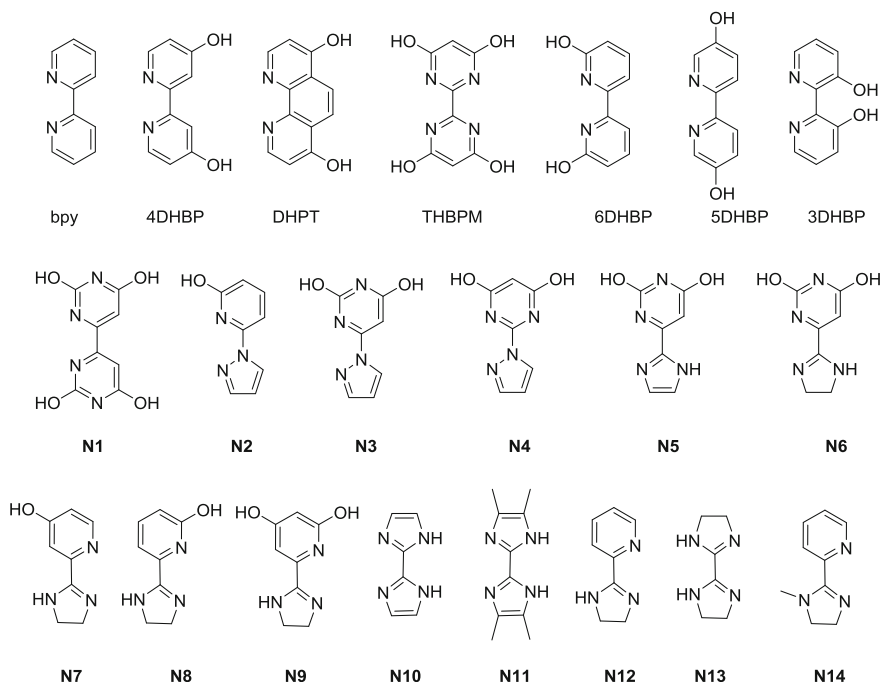
Fig. 2.4 Proton-responsive ligands used for CO$_2$ hydrogenation
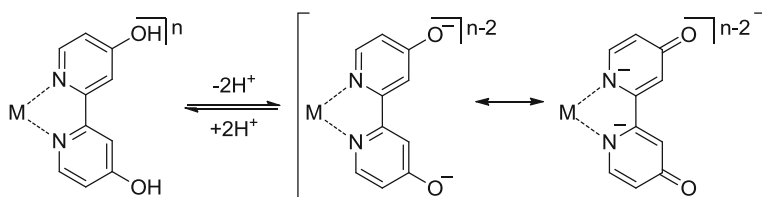
Scheme 2.8 Acid–base equilibrium between hydroxy and oxyanion forms and resonance structures of oxyanion form

H$_2$ = 1). The significant improvement of the activity can be attributed to the strong electron-donating ability of the oxyanion. The catalytic activity of [Cp*Ir(6DHBP)(OH$_2$)]$^{2+}$ and its analogues [Cp*Ir(6,6′-R$_2$-bpy)(OH$_2$)]SO$_4$ (R = OMe, Me, H) was also investigated [16]. As shown in the Hammett plots (Fig. 2.3), similar to the 4,4′-substituted analogues, stronger electron-donating substituents lead to higher reaction rates.

Most recently, Himeda et al. reported iridium catalysts with electron-donating imidazoline moieties as ligands for the hydrogenation of CO$_2$ to formate in aqueous solution. These complexes are considerably more effective than the imidazole
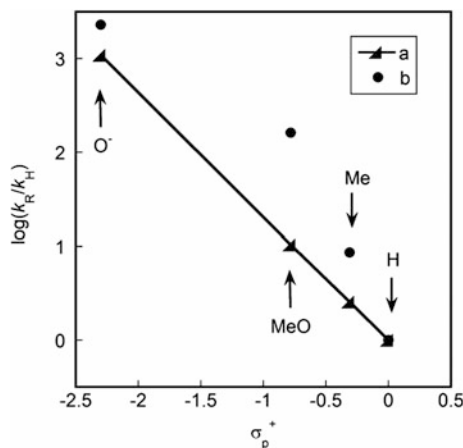
Fig. 2.5 Correlation between initial TOFs and σ_p^+ values of substituents (R) for the CO_2 hydrogenation catalyzed by (a) $[Cp^*Ir(4,4'-R_2-bpy)(OH_2)]SO_4$ (R = OH, OMe, Me, H; triangles) and (b) $[Cp^*Ir(6,6'-R_2-bpy)(OH_2)]SO_4$ (R = OH, OMe, Me, H; circles). Reaction conditions: 1 MPa of H_2/CO_2 (1/1), 80 °C; **a** 0.02–0.2 mM catalyst in 1 M KOH and **b** 0.01–0.2 mM catalyst in 1 M $NaHCO_3$. Reproduced from Ref. [16] with permission from the Royal Society of Chemistry

analogues [79]. The reaction rate (1290 h^{-1}) of the bisimidazoline complex $[Cp^*Ir(N13)(OH_2)]^{2+}$ was considerably higher than that (20 h^{-1}) of bisimidazole complex $[Cp^*Ir(N10)(OH_2)]^{2+}$ under 1 MPa at 50 °C. Under atmospheric pressure at room temperature, the bisimidazoline complexes exhibited a TOF of 43 h^{-1}, which is comparable to that of the most efficient dinuclear complex $[(Cp^*IrCl)_2(THBPM)]^{2+}$ (70 h^{-1}) [18]. The catalytic activity of the complex $[Cp^*Ir(N14)(OH_2)]^{2+}$ with an N-methylated imidazoline moiety was the same as that of the unsubstituted pyridylimidazoline analogue $[Cp^*Ir(N12)(OH_2)]^{2+}$. The high activity was not attributable to the deprotonation of NH in the imidazoline cycle under the reaction conditions.

Pendant base effects. A hydroxy group near the metal center may act as an important functional group, which can facilitate hydrogen dissociation and production as found in Fe-guanylpyridinol cofactor in [Fe]-hydrogenase [80–82]. A computational study revealed that the pendant hydroxy group played an important role in the activation of H_2 by forming a hydrogen bond [83]. Inspired by these works, Himeda and Wang et al. developed a series of iridium complexes, $[Cp^*Ir(nDHBP)(OH_2)]^{2+}$ (nDHBP: n,n'-dihydroxy-2,2'-bipyridine, n = 3, 4, 5, 6), $[(Cp^*IrCl)_2(THBPM)]^{2+}$, and $[Cp^*Ir(Nn)(OH_2)]^{2+}$ (n = 2–6, Fig. 2.4), as catalysts for CO_2 hydrogenation and the reverse reaction formic acid dehydrogenation under mild conditions in water solvent [16, 18, 19, 84–86].

As shown in the Hammett plots (Fig. 2.3), the TOF (8050 h^{-1}) of $[Cp^*Ir(6DHBP)(OH_2)]^{2+}$ was considerably higher than that (5100 h^{-1}) of $[Cp^*Ir(4DHBP)(OH_2)]^{2+}$ under the same conditions. As the hydroxy groups at the *para* and *ortho*

positions have almost the same electron-donating ability, additional rate enhancement is attributed to the proximity of the hydroxy groups in 6DHBP to the metal center. The possible cooperative effect of the adjacent OH, namely, pendant base effect, was studied in detail by experimental and computational methods [16, 19, 86].

The mechanism study suggested that CO$_2$ hydrogenation generally involves three steps: H$_2$ heterolysis to generate metal hydride, CO$_2$ insertion into the hydride to give formato intermediate, and dissociation of formate. NMR experiments indicated that [Cp*Ir(6DHBP)(OH$_2$)]$^{2+}$ forms the Ir–H species considerably more easily than [Cp*Ir(4DHBP)(OH$_2$)]$^{2+}$ in the presence of H$_2$. For instance, 95% of [Cp*Ir(6DHBP)(OH$_2$)]$^{2+}$ converted to the Ir–H complex over 0.5 h under 0.2 MPa H$_2$, whereas only 90% of [Cp*Ir(4DHBP)(OH$_2$)]$^{2+}$ transformed to the corresponding Ir–H complex over 40 h under 0.5 MPa H$_2$. DFT calculations using complex [Cp*Ir(6DHBP)(OH$_2$)]$^{2+}$ suggested that the heterolysis of dihydrogen is the RDS under basic conditions (pH 8.3) [16]. Furthermore, the calculations showed that the adjacent oxyanions, which deprotonated from hydroxy groups under basic conditions, became pendant bases and assisted the heterolysis of H$_2$ (Scheme 2.9A–D).

A study on the deuterium kinetic isotope effect (KIE) further found clear evidence for the involvement of a water molecule in the heterolysis of H$_2$ using [Cp*Ir(6DHBP)(OH$_2$)]$^{2+}$ and [Cp*Ir(N2)(OH$_2$)]$^{2+}$ bearing a pendant base [19]. Water participation enhanced proton transfer through the formation of a water bridge in
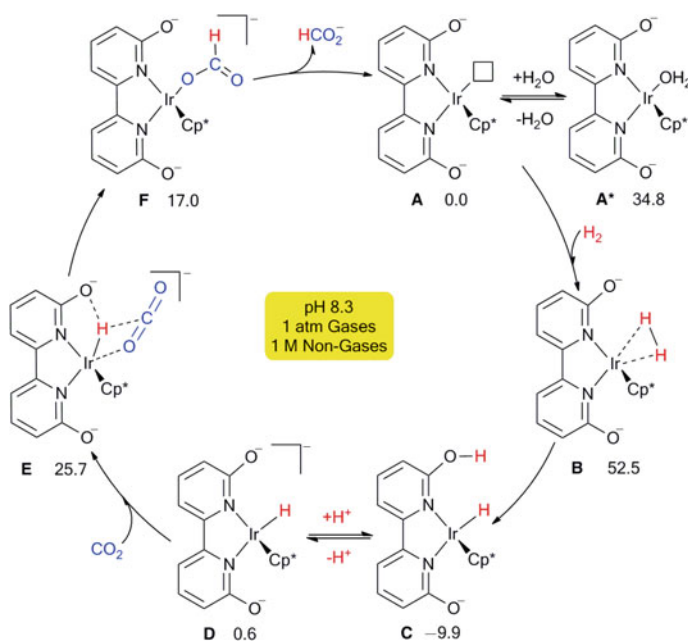
Scheme 2.9 Proposed mechanism for CO$_2$ hydrogenation by [Cp*Ir(6DHBP)(OH$_2$)]$^{2+}$. Reproduced from Ref. [16] with permission from the Royal Society of Chemistry

rate-limiting H$_2$ heterolysis. The KIE study was implemented with D$_2$/KDCO$_3$/D$_2$O instead of H$_2$/KHCO$_3$/H$_2$O. When D$_2$ was used instead of H$_2$, an apparent decrease in reaction rate was found both in KHCO$_3$/H$_2$O (KIE: 1.19) and KDCO$_3$/D$_2$O (KIE: 1.20) solution using [Cp*Ir(4DHBP)(OH$_2$)]$^{2+}$, which bears no pendant OH. Replacing H$_2$O with D$_2$O did not lead to a substantial rate decrease in H$_2$/KDCO$_3$ (KIE: 0.98). This result indicated that D$_2$ participated in the RDS for [Cp*Ir (4DHBP)(OH$_2$)]$^{2+}$. By contrast, for [Cp*Ir(6DHBP)(OH$_2$)]$^{2+}$ and [Cp*Ir(N2) (OH$_2$)]$^{2+}$ bearing pendant OH groups, D$_2$O led to a larger rate decrease than that with D$_2$. This result suggested that D$_2$O participated in the RDS for [Cp*Ir(6DHBP) (OH$_2$)]$^{2+}$ and [Cp*Ir(N2)(OH$_2$)]$^{2+}$. Therefore, it can be concluded that water participated in the rate-limiting heterolysis of H$_2$ for [Cp*Ir(6DHBP)(OH$_2$)]$^{2+}$ and [Cp*Ir(N2)(OH$_2$)]$^{2+}$ and not for [Cp*Ir(4DHBP)(OH$_2$)]$^{2+}$. This study suggests that a water molecule interacts with the pendant base and H$_2$ at the metal center, and assists the heterolysis of H$_2$ via a proton relay (Scheme 2.10). DFT calculations supported the participation of H$_2$O in the transition state. The calculated transition state with a water molecule is 14.2 kJ mol^{-1} lower than that without H$_2$O. This finding first proved the involvement of a water molecule in the H$_2$ heterolysis using complexes bearing pendant OH groups.

Recently, Wang et al. developed a series of new proton-responsive imidazoline-based complexes [Cp*Ir(Nn)(OH$_2$)]$^{2+}$ (n = 6–9) for highly efficient CO$_2$ hydrogenation in aqueous systems [87]. [Cp*Ir(N9)(OH$_2$)]$^{2+}$, which contains two OH groups at the *ortho* and *para* positions on a coordinating pyridine ring, achieved an unprecedented TOF of 106 h^{-1} and TON of 7280 for 336 h at 25 °C under 0.1 MPa CO$_2$ and H$_2$. The high efficiency of this system was attributed to the combined effects of the strong electron-rich imidazoline moiety and pendant base (OH groups).

The combined electronic and pendant base effects significantly improved the activity of the bioinspired complexes [Cp*Ir(6DHBP)(OH$_2$)]$^{2+}$, [Cp*Ir(N$_2$)(OH$_2$)]$^{2+}$ (N$_2$ = 2,2′,6,6′-tetrahydroxy-4,4′-bipyrimidine), and [(Cp*IrCl)$_2$(THBPM)]$^{2+}$. [(Cp*IrCl)$_2$(THBPM)]$^{2+}$ provided an extraordinary TOF of 65 h^{-1} and TON of 7200 (336 h) under ambient conditions (25 °C, 1 atm H$_2$/CO$_2$) in CO$_2$ hydrogenation. [Cp*Ir(N2)(OH$_2$)]$^{2+}$ showed comparable activity with [(Cp*IrCl)$_2$(THBPM)]$^{2+}$.
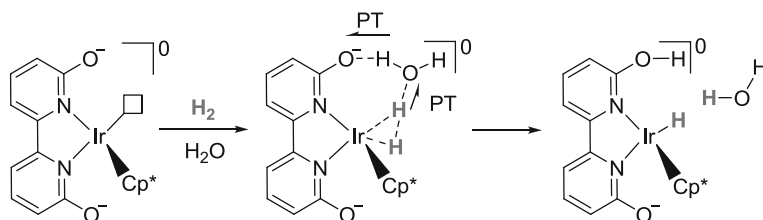
Scheme 2.10 Proposed mechanism for H$_2$ heterolysis assisted by the pendant base and a water molecule through proton relay. PT indicates proton transfer. Reprinted with permission from Ref. [19]. Copyright (2013) American Chemical Society

2.1.3.3 Ir Complexes with *C,C*- and *C,N*-Chelated Ligands

Peris et al. developed a series of water-soluble complexes **44–46** using *bis*-NHC (*N*-heterocyclic carbenes) as electron-donating ligands (Fig. 2.6) [21, 88]. By introducing hydroxy or sulfonate groups to the side carbon chains, the water solubility was improved. Thus, the activity was remarkably enhanced for the CO$_2$ hydrogenation to HCO$_2$K. Another merit of *bis*-NHC ligands is that they endowed high thermal stability to the corresponding complexes. Finally, a high TON of 190,000 was achieved with complex IrI$_2$(AcO)(bis-NHC) **46**, under 6 MPa H$_2$/CO$_2$ (1/1) at 200 °C for 75 h.

Fukuzumi et al. developed *C,N*-chelated water-soluble Ir complex **47** bearing a carboxyl group [22]. Aqua complex **47** can be deprotonated to give benzoate complex **48** and hydroxo complex **49**. The pK_a values of complexes **47** and **48** are determined to be 4.0 and 9.5, respectively (Fig. 2.7). Complex **48** was utilized for CO$_2$ hydrogenation in 0.1 M K$_2$CO$_3$ solution (pH 8.8) by bubbling H$_2$/CO$_2$ (1/1, 50 mL/min) under atmospheric pressure at 30 °C. A TOF of 6.8 h^{-1} and a TON of more than 100 were obtained over 20 h. In the same manner, the TOF increased to 22.1 h^{-1} at 60 °C.
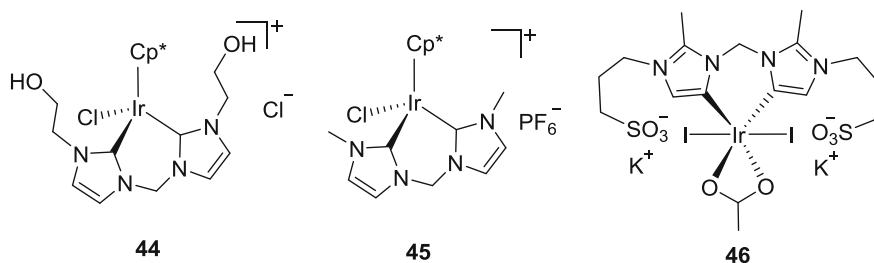
Fig. 2.6 Peris et al.'s NHC Ir complexes for CO$_2$ hydrogenation in water
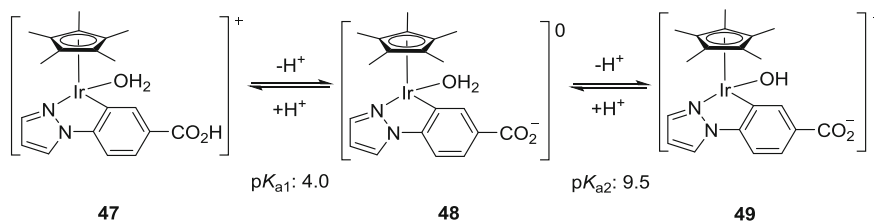
Fig. 2.7 Fukuzumi et al.'s catalyst for CO$_2$ hydrogenation in water. Reprinted with permission from Ref. [22]. Copyright (2012) Royal Society of Chemistry

2.2 CO_2 Hydrogenation Using Non-precious Metals

Although noble metals, such as Ir, Rh, and Ru, are widely used for CO_2 hydrogenation and great success has been achieved, their high cost is one drawback for their practical application. Therefore, various non-precious metals, such as Ni, Fe, Co, and Mo, were investigated. Efficient ligands for noble metals-based complexes are usually also capable to construct effective complexes of non-precious metals. However, some exceptions exist; for example, the Co analogues of the highly efficient Ir complexes $[Cp^{*}Ir(nDHBP)(OH_2)]^{2+}$ (n = 4 or 6) showed low activity because of their low stability [89]. Nevertheless, versatile phosphine and pincer ligands are applied to develop efficient non-precious metal complexes.

2.2.1 Using Phosphine Ligands

In the pioneer work of Inoue, they used a complex $Ni(dppe)_2$ (dppe: 1,2-bis (diphenylphosphino)ethane) as catalyst and obtained a TON of 7 for 20 h at room temperature under 5 MPa H_2/CO_2 (1/1) [1]. In 2010, Beller and Laurenczy et al. reported the first hydrogenation of bicarbonate to formate with $Fe(BF_4)_2 \cdot 6H_2O$ and $P(CH_2CH_2PPh_2)_3$ (PP_3), which forms iron hydride complexes $[FeH(PP_3)]BF_4$ and $[FeH(H_2)(PP_3)]BF_4$ under the reaction conditions [40]. The catalytic reaction under 60 bar H_2 at 80 °C provided sodium formate with an excellent yield of 88% and a high TON of 610 for 20 h. The activity of the iron catalyst is comparable to that of a noble metal analogue $[\{RuCl_2(benzene)\}_2]/PP_3$ (TON = 624). Two years later, Beller et al. reported the cobalt analogue $Co(BF_4)_2 \cdot 6H_2O$ and PP_3 for hydrogenation of sodium bicarbonate [41]. A high TON of 3880 was obtained under 60 bar H_2 at 120 °C with a yield of 71%. They further prepared a phosphine ligand tris(2-(diphenylphosphino)phenyl)phosphine in a one-pot reaction [90]. The multidentate ligand combined with $Fe(BF_4)_2 \cdot 6H_2O$ served as an efficient catalyst for CO_2 or bicarbonate hydrogenation. The in situ catalyst provided a high TON of 1600 under 60 bar H_2 at 80 °C for bicarbonate substrate in MeOH over 20 h.

Linehan et al. utilized $Co(dmpe)_2H$ (dmpe: 1,2-bis(dimethylphosphino)ethane) for CO_2 hydrogenation and achieved a remarkable TON of 9400 after 1 h in THF under 20 atm H_2/CO_2 (1/1) at 21 °C in the presence of Verkade's base [43]. The cobalt-based system is similar to the fastest catalysts based on iridium at room temperature [12]. The mechanism study indicated a significant effect of the strong base [91].

Copper catalysts are less investigated [92]. Copper complexes with tridentate 1,1,1-tris-(diphenylphosphinomethyl)ethane were studied by Appel et al. and provided a TON up to 500 under 4 MPa H_2/CO_2 (1/1) at 140 °C for 20 h [93, 94].

2.2.2   *Using Pincer Ligands*

In 2011, Milstein and co-workers reported an active pincer iron complex, *trans*-[FeH$_2$(CO)(PNP)] (**50**), which provided a high TON of 788 and TOF of 156 h^{-1} under low pressure (0.6–1 MPa) in H$_2$O/THF (10/1) at 80 °C [42]. The observed activity was comparable to known noble metal catalysts and highlighted the enormous potential of iron-based catalysts for possible applications. The mechanism study suggested that the reaction proceeds through direct attack of the iron hydride to CO$_2$, followed by replacement of the resulting formate ligand by water. Dihydrogen coordination, prior to heterolytic cleavage of H$_2$ by hydroxide or de-aromatization, and subsequent proton migration were plausible pathways for the regeneration of the *trans*-dihydride complex **50** (Fig. 2.8). Milstein and co-workers also developed pyrazine-based pincer Fe complex **51** (Fig. 2.8), which provided a moderate TON of 388 for CO$_2$ hydrogenation in H$_2$O/THF (10/1) under 10 bar H$_2$/CO$_2$ (6.3/3.3) for 16 h [95].

   In 2016, Kirchner and Gonsalvi prepared several iron pincer complexes, among which complexes [Fe(PNP^H-^{i}Pr)(H)(CO)(Br)] (**52**) and [Fe(PNP^{Me}-^{i}Pr)(H)(CO)(Br)] (**53**) were found to be active catalysts for hydrogenation of CO$_2$ and NaHCO$_3$ to formate under mild conditions (Fig. 2.8) [45]. Notably, the hydrogenation of NaHCO$_3$ to HCO$_2$Na with complex **52** proceeded even at room temperature in H$_2$O/THF (4/1), giving a TON of 188 after 72 h. In the presence of DBU, complex **53** afforded sodium formate with a TON of 856 after 21 h and 1032 after 72 h under an initial pressure of 80 bar in EtOH at 25 °C. A catalytic cycle with **53** was proposed based on the NMR study (Scheme 2.11). Dihydrido intermediate **54** was first formed from **53** in the presence of H$_2$ and DBU. CO$_2$ insertion into **54** gave hydrido formate complex **55**. Further formate elimination and hydrogenolysis regenerated **54** with the assistance of DBU. Solvent-assisted formate decoordination may occur to afford a pentacoordinate cationic Fe(II) hydrido carbonyl species. However, it was not observed. Under NMR, EtOH stabilized intermediate **56** was detected. DFT studies indicated an outer sphere mechanism with hydrido formate

Fig. 2.8 Pincer Fe complexes for CO$_2$ hydrogenation
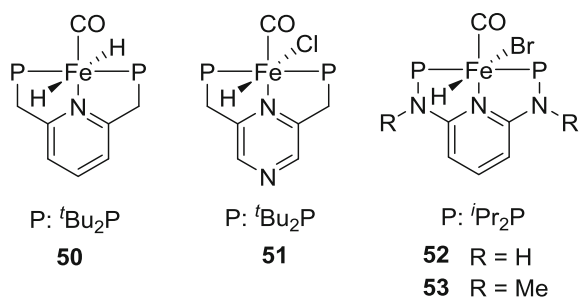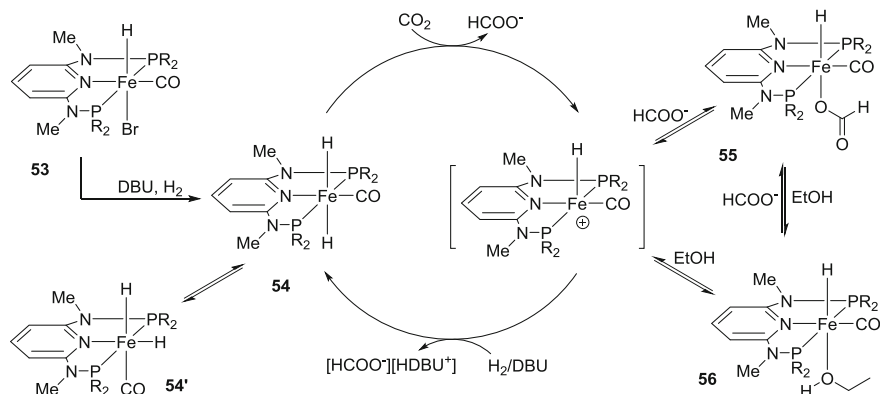
Scheme 2.11 Proposed catalytic cycle for CO$_2$ hydrogenation with complex **53**. Redrawn based on Ref. [45]

complex **55** as the catalyst resting state. Water molecule is involved in the catalytic process and stabilizes the reaction intermediates by forming hydrogen bond with the free formate ion. It facilitates formate elimination from the coordination sphere of the metal, thereby promoting catalysis. The excess DBU enhances the overall reaction by acid base reaction with the formic acid product.

In 2015, Bernskoetter and Hazari et al. developed a family of pincer iron complexes supported by PNP ligands containing a secondary or tertiary amine (Fig. 2.9) [96]. Among them, complexes **57** and **58** exhibited high activity. Using Lewis acid, such as LiOTf, as a cocatalyst can significantly enhance the reactivity. Complex **57** with secondary amine gave a TON of 8910 in THF under 6.9 MPa H$_2$/CO$_2$ (1/1) for 24 h in the presence of DBU at 80 °C. By contrast, under the same conditions, complex **58** bearing a tertiary amine achieved an unprecedented TON of 58,990 and initial TOF up to 18,050 h^{-1}. The formato complex, which was stabilized by an intramolecular hydrogen bond between the N–H moiety of PNP ligand and the carbonyl oxygen of a formate ligand, was identified as the catalytic resting state. The primary roles of LA are to disrupt the intramolecular hydrogen bond and assist formate extrusion. In 2016, Bernskoetter et al. reported a cobalt analogue for hydrogenation of CO$_2$ [44]. When paired with the Lewis acid lithium triflate, pincer cobalt complex **59** afforded a TON near 30,000 (at 1000 psi, 45 °C). This finding represents a notable improvement in for the activity for cobalt catalysts. The authors successfully synthesized a series of low-valent pincer–molybdenum catalysts for CO$_2$ hydrogenation [46]. Complexes **60** with PN^{Me}P (MeN(CH$_2$CH$_2$PPh$_2$)$_2$) ligand provided a modest TON of 35 under 6.9 MPa H$_2$/CO$_2$ (1/1) for 24 h with the addition of Lewis acid LiOTf (Fig. 2.9).
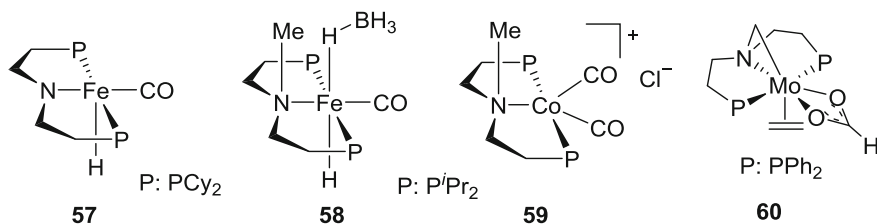
Fig. 2.9 Bernskoetter's catalysts for CO$_2$ hydrogenation

2.3 CO$_2$ Hydroboration and Hydrosilylation to Formate

Formic acid production from CO$_2$ hydrogenation with H$_2$ is thermodynamically unfavorable. The addition of a base is one strategy to promote the reaction because stable formate salt is generated. Hydrosilane and boranes are used as hydrogen sources for CO$_2$ reduction to overcome the unfavorable thermodynamics. The reduction of CO$_2$ to formate, acetal, methoxide (see Chap. 4), and methane is feasible by using appropriate catalysts [97–103]. The products, silyl formate or boron formate, can readily release formic acid by the addition of water. This reaction pathway is a simple method to produce formic acid from CO$_2$. A number of catalytic systems have been reported.

2.3.1 CO$_2$ Hydrosilylation

The hydrosilylation of CO$_2$ to formate dates back to 1981. Koinuma et al. first reported the reaction with complex RuCl$_2$(PPh$_3$)$_3$ using hydrosilanes HSiMeEt$_2$ or HSiMe(OMe)$_2$ to produce HCO$_2$SiR$_3$ albeit in low yields (up to 14%) [104].

Pitter et al. found that commercially available RuCl$_3$ · nH$_2$O is a good catalyst for hydrosilylation of CO$_2$ in MeCN with n-Hex$_3$SiH into n-Hex$_3$SiOOCH and with Me$_2$PhSiH into Me$_2$PhSiOOCH [105]. The initially formed [Ru^{II}Cl(MeCN)$_5$] [Ru^{III}Cl$_4$(MeCN)$_2$] (**61**) was found to be the most active catalyst, which provided a TON of 465 and a TOF of 233 h^{-1} within 2 h at 60 °C. In addition, the reactions using Et$_2$SiH$_2$, Ph$_2$SiH$_2$, and p-C$_6$H$_4$-(Me$_2$SiH)$_2$ yielded Et$_2$Si(OOCH)$_2$, Ph$_2$Si (OOCH)$_2$, and p-C$_6$H$_4$-(Me$_2$SiOOCH)$_2$, respectively. When silyl formate was exposed to moisture, formic aid was readily released and simultaneously gave silanediols. Using complex Ru$_2$Cl$_5$(MeCN)$_7$ (**61**), the authors performed a recycling test. They found that Me$_2$PhSi(OOCH) could be isolated by distillation. Therefore, the residue was reused for the next run. After 10 successive experiments, they achieved a high TON of 4619 [106].

In 2012, Baba et al. utilized cheap Cu(OAc)$_2$ · H$_2$O and 1,2-bis(diphenylphos-phino)benzene ligand as a catalyst and achieved a high TON of 8100 under 1 atm CO$_2$ at 60 °C after 6 h using an inexpensive hydrosilane polymethylhydrosiloxane

(PMHS) [107]. Afterward, they investigated the ligand effect by using other diphosphines [108]. 1,2-Bis(diisopropylphosphino)benzene was demonstrated to be the most effective ligand, which achieved a high TON of approximately 70,000 and TOF of 2900 h^{-1} after 24 h under 1 atm of CO_2 at 60 °C.

In 2013, Hou et al. reported N-heterocyclic carbene–copper complex [Cu(O^{t}Bu) (IPr)] (IPr: 1,3-bis(2,6-diisopropylphenyl)imidazol-2-ylidene) as a highly efficient catalyst, which showed a high TON of 7489 and a TOF of 1248 h^{-1} under the same conditions [109]. The reaction of [Cu(O^{t}Bu)(IPr)] with triethoxysilane at room temperature instantly afforded [CuH(IPr)]. Subsequent reaction with CO_2 gave a Cu formate complex [Cu(OCHO)(IPr)], which was isolated and characterized with single-crystal X-ray diffraction. This study provided an important insight into the catalytic mechanism.

In 2013, García et al. reported the first hydrosilylation of CO_2 using the nickel complex [(dippe)Ni(μ-H)]$_2$ (62) (dippe: 1,2-bis(diisopropylphosphino)ethane) as a catalytic precursor in combination with Et$_3$B to give silyl formate (Et$_3$SiOC(O)H) in high yields (85–89%) at 80 °C for 1 h [110]. Ninety-five percent of Et$_3$SiH was converted to yield 88% of silyl formate corresponding to a TOF of 87.7 h^{-1}. The proposed two pathways for CO_2 hydrosilylation are depicted in Scheme 2.12. In one pathway, CO_2 coordination to the nickel center gives intermediate **I**. Next, the coordination of Et$_3$B to CO_2 and silane assists a nucleophilic attack of the hydride over CO_2 yielding species **II**. Reductive elimination releases the product Et$_3$SiOOH and regenerates the nickel catalyst. In another pathway, an oxidative addition of Et$_3$SiH over nickel(0) afforded hydride intermediate **I'**. The insertion of the $CO_2 \cdot BEt_3$ adduct into the Ni–H bond generates nickel formate **II**, which releases Et$_3$SiOOH.

Okuda et al. reported triphenylborane (BPh$_3$) as an efficient catalyst in highly polar, aprotic solvents (CH$_3$CN or CH$_3$NO$_2$) for CO_2 hydrosilylation. Under mild conditions (1 bar CO_2, 40 °C), it provided silyl formates with high chemoselectivity (>95%) within 7 h [111]. Okuda et al. proposed a similar mechanism as García's (Scheme 2.13). Weak or dynamic coordination of BPh$_3$ to CO_2 and to the Si–H moiety generates two partially polarized species, respectively. Hydridic H attacks C of CO_2, ultimately resulting in the formate product. Highly polar solvents are supposed to enhance the reaction by stabilizing partially charged species.

Rodríguez and Conejero et al. have prepared platinum complex [Pt(I^{t}Bu′)(I^{t}Bu)] [BAr^F] (63) (BAr^F: tetrakis[(3,5-trifluoromethyl)phenyl]borate) [112]. Although complex 63 is inert in the presence of CO_2, it can be transferred into Pt silyl derivative [Pt(SiHEt$_2$)(I^{t}Bu)$_2$][BAr^F] (64) and platinum hydride [Pt(H)(I^{t}Bu)$_2$] [BAr^F] (65) with Et$_2$SiH$_2$ (Scheme 2.14). Among these complexes, 63 is proven to be the most efficient for CO_2 hydrosilylation. When catalyst 63 (0.5%) was used with nBuSiH$_3$ under 5 atm of CO_2, silylformate nBuSiH$_2$(OCOH) was almost quantitatively obtained at approximately 15 min at room temperature corresponding to TON and TOF values of 200 and 714 h^{-1}, respectively. The high reactivity and selectivity toward mono-silylformates were attributed to the enhanced electrophilicity of the silicon atom in the silane through its coordination to platinum.
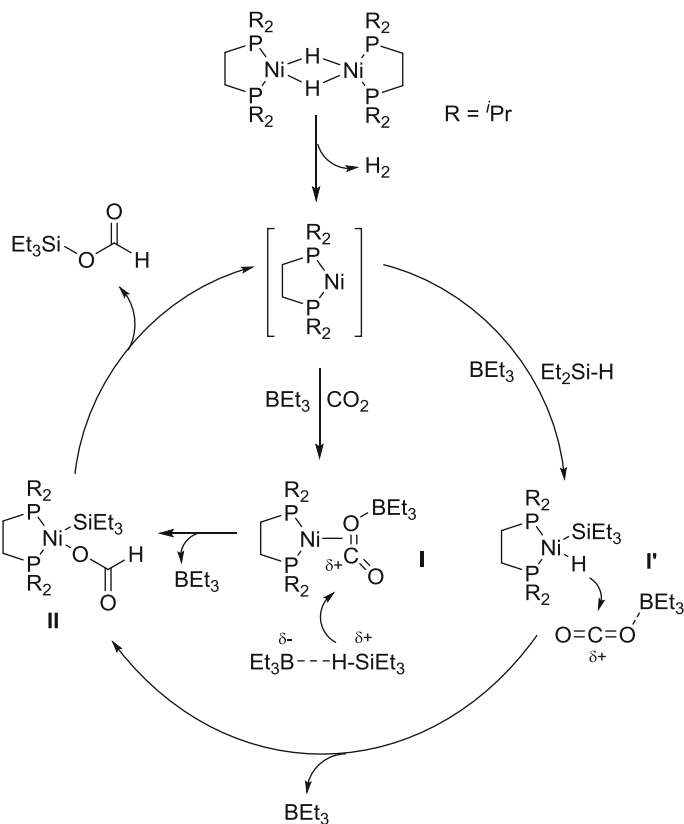
Scheme 2.12 Mechanistic proposal for CO$_2$ hydrosilylation. Reprinted with permission from Ref. [110]. Copyright (2013) American Chemical Society
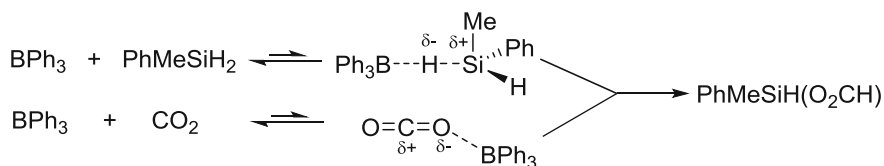
Scheme 2.13 Proposed dual activation mechanism for BPh$_3$-catalyzed CO$_2$ hydrosilylation in highly polar solvents

2.3.2   CO$_2$ Hydroboration

Compared with CO$_2$ hydrosilylation to formate, CO$_2$ hydroboration to formate is less reported because of its low selectivity to formate. Most of the CO$_2$ reductions
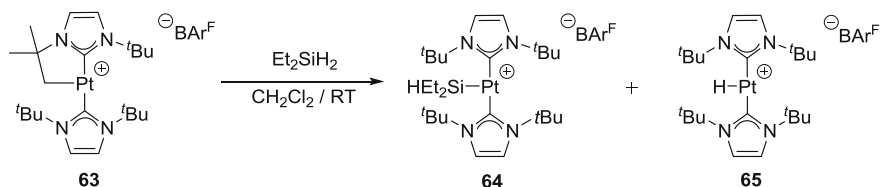
Scheme 2.14 Transformation of **63** to **64** and **65** in the presence of Et_2SiH_2. Redrawn based on Ref. [112]. Copyright (2016) Wiley-VCH GmbH & Co. KGaA, Weinheim

with hydroboranes generated mixtures or methoxyboranes as the end product (see Chap. 4) [113–115].

In 2013, Shintani and Nozaki first developed a copper/*N*-heterocyclic carbene-catalyzed hydroboration of CO_2 under mild conditions to give formic acid selectively [116]. When pinacolborane (HBpin) and catalyst [Cu(O^{t}Bu)(IPr)] (**66**, 10 mol%) were treated with 1 atm CO_2 under 35 °C, single product formic acid was obtained with 85% yield. Based on a series of experiments, the authors proposed a mechanism (Scheme 2.15). The hydroboration of CO_2 initially underwent the reaction of [Cu(O^{t}Bu)(IPr)] with HBpin generating [CuH(IPr)] (**67**). CO_2 insertion to **67** gave [Cu(OCHO)(IPr)] (**68**). Subsequent reaction of [Cu(OCHO)(IPr)] with HBpin was turnover limiting and provided boron formate along with the regeneration of copper hydride. Finally, boron formate afforded formic acid by treatment with aqueous HCl.
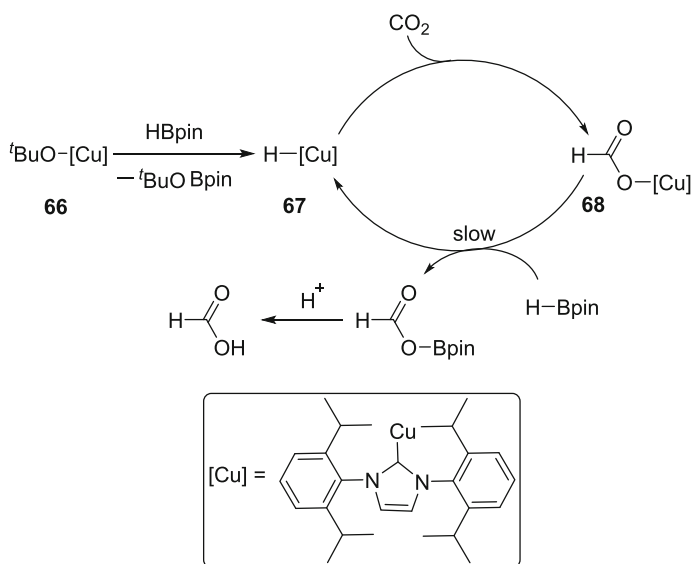
Scheme 2.15 Proposed catalytic cycle for the copper-catalyzed hydroboration of CO_2. Reprinted with permission from Ref. [116]. Copyright (2013) American Chemical Society

$$CO_2 \; + \; HBpin \xrightarrow[C_6D_6, \; rt]{\textbf{69}} \; HCOOBpin$$

TON 63500, TOF 529 h^{-1}, 64% yield
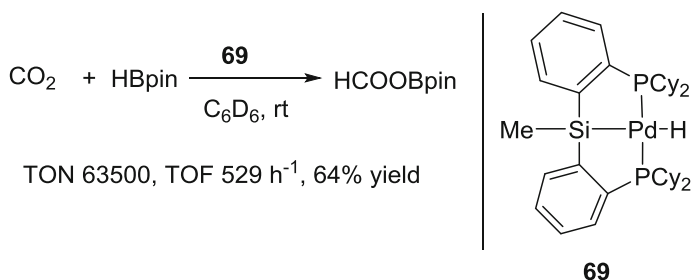
Scheme 2.16 Selective reduction of CO$_2$ with HBpin into formic acid catalyzed by Pd(II) pincer complex **69**

In 2014, Hazari et al. described selective reduction of CO$_2$ with HBpin into formic acid catalyzed by Pd(II) pincer complex **69** (Scheme 2.16) [117]. An excellent TON of 63,500 was obtained in the hydroboration of CO$_2$ under room temperature. The selectivity was ascribed to the bulky steric hindrance of HBpin. The decline in selectivity was observed when HBpin was replaced with less steric hindrance HBcat (catecholborane).

References

1. Inoue Y, Izumida H, Sasaki Y, Hashimoto H (1976) Catalytic fixation of carbon dioxideto formic acid by transition-metal complexes under mild conditions. Chem Lett 5(8):863–864
2. Ezhova NN, Kolesnichenko NV, Bulygin AV, Slivinskii EV, Han S (2002) Hydrogenation of CO$_2$ to formic acid in the presence of the Wilkinson complex. Russ Chem Bull 51 (12):2165–2169. doi:10.1023/A:1022162713837
3. Jessop PG, Ikariya T, Noyori R (1994) Homogeneous catalytic hydrogenation of supercritical carbon dioxide. Nature 368(6468):231–233. doi:10.1038/368231a0
4. Munshi P, Main AD, Linehan JC, Tai CC, Jessop PG (2002) Hydrogenation of carbon dioxide catalyzed by ruthenium trimethylphosphine complexes: The accelerating effect of certain alcohols and amines. J Am Chem Soc 124(27):7963–7971. doi:10.1021/ja0167856
5. Wang W-H, Himeda Y (2012) Recent Advances in transition metal-catalysed homogeneous hydrogenation of carbon dioxide in aqueous media. In: Hydrogenation. InTech, pp 249–268. doi:10.5772/48658
6. Wang W, Wang S, Ma X, Gong J (2011) Recent advances in catalytic hydrogenation of carbon dioxide. Chem Soc Rev 40(7):3703–3727. doi:10.1039/c1cs15008a
7. Leitner W (1995) Carbon dioxide as a raw material: synthesis of formic acid and its derivatives from CO$_2$. Angew Chem Int Ed 34(20):2207–2221. doi:10.1002/anie.199522071
8. Jessop PG, Ikariya T, Noyori R (1995) Homogeneous hydrogenation of carbon-dioxide. Chem Rev 95(2):259–272. doi:10.1021/cr00034a001
9. Leitner W, Dinjus E, Gassner F (1998) CO$_2$ Chemistry. In: Cornils B, Herrmann WA (eds) Aqueous-phase organometallic catalysis, concepts and applications. Wiley-VCH, Weinheim, pp 486–498
10. Jessop PG, Joó F, Tai CC (2004) Recent advances in the homogeneous hydrogenation of carbon dioxide. Coord Chem Rev 248(21–24):2425–2442. doi:10.1016/j.ccr.2004.05.019

11. Jessop PG (2007) Homogeneous hydrogenation of carbon dioxide. In: De Vries JG, Elsevier CJ (eds) Handbook of homogeneous hydrogenation, vol 1. Wiley-VCH, Weinheim, pp 489–511

12. Tanaka R, Yamashita M, Nozaki K (2009) Catalytic hydrogenation of carbon dioxide using Ir(III)-Pincer complexes. J Am Chem Soc 131(40):14168–14169. doi:10.1021/ja903574e

13. Tanaka R, Yamashita M, Chung LW, Morokuma K, Nozaki K (2011) Mechanistic studies on the reversible hydrogenation of carbon dioxide catalyzed by an Ir-PNP complex. Organometallics 30(24):6742–6750. doi:10.1021/om2010172

14. Schmeier TJ, Dobereiner GE, Crabtree RH, Hazari N (2011) Secondary coordination sphere interactions facilitate the insertion step in an Iridium(III) CO$_2$ reduction catalyst. J Am Chem Soc 133(24):9274–9277. doi:10.1021/ja2035514

15. Himeda Y (2007) Conversion of CO$_2$ into formate by homogeneously catalyzed hydrogenation in water: tuning catalytic activity and water solubility through the acid-base equilibrium of the ligand. Eur J Inorg Chem 25:3927–3941. doi:10.1002/ejic.200700494

16. Wang W-H, Hull JF, Muckerman JT, Fujita E, Himeda Y (2012) Second-coordination-sphere and electronic effects enhance iridium(III)-catalyzed homogeneous hydrogenation of carbon dioxide in water near ambient temperature and pressure. Energy Environ Sci 5(7):7923–7926. doi:10.1039/c2ee21888g

17. Himeda Y, Onozawa-Komatsuzaki N, Sugihara H, Kasuga K (2007) Simultaneous tuning of activity and water solubility of complex catalysts by acid-base equilibrium of ligands for conversion of carbon dioxide. Organometallics 26(3):702–712. doi:10.1021/om060899e

18. Hull JF, Himeda Y, Wang W-H, Hashiguchi B, Periana R, Szalda DJ, Muckerman JT, Fujita E (2012) Reversible hydrogen storage using CO$_2$ and a proton-switchable iridium catalyst in aqueous media under mild temperatures and pressures. Nat Chem 4(5):383–388. doi:10.1038/nchem.1295

19. Wang W-H, Muckerman JT, Fujita E, Himeda Y (2013) Mechanistic insight through factors controlling effective hydrogenation of CO$_2$ catalyzed by bioinspired proton-responsive Iridium(III) complexes. ACS Catal 3(5):856–860. doi:10.1021/cs400172j

20. Onishi N, Xu S, Manaka Y, Suna Y, Wang W-H, Muckerman JT, Fujita E, Himeda Y (2015) CO$_2$ hydrogenation catalyzed by iridium complexes with a proton-responsive ligand. Inorg Chem 54(11):5114–5123. doi:10.1021/ic502904q

21. Azua A, Sanz S, Peris E (2011) Water-soluble Ir(III) N-Heterocyclic Carbene based catalysts for the reduction of CO$_2$ to formate by transfer hydrogenation and the deuteration of Aryl Amines in water. Chem-Eur J 17(14):3963–3967. doi:10.1002/chem.201002907

22. Maenaka Y, Suenobu T, Fukuzumi S (2012) Catalytic interconversion between hydrogen and formic acid at ambient temperature and pressure. Energy Environ Sci 5(6):7360–7367. doi:10.1039/c2ee03315a

23. Muller K, Sun Y, Thiel WR (2013) Ruthenium(II) phosphite complexes as catalysts for the hydrogenation of carbon dioxide. ChemCatChem 5(6):1340–1343. doi:10.1002/cctc.201200818

24. Moret S, Dyson PJ, Laurenczy G (2014) Direct synthesis of formic acid from carbon dioxide by hydrogenation in acidic media. Nature Commun 5:4017–4023. doi:10.1038/ncomms5017

25. Lau CP, Chen YZ (1995) Hydrogenation of carbon dioxide to formic acid using a 6,6'-cichloro-2,2'-bipyridine complex of ruthenium, cis-[Ru(6,6'-Cl$_2$bpy)$_2$(H$_2$O)$_2$](CF$_3$SO$_3$)$_2$. J Mol Catal A 101(1):33–36. doi:10.1016/1381-1169(95)00068-2

26. Khan MMT, Halligudi SB, Shukla S (1989) Reduction of CO$_2$ by molecular-hydrogen to formic acid and formaldehyde and their decomposition to CO and H$_2$O. J Mol Catal 57(1):47–60. doi:10.1016/0304-5102(89)80126-9

27. Laurenczy G, Joó F, Nadasdi L (2000) Formation and characterization of water-soluble hydrido-ruthenium(II) complexes of 1,3,5-triaza-7-phosphaadamantane and their catalytic activity in hydrogenation of CO$_2$ and HCO$_3$in aqueous solution. Inorg Chem 39(22):5083–5088. doi:10.1021/ic000200b

28. Elek J, Nadasdi L, Papp G, Laurenczy G, Joó F (2003) Homogeneous hydrogenation of carbon dioxide and bicarbonate in aqueous solution catalyzed by water-soluble ruthenium(II) phosphine complexes. Appl Catal A-Gen 255(1):59–67. doi:10.1016/S0926-860X(03)00644-6

29. Federsel C, Jackstell R, Boddien A, Laurenczy G, Beller M (2010) Ruthenium-catalyzed hydrogenation of bicarbonate in water. Chemsuschem 3(9):1048–1050. doi:10.1002/cssc.201000151

30. Hsu S-F, Rommel S, Eversfield P, Muller K, Klemm E, Thiel WR, Plietker B (2014) A rechargeable hydrogen battery based on Ru catalysis. Angew Chem Int Ed 53(27):7074–7078. doi:10.1002/anie.201310972

31. Filonenko GA, van Putten R, Schulpen EN, Hensen EJM, Pidko EA (2014) Highly efficient reversible hydrogenation of carbon dioxide to formates using a Ruthenium PNP-Pincer catalyst. ChemCatChem 6(6):1526–1530. doi:10.1002/cctc.201402119

32. Huff CA, Sanford MS (2013) Catalytic CO_2 hydrogenation to formate by a Ruthenium Pincer complex. ACS Catal 3(10):2412–2416. doi:10.1021/cs400609u

33. Filonenko GA, Conley MP, Coperet C, Lutz M, Hensen EJM, Pidko EA (2013) The impact of metal-ligand cooperation in hydrogenation of carbon dioxide catalyzed by Ruthenium PNP Pincer. ACS Catal 3(11):2522–2526. doi:10.1021/cs4006869

34. Graf E, Leitner W (1992) Direct formation of formic-acid from carbon-dioxide and dihydrogen using the $[(Rh(Cod)Cl)_2]Ph_2P(CH_2)_4PPh_2$ catalyst system. Chem Commun (8):623–624. doi:10.1039/C39920000623

35. Gassner F, Leitner W (1993) Hydrogenation of carbon dioxide to formic acid using water-soluble rhodium catalyststs. Chem Commun (19):1465–1466. doi:10.1039/C39930001465

36. Zhao G, Joó F (2011) Free formic acid by hydrogenation of carbon dioxide in sodium formate solutions. Catal Commun 14(1):74–76. doi:10.1016/j.catcom.2011.07.017

37. Bays JT, Priyadarshani N, Jeletic MS, Hulley EB, Miller DL, Linehan JC, Shaw WJ (2014) The influence of the second and outer coordination spheres on $Rh(diphosphine)_2$ CO_2 hydrogenation catalysts. ACS Catal 4(10):3663–3670. doi:10.1021/cs5009199

38. Wesselbaum S, Hintermair U, Leitner W (2012) Continuous-flow hydrogenation of carbon dioxide to pure formic acid using an integrated $scCO_2$ process with immobilized catalyst and base. Angew Chem Int Ed 51(34):8585–8588. doi:10.1002/anie.201203185

39. Jantke D, Pardatscher L, Drees M, Cokoja M, Herrmann WA, Kuhn FE (2016) Hydrogen production and storage on a formic acid/bicarbonate platform using water-soluble N-Heterocyclic Carbene complexes of late transition metals. Chemsuschem 9(19):2849–2854. doi:10.1002/cssc.201600861

40. Federsel C, Boddien A, Jackstell R, Jennerjahn R, Dyson PJ, Scopelliti R, Laurenczy G, Beller M (2010) A well-defined iron catalyst for the reduction of bicarbonates and carbon dioxide to formates, alkyl formates, and formamides. Angew Chem Int Ed 49(50):9777–9780. doi:10.1002/anie.201004263

41. Federsel C, Ziebart C, Jackstell R, Baumann W, Beller M (2012) Catalytic hydrogenation of carbon dioxide and bicarbonates with a well-defined cobalt dihydrogen complex. Chem-Eur J 18(1):72–75. doi:10.1002/chem.201101343

42. Langer R, Diskin-Posner Y, Leitus G, Shimon LJW, Ben-David Y, Milstein D (2011) Low-pressure hydrogenation of carbon dioxide catalyzed by an iron pincer complex exhibiting noble metal activity. Angew Chem Int Ed 50(42):9948–9952. doi:10.1002/anie.201104542

43. Jeletic MS, Mock MT, Appel AM, Linehan JC (2013) A cobalt-based catalyst for the hydrogenation of CO_2 under ambient conditions. J Am Chem Soc 135(31):11533–11536. doi:10.1021/ja406601v

44. Spentzos AZ, Barnes CL, Bernskoetter WH (2016) Effective Pincer Cobalt precatalysts for Lewis acid assisted CO$_2$ hydrogenation. Inorg Chem 55(16):8225–8233. doi:10.1021/acs.inorgchem.6b01454

45. Bertini F, Gorgas N, Stöger B, Peruzzini M, Veiros LF, Kirchner K, Gonsalvi L (2016) Efficient and mild carbon dioxide hydrogenation to formate catalyzed by Fe(II) Hydrido Carbonyl complexes bearing 2,6-(Diaminopyridyl)diphosphine Pincer ligands. ACS Catal 6 (5):2889–2893. doi:10.1021/acscatal.6b00416

46. Zhang Y, Williard PG, Bernskoetter WH (2016) Synthesis and characterization of Pincer-Molybdenum precatalysts for CO$_2$ hydrogenation. Organometallics 35(6):860–865. doi:10.1021/acs.organomet.5b00955

47. Jessop PG, Hsiao Y, Ikariya T, Noyori R (1996) Homogeneous catalysis in supercritical fluids: hydrogenation of supercritical carbon dioxide to formic acid, alkyl formates, and formamides. J Am Chem Soc 118(2):344–355. doi:10.1021/ja953097b

48. Joó F, Laurenczy G, Nadasdi L, Elek J (1999) Homogeneous hydrogenation of aqueous hydrogen carbonate to formate under exceedingly mild conditions—a novel possibility of carbon dioxide activation. Chem Commun (11):971–972. doi:10.1039/A902368B

49. Katho A, Opre Z, Laurenczy G, Joó F (2003) Water-soluble analogs of [RuCl$_3$(NO)(PPh$_3$)$_2$] and their catalytic activity in the hydrogenation of carbon dioxide and bicarbonate in aqueous solution. J Mol Catal A-Chem 204:143–148. doi:10.1016/S1381-1169(03)00293-0

50. Kovacs G, Schubert G, Joó F, Papai I (2006) Theoretical investigation of catalytic HCO$_3^-$ hydrogenation in aqueous solutions. Catal Today 115(1):53–60. doi:10.1016/j.cattod.2006.02.018

51. Horvath H, Laurenczy G, Katho A (2004) Water-soluble (η^6-arene)ruthenium(II)-phosphine complexes and their catalytic activity in the hydrogenation of bicarbonate in aqueous solution. J Organometal Chem 689(6):1036–1045. doi:10.1016/j.jorganchem.2003.11.036

52. Erlandsson M, Landaeta VR, Gonsalvi L, Peruzzini M, Phillips AD, Dyson PJ, Laurenczy G (2008) (Pentamethylcyclopentadienyl)iridium-PTA (PTA = 1,3,5-triaza-7-phosphaadamantane) complexes and their application in catalytic water phase carbon dioxide hydrogenation. Eur J Inorg Chem 4:620–627. doi:10.1002/ejic.200700792

53. Laurenczy G, Jedner S, Alessio E, Dyson PJ (2007) In situ NMR characterisation of an intermediate in the catalytic hydrogenation of CO$_2$ and HCO$_3^-$ in aqueous solution. Inorg Chem Commun 10(5):558–562. doi:10.1016/j.inoche.2007.01.020

54. Muller K, Sun Y, Heimermann A, Menges F, Niedner-Schatteburg G, van Wullen C, Thiel WR (2013) Structure-reactivity relationships in the hydrogenation of carbon dioxide with ruthenium complexes bearing pyridinylazolato ligands. Chem-Eur J 19(24):7825–7834. doi:10.1002/chem.201204199

55. Drake JL, Manna CM, Byers JA (2013) Enhanced carbon dioxide hydrogenation facilitated by catalytic quantities of bicarbonate and other inorganic salts. Organometallics 32 (23):6891–6894. doi:10.1021/om401057p

56. Zhang P, Ni SF, Dang L (2016) Steric and electronic effects of bidentate phosphine ligands on ruthenium(II)-catalyzed hydrogenation of carbon dioxide. Chem Asian J 11(18):2528–2536. doi:10.1002/asia.201600611

57. Gunanathan C, Milstein D (2011) Metal-ligand cooperation by aromatization-dearomatization: a new paradigm in bond activation and "Green" catalysis. Acc Chem Res 44(8):588–602. doi:10.1021/ar2000265

58. Zhang J, Leitus G, Ben-David Y, Milstein D (2006) Efficient homogeneous catalytic hydrogenation of esters to alcohols. Angew Chem Int Ed 45(7):1113–1115. doi:10.1002/anie.200503771

59. Praneeth VKK, Ringenberg MR, Ward TR (2012) Redox-active ligands in catalysis. Angew Chem Int Ed 51(41):10228–10234. doi:10.1002/anie.201204100

60. Vogt M, Gargir M, Iron MA, Diskin-Posner Y, Ben-David Y, Milstein D (2012) A new mode of activation of CO$_2$ by metal-ligand cooperation with reversible C–C and M–O bond formation at ambient temperature. Chem-Eur J 18(30):9194–9197. doi:10.1002/chem.201201730

61. Huff CA, Kampf JW, Sanford MS (2012) Role of a noninnocent pincer ligand in the activation of CO_2 at (PNN)Ru(H)(CO). Organometallics 31(13):4643–4645. doi:10.1021/om300403b

62. Filonenko GA, Hensen EJM, Pidko EA (2014) Mechanism of CO_2 hydrogenation to formates by homogeneous Ru-PNP pincer catalyst: from a theoretical description to performance optimization. Catal Sci Technol 4(10):3474–3485. doi:10.1039/c4cy00568f

63. Kothandaraman J, Goeppert A, Czaun M, Olah GA, Surya Prakash GK (2016) CO_2 capture by amines in aqueous media and its subsequent conversion to formate with reusable ruthenium and iron catalysts. Green Chem 18(21):5831–5838. doi:10.1039/c6gc01165a

64. Tsai JC, Nicholas KM (1992) Rhodium-catalyzed hydrogenation of carbon-dioxide to formic acid. J Am Chem Soc 114(13):5117–5124. doi:10.1021/ja00039a024

65. Lilio AM, Reineke MH, Moore CE, Rheingold AL, Takase MK, Kubiak CP (2015) Incorporation of pendant bases into Rh(diphosphine)$_2$ complexes: synthesis, thermodynamic studies, and catalytic CO_2 hydrogenation activity of [Rh(P$_2$N$_2$)$_2$]$^+$ complexes. J Am Chem Soc 137(25):8251–8260. doi:10.1021/jacs.5b04291

66. Yang XZ (2011) Hydrogenation of carbon dioxide catalyzed by pnp pincer iridium, iron, and cobalt complexes: a computational design of base metal catalysts. ACS Catal 1(8):849–854. doi:10.1021/cs2000329

67. Li J, Yoshizawa K (2011) Catalytic hydrogenation of carbon dioxide with a highly active hydride on Ir(III)-Pincer complex: mechanism for CO_2 insertion and nature of metal-hydride bond. Bull Chem Soc Jpn 84(10):1039–1048. doi:10.1246/bcsj.20110128

68. Feller M, Gellrich U, Anaby A, Diskin-Posner Y, Milstein D (2016) Reductive cleavage of CO_2 by metal-ligand-cooperation mediated by an iridium pincer complex. J Am Chem Soc 138(20):6445–6454. doi:10.1021/jacs.6b00202

69. Kang P, Cheng C, Chen Z, Schauer CK, Meyer TJ, Brookhart M (2012) Selective electrocatalytic reduction of CO_2 to formate by water-stable iridium dihydride pincer complexes. J Am Chem Soc 134(12):5500–5503. doi:10.1021/ja300543s

70. Bolinger CM, Sullivan BP, Conrad D, Gilbert JA, Story N, Meyer TJ (1985) Electrocatalytic reduction of CO_2 based on polypyridyl complexes of rhodium and ruthenium. Chem Commun (12):796–797. doi:10.1039/C39850000796

71. Caix C, ChardonNoblat S, Deronzier A (1997) Electrocatalytic reduction of CO_2 into formate with [(η^5-Me$_5$C$_5$)M(L)Cl]$^+$ complexes (L = 2,2'-bipyridine ligands; M = Rh(III) and Ir(III)). J Electroanal Chem 434(1):163–170. doi:10.1016/S0022-0728(97)00058-2

72. Hayashi H, Ogo S, Abura T, Fukuzumi S (2003) Accelerating effect of a proton on the reduction of CO_2 dissolved in water under acidic conditions. Isolation, crystal structure, and reducing ability of a water-soluble ruthenium hydride complex. J Am Chem Soc 125(47):14266–14267. doi:10.1021/ja036117f

73. Wang WH, Himeda Y, Muckerman JT, Manbeck GF, Fujita E (2015) CO_2 Hydrogenation to formate and methanol as an alternative to photo- and electrochemical CO_2 reduction. Chem Rev 115(23):12936–12973. doi:10.1021/acs.chemrev.5b00197

74. Ohnishi YY, Matsunaga T, Nakao Y, Sato H, Sakaki S (2005) Ruthenium(II)-catalyzed hydrogenation of carbon dioxide to formic acid. theoretical study of real catalyst, ligand effects, and solvation effects. J Am Chem Soc 127(11):4021–4032. doi:10.1021/ja043697n

75. Himeda Y, Onozawa-Komatsuzaki N, Sugihara H, Arakawa H, Kasuga K (2004) Half-sandwich complexes with 4,7-dihydroxy-1,10-phenanthroline: water-soluble, highly efficient catalysts for hydrogenation of bicarbonate attributable to the generation of an oxyanion on the catalyst ligand. Organometallics 23(7):1480–1483. doi:10.1021/om030382s

76. Himeda Y, Onozawa-Komatsuzaki N, Sugihara H, Kasuga K (2006) Highly efficient conversion of carbon dioxide catalyzed by half-sandwich complexes with pyridinol ligand: the electronic effect of oxyanion. J Photochem Photobio A 182(3):306–309. doi:10.1016/j.jphotochem.2006.04.025

77. Himeda Y, Miyazawa S, Hirose T (2011) Interconversion between formic acid and H$_2$/CO$_2$ using rhodium and ruthenium catalysts for CO_2 fixation and H$_2$ storage. Chemsuschem 4(4):487–493. doi:10.1002/cssc.201000327

78. Crabtree RH (2011) Multifunctional ligands in transition metal catalysis. New J Chem 35 (1):18–23. doi:10.1039/c0nj00776e

79. Xu S, Onishi N, Tsurusaki A, Manaka Y, Wang W-H, Muckerman JT, Fujita E (2015) Himeda Y (2015) efficient Cp*Ir catalysts with imidazoline ligands for CO$_2$ hydrogenation. Eur J Inorg Chem 34:5591–5594. doi:10.1002/ejic.201501030

80. Shima S, Lyon EJ, Sordel-Klippert MS, Kauss M, Kahnt J, Thauer RK, Steinbach K, Xie XL, Verdier L, Griesinger C (2004) The cofactor of the iron-sulfur cluster free hydrogenase Hmd: structure of the light-inactivation product. Angew Chem Int Ed 43 (19):2547–2551. doi:10.1002/anie.200353763

81. Shima S, Pilak O, Vogt S, Schick M, Stagni MS, Meyer-Klaucke W, Warkentin E, Thauer RK, Ermler U (2008) The crystal structure of Fe-hydrogenase reveals the geometry of the active site. Science 321(5888):572–575. doi:10.1126/science.1158978

82. Shima S, Ermler U (2011) Structure and function of Fe-Hydrogenase and its Iron-Guanylylpyridinol (FeGP) cofactor. Eur J Inorg Chem 7:963–972. doi:10.1002/ejic.201000955

83. Yang X, Hall MB (2009) Monoiron hydrogenase catalysis: hydrogen activation with the formation of a dihydrogen, Fe–H–H–O, bond and methenyl-H4MPT$^+$ triggered hydride transfer. J Am Chem Soc 131(31):10901–10908. doi:10.1021/ja902689n

84. Manaka Y, Wang W-H, Suna Y, Kambayashi H, Muckerman JT, Fujita E, Himeda Y (2014) Efficient H$_2$ generation from formic acid using azole complexes in water. Catal Sci Technol 4(1):34–37. doi:10.1039/c3cy00830d

85. Wang W-H, Xu S, Manaka Y, Suna Y, Kambayashi H, Muckerman JT, Fujita E, Himeda Y (2014) Formic acid dehydrogenation with bioinspired Iridium complexes: a kinetic isotope effect study and mechanistic insight. Chemsuschem 7(7):1976–1983. doi:10.1002/cssc.201301414

86. Suna Y, Ertem MZ, Wang W-H, Kambayashi H, Manaka Y, Muckerman JT, Fujita E, Himeda Y (2014) Positional effects of hydroxy groups on catalytic activity of proton-responsive half-sandwich Cp*Iridium(III) complexes. Organometallics 33(22):6519–6530. doi:10.1021/om500832d

87. Wang L, Onishi N, Murata K, Hirose T, Muckerman JT, Fujita E, Himeda Y (2017) Efficient hydrogen storage and production using a catalyst with an Imidazoline-based, proton-responsive ligand. ChemSusChem 10(6):1071–1075. doi:10.1002/cssc.201601437

88. Sanz S, Benitez M, Peris E (2010) A new approach to the reduction of carbon dioxide: CO$_2$ reduction to formate by transfer hydrogenation in iPrOH. Organometallics 29(1):275–277. doi:10.1021/om900820x

89. Badiei YM, Wang W-H, Hull JF, Szalda DJ, Muckerman JT, Himeda Y, Fujita E (2013) Cp*Co(III) catalysts with proton-responsive ligands for carbon dioxide hydrogenation in aqueous media. Inorg Chem 52(21):12576–12586. doi:10.1021/ic401707u

90. Ziebart C, Federsel C, Anbarasan P, Jackstell R, Baumann W, Spannenberg A, Beller M (2012) Well-defined iron catalyst for improved hydrogenation of carbon dioxide and bicarbonate. J Am Chem Soc 134(51):20701–20704. doi:10.1021/ja307924a

91. Jeletic MS, Helm ML, Hulley EB, Mock MT, Appel AM, Linehan JC (2014) A cobalt hydride catalyst for the hydrogenation of CO$_2$: pathways for catalysis and deactivation. ACS Catal 4(10):3755–3762. doi:10.1021/cs5009927

92. Watari R, Kayaki Y, Hirano S-I, Matsumoto N, Ikariya T (2015) Hydrogenation of carbon dioxide to formate catalyzed by a Copper/1,8-Diazabicyclo[5.4.0]undec-7-ene System. Adv Syn Catal 357(7):1369–1373. doi:10.1002/adsc.201500043

93. Zall CM, Linehan JC, Appel AM (2015) A molecular copper catalyst for hydrogenation of CO$_2$ to formate. ACS Catal 5(9):5301–5305. doi:10.1021/acscatal.5b01646

94. Zall CM, Linehan JC, Appel AM (2016) Triphosphine-Ligated copper hydrides for CO$_2$ hydrogenation: structure, reactivity, and thermodynamic studies. J Am Chem Soc 138 (31):9968–9977. doi:10.1021/jacs.6b05349

95. Rivada-Wheelaghan O, Dauth A, Leitus G, Diskin-Posner Y, Milstein D (2015) Synthesis and reactivity of iron complexes with a new pyrazine-based pincer ligand, and application in

catalytic low-pressure hydrogenation of carbon dioxide. Inorg Chem 54(9):4526–4538. doi:10.1021/acs.inorgchem.5b00366

96. Zhang Y, MacIntosh AD, Wong JL, Bielinski EA, Williard PG, Mercado BQ, Hazari N, Bernskoetter WH (2015) Iron catalyzed CO_2 hydrogenation to formate enhanced by Lewis acid co-catalysts. Chem Sci 6(7):4291–4299. doi:10.1039/c5sc01467k

97. LeBlanc FA, Piers WE, Parvez M (2014) Selective hydrosilation of CO_2 to a bis(silylacetal) using an anilido bipyridyl-ligated organoscandium catalyst. Angew Chem Int Ed 53(3):789–792. doi:10.1002/anie.201309094

98. Deglmann P, Ember E, Hofmann P, Pitter S, Walter O (2007) Experimental and theoretical investigations on the catalytic hydrosilylation of carbon dioxide with ruthenium nitrile complexes. Chem-Eur J 13(10):2864–2879. doi:10.1002/chem.200600396

99. Lalrempuia R, Iglesias M, Polo V, Sanz Miguel PJ, Fernández-Alvarez FJ, Pérez-Torrente JJ, Oro LA (2012) Effective fixation of CO_2 by Iridium-catalyzed hydrosilylation. Angew Chem Int Ed 51(51):12824–12827. doi:10.1002/anie.201206165

100. Jiang Y, Blacque O, Fox T, Berke H (2013) Catalytic CO_2 activation assisted by rhenium hydride/$B(C_6F_5)_3$ frustrated Lewis pairs–metal hydrides functioning as FLP bases. J Am Chem Soc 135(20):7751–7760. doi:10.1021/ja402381d

101. Scheuermann ML, Semproni SP, Pappas I, Chirik PJ (2014) Carbon dioxide hydrosilylation promoted by cobalt pincer complexes. Inorg Chem 53(18):9463–9465. doi:10.1021/ic501901n

102. Itagaki S, Yamaguchi K, Mizuno N (2013) Catalytic synthesis of silyl formates with 1 atm of CO_2 and their utilization for synthesis of formyl compounds and formic acid. J Mol Catal A-Chem 366:347–352. doi:10.1016/j.molcata.2012.10.014

103. Rios P, Curado N, Lopez-Serrano J, Rodriguez A (2016) Selective reduction of carbon dioxide to bis(silyl)acetal catalyzed by a PBP-supported nickel complex. Chem Commun 52 (10):2114–2117. doi:10.1039/C5CC09650B

104. Koinuma H, Kawakami F, Kato H, Hirai H (1981) Hydrosilylation of carbon dioxide catalyzed by ruthenium complexes. Chem Commun (5):213–214. doi:10.1039/C39810000213

105. Jansen A, Gorls H, Pitter S (2000) trans-[(Ru^{II}Cl)(MeCN)$_5$][(Ru^{III}Cl$_4$)(MeCN)$_2$]: a reactive intermediate in the homogeneous catalyzed hydrosilylation of carbon dioxide. Organometallics 19(2):135–138. doi:10.1021/om990654k

106. Jansen A, Pitter S (2004) Homogeneously catalysed reduction of carbon dioxide with silanes: a study on solvent and ligand effects and catalyst recycling. J Mol Catal A-Chem 217(1–2):41–45. doi:10.1016/j.molcata.2004.03.041

107. Motokura K, Kashiwame D, Miyaji A, Baba T (2012) Copper-catalyzed formic acid synthesis from CO_2 with Hydrosilanes and H_2O. Org Lett 14(10):2642–2645. doi:10.1021/ol301034j

108. Motokura K, Kashiwame D, Takahashi N, Miyaji A, Baba T (2013) Highly active and selective catalysis of Copper Diphosphine complexes for the transformation of carbon dioxide into Silyl formate. Chem-Eur J 19(30):10030–10037. doi:10.1002/chem.201300935

109. Zhang L, Cheng J, Hou Z (2013) Highly efficient catalytic hydrosilylation of carbon dioxide by an N-heterocyclic carbene copper catalyst. Chem Commun 49(42):4782–4784. doi:10.1039/c3cc41838c

110. González-Sebastián L, Flores-Alamo M, García JJ (2013) Nickel-catalyzed hydrosilylation of CO_2 in the presence of Et_3B for the synthesis of formic acid and related formates. Organometallics 32(23):7186–7194. doi:10.1021/om400876j

111. Mukherjee D, Sauer DF, Zanardi A, Okuda J (2016) Selective metal-free hydrosilylation of CO_2 catalyzed by Triphenylborane in highly polar, Aprotic solvents. Chem-Eur J 22 (23):7730–7733. doi:10.1002/chem.201601006

112. Rios P, Diez J, Lopez-Serrano J, Rodriguez A, Conejero S (2016) Cationic Platinum(II) sigma-SiH complexes in carbon dioxide hydrosilation. Chem-Eur J 22(47):16791–16795. doi:10.1002/chem.201603524

113. Zeng G, Maeda S, Taketsugu T, Sakaki S (2016) Catalytic hydrogenation of carbon dioxide with Ammonia-Borane by Pincer-type phosphorus compound: a theoretical prediction. J Am Chem Soc 138(41):13481–13484. doi:10.1021/jacs.6b07274
114. Bontemps S, Vendier L, Sabo-Etienne S (2014) Ruthenium-catalyzed reduction of carbon dioxide to formaldehyde. J Am Chem Soc 136(11):4419–4425. doi:10.1021/ja500708w
115. Bontemps S, Vendier L, Sabo-Etienne S (2012) Borane-mediated carbon dioxide reduction at Ruthenium: formation of C$_1$ and C$_2$ compounds. Angew Chem Int Ed 51(7):1671–1674. doi:10.1002/anie.201107352
116. Shintani R, Nozaki K (2013) Copper-catalyzed hydroboration of carbon dioxide. Organometallics 32(8):2459–2462. doi:10.1021/om400175h
117. Suh H-W, Guard LM, Hazari N (2014) A mechanistic study of allene carboxylation with CO$_2$ resulting in the development of a Pd(ii) pincer complex for the catalytic hydroboration of CO$_2$. Chem Sci 5(10):3859–3872. doi:10.1039/c4sc01110d

Chapter 3
Transformation of CO_2 to Formic Acid or Formate Over Heterogeneous Catalysts

Abstract Although heterogeneously catalytic CO_2 hydrogenation to formate was discovered 100 years ago, only recently important progress has been achieved. This chapter covers the most recent reported heterogeneous catalysts using Ni, Pd, Ru, Ir, and Au. The catalyst design and catalytic performance are described. Traditional supports such as carbon, alumina, silica, and titania are widely used. Cooperative effect of metals and supports is one important factor for the design of effective catalyst. Novel catalysts based on nanoporous material or nanoparticle and covalent framework are attractive due to their high activity.

Keywords CO_2 hydrogenation · Heterogeneous catalyst
Formic acid · Formate · Immobilization · Support

Heterogeneous catalysts can be reused repeatedly because they can be easily separated from the reaction mixture by simple filtration. They are environmentally benign and can be easily operated in continuous processes. In addition, the use of heterogeneous catalysts in molecule transformation makes the product separation easier. In 1914, heterogeneous CO_2 hydrogenation to formate was first observed [1]. However, using heterogeneous catalysts for formate or formic acid (FA) synthesis from CO_2 have only recently attracted renewed attention [2], although many kinds of heterogeneous catalysts were prepared and used to reduce CO_2 to formic acid during the past decades. In this chapter, we introduce the most recent progress of CO_2 transformation to formic acid with heterogeneous catalysts. It is classified according to different metal catalysts applied.

3.1 Nickel-Based Catalyst

The synthesis of FA from carbon dioxide with a heterogeneous catalyst was reported in 1935 by Farlow and Adkins [3]. The reaction was carried out using Raney® nickel as catalyst in the presence various amines and under 200–400 atm overall hydrogen pressure and 80–150 °C. In addition, amine was added to shift the thermodynamic equilibrium toward product formation (Eq. 3.1).

$$CO_2 + H_2 \xrightarrow[\text{EtOH, 1-Ph-2-aminopropanol}]{\text{Raney nickel, 80 °C, 1 h}} HCOOH \bullet Base \quad (3.1)$$

6 MPa   14 MPa   55% yield
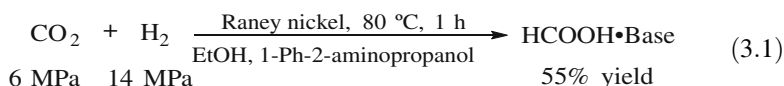
In 2006, Takahashi et al. studied the reduction of CO_2 through a hydrothermal method to explore the selective formation of organic compounds [4]. They were able to form FA selectively at 300 °C when K_2CO_3 was employed as a CO_2 source in the presence of Fe-powder, Ni-powder, and water (Eq. 3.2).

$$HCO_3^- + H_2O \xrightarrow[\text{300 °C, 6 h}]{\text{Ni-powder, Fe-powder}} HCO_2^- \quad (3.2)$$
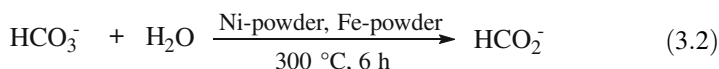
In 2016, Huo et al. reported the unsupported hydrogenation of carbonates to FA in aqueous phase for the first time [5]. The hydrogenation was catalyzed by nanoporous nickel (NiNPore), which was found to exhibit significant catalytic activity during the reduction of $NaHCO_3$. FA was obtained in 86.6% yield with turnover frequency (TOF) of 1738 h^{-1} and turnover number (TON) of 3476 in the presence of 22 mol% catalyst under 6 MPa hydrogen pressure in an aqueous phase at 200 °C for 2 h (Eq. 3.3). Interestingly, they found that extending the scope of the feedstock enables the $KHCO_3$ to afford a 92% FA yield, which is higher than that of $NaHCO_3$. The hydrogen pressures and pKa values of the carbonates had a significant influence on the formation of formic acid. The NiNPore catalyst was easily recovered and could be recycled at least five times without loss of catalytic activity.

$$CO_3^{2-}/HCO_3^- + H_2 \xrightarrow[\text{200 °C, 2 h, } H_2O]{\text{Cat. NiNPore}} HCOOH \quad (3.3)$$
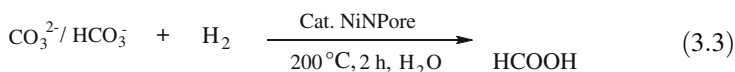
In 2016, Zhao et al. developed another nickel-based catalyst $Ni–P/Al_2O_3$ for the reduction of CO_2 into HCO_2^- by using $NaBH_4$ as hydrogen source [6]. The optimum preparation conditions for the $Ni–P/Al_2O_3$ catalyst were Ni to P ratio of 1:1, impregnation time of 12 h, and calcination temperature of 550 °C. The $Ni–P/Al_2O_3$ catalyst obtained was used in industrial applications involving CO_2 reduction, and 41.37% of the average efficiency of CO_2 reduction was achieved under optimal conditions (addition amount of $Ni–P/Al_2O_3$ of 1%, $NaBH_4$ concentration of 0.175 mol L^{-1}, reaction temperature of 55 °C, pH of 8.0, ethanol concentration of 90%, and residence time of 15 s). Ni_2P species distributed evenly on the $Ni–P/Al_2O_3$ catalyst were the active components for the reduction of CO_2 into HCO_2^-. These components were determined by scanning electron microscopy (SEM) and X-ray diffraction (XRD) analysis. Through the hydrogenation of Ni_2P, an increasing amount of boron substances of $BH_i(OH)_{4-i}^{-1}$ (i = 4, 3, 2, 1) and

$HCO_2BH_j(OH)_{3-j}^{-1}$ (j = 3, 2, 1, 0) was generated, and CO_2 reduction by $NaBH_4$ was promoted.

3.2 Palladium-Based Catalyst

In 1982, Klibanov et al. have found that palladium adsorbed on activated carbon (Pd/C) not only can be used as a catalyst for FA decomposition but also can be used as a catalyst for the synthesis of formate from H_2 and bicarbonate (Eq. 3.4) [7]. They were able to obtain 13 mM of formate by shaking 100 mg of catalyst in 5 mL of 0.3 M sodium bicarbonate for 20 h and under 1 atm of H_2 and room temperature. The heterogeneous catalysts Pd/C, Pd/γ-Al_2O_3, Pd/$BaSO_4$, and [W/($PQ^{2+/+/0}$)$_n$/Pd] (a polymer-supported palladium catalyst) were then investigated by Wrighton et al. [8]. The Pd-based catalysts equilibrated the H_2/$NaCO_3H$(aq)/$NaHCO_2$(aq) system at 298 K to a formate to bicarbonate ratios of ~1:1 to ~1.5:1 under 1–1.7 atm of H_2. Owing to the chemical equilibrium between carbonate and formate, the reaction was incomplete. Similar observation was also reported by Feilchenfeld et al. [9]. They were able to reduce alkali metal bicarbonates to their respective formate salts over a Pd/C catalyst under mild temperature and pressure conditions. A strong influence of carbonate and hydrogen concentration on the initial reaction rates was then observed. The rate increased at elevated H_2 pressure in accordance with the Langmuir isotherm law. At increased HCO_3^- concentrations, the rate passed through a maximum. Measurements of the equilibrium at 35 °C indicated a Gibbs free energy change of approximately −2.2 kcal/mole. The highest concentration of HCO_2^- obtainable at 6 atm H_2 was limited by the common ion effect to 5.8 M.

$$HCO_3^- + H_2 \xrightarrow[\text{1 atm}]{\text{Pd/C} \atop \text{298 K}} HCO_2^- + H_2O \qquad (3.4)$$
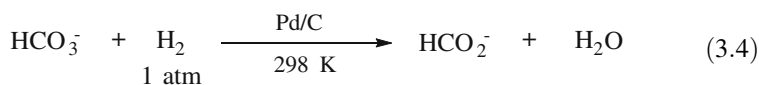
In 2015, Lin et al. systematically studied the hydrogenation of CO_2-derived ammonium carbamates/carbonates at room temperature [10]. A high yield of formate (~92%) was achieved after hydrogenating ammonium carbamate in 70 wt% ethanol–water solution at room temperature with carbon-supported palladium nano-catalyst (Pd/AC) and 2.75 MPa of H_2 (Eq. 3.5). The solvent effect on the distribution of the reactive intermediates was analyzed by ^{13}C NMR spectroscopy. The results indicated that ethyl carbonate ions were formed by dissolving either ammonium carbamate or ammonium carbonate in ethanol. Ammonium ions promote the formation of ethyl carbonate ions in the presence of ethanol, which can be readily converted to formates through hydrogenation over the Pd/AC catalyst. These findings may open a new avenue for sustainable carbon recycling.

$$NH_2CO_2NH_4 \; + \; H_2 \; \xrightarrow[\text{70 wt\% ethnol-water}]{\text{Pd/AC, 20 °C, 8 h}} \; HCOONEt_4 \; + \; NH_3 \quad (3.5)$$

2.75MPa   92% yield
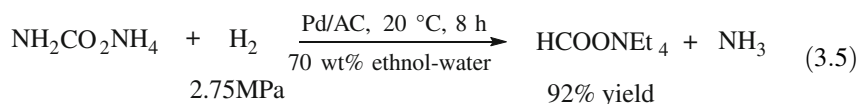
3.3   Ruthenium-Based Catalyst

In 2004, Zheng et al. reported the preparation and application of amine-functionalized silica-immobilized ruthenium catalysts for the hydrogenation of CO_2 to FA for the first time [11]. The heterogeneous catalyst Si–$(CH_2)_3$–NH $(CH_2)_3CH_3$–Ru exhibited higher catalytic activity than homogeneous catalysts. FA was obtained with TOF of 1384 h^{-1} and selectivity of 100% when the hydrogenation reaction of CO_2 with H_2 was performed in ethanol under 16.0 MPa and in the presence of PPh_3 and NEt_3 at 80 °C for 1 h (Eq. 3.6). Subsequently, they investigated the effect of CO_2 pressure on the hydrogenation reaction. A TOF of 1482 h^{-1} for HCOOH generation was achieved on immobilized ruthenium catalyst [Si–$(CH_2)_3$–NH_2–Ru] under scCO_2 with H_2 pressure of 4.0 MPa at reaction temperature of 80 °C, PPh_3/Ru molar ratio of 6:1, and stirring speed of 750 r/min [12].

$$CO_2 \; + \; H_2 \; \xrightarrow[\text{80 °C, ethanol}]{\text{NEt}_3, \text{Cat.}, \text{PPh}_3} \; HCOOH/NEt_3$$

12 MPa   4.0 MPa

TOF $=$ 1384 h^{-1} (3.6)

100% selectivity

Cat. $=$ Si-$(CH_2)_3$-NH$(NH_2)_3CH_3$-Ru
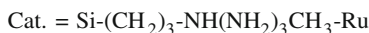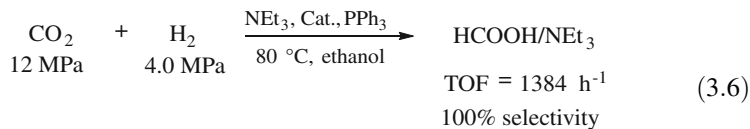
In 2008, Han et al. demonstrated the first use of an ionic liquid (IL) as a base in the silica-immobilized-ruthenium-complex-catalyzed hydrogenation of CO_2 to FA (Eq. 3.7) [13]. The HCOOH had a TOF of 103 h^{-1} on the immobilized ruthenium catalyst [Si–$(CH_2)_3$–NH$(CSCH_3)$–$RuCl_3$–PPh_3] under a total pressure of 18 bar (H_2:CO_2 = 1:1) at reaction temperature of 60 °C in the IL 1-(N,N-dimethylaminoethyl)-2,3-dimethylimidazolium trifluoromethane-sulfonate ([mammim][TfO]) aqueous solution. And then, they designed and prepared a novel IL 1,3-di(N,N-dimethylaminoethyl)-2-methylimidazolium ([DAMI][TFO]) for CO_2 hydrogenation promoted by ruthenium heterogeneous catalysts, which they used to improve the reaction efficiency. A maximum TOF of 920 h^{-1} was achieved in the presence of [DAMI][TFO] at 80 °C under H_2 pressure of 9.0 MPa [14]. The molar ratio of formic acid formed to the IL used can reach 2:1 (0.246:1 w/w) in one reaction cycle. The unique feature of this approach is that the formic acid can be recovered easily, and the IL and catalyst can be both reused after a simple separation process.

$$CO_2 + H_2 \xrightarrow[\text{60 °C, water}]{\text{IL, Cat.,}} HCOOH$$

9.0 MPa 9.0 MPa

Cat. = Si-$(CH_2)_3$-NH$(CSCH_3)_3$-$RuCl_3$-PPh_3

$$(3.7)$$

IL =

[mammim][TfO] or [DAMI][TfO]
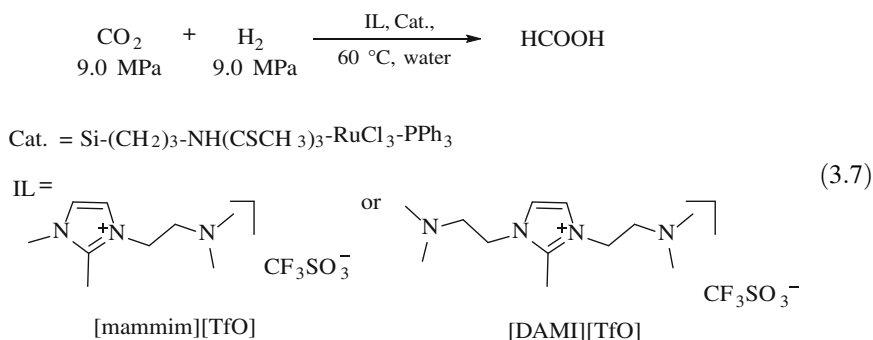
In 2016, Wang et al. synthesized a novel heterogeneous Ru–DBU/Al_2O_3 catalyst (DBU: 1,8-diazabicyclo[5.4.0]undec-7-ene) for the hydrogenation of CO_2 to formic acid [15]. They then characterized the Ru–DBU/Al_2O_3 by a combination of FTIR, XRD, and XPS and found that an amorphous Ru(III)–DBU species was formed. A maximum TOF of 239 h^{-1} was achieved at 80 °C in a highly polar solvent DMSO in the presence of NEt_3 and KH_2PO_4 as Lewis organic base and protonic additive, respectively (Eq. 3.8). The polar solvent improved the productivity of formic acid by promoting the insertion of CO_2 into the Ru–H bond. The CO_2 insertion is the rate-determining step of CO_2 hydrogenation.

$$CO_2 + H_2 \xrightarrow[\substack{\text{80 °C, DMSO} \\ KHCO_3}]{\text{Ru-DBU/Al}_2\text{O}_3} HCOOH$$

9.0 MPa 6.0 MPa

$$(3.8)$$
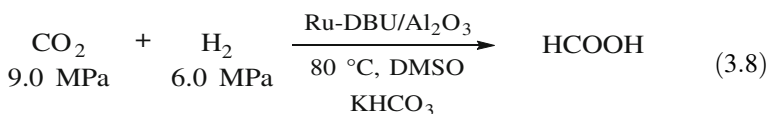
Recently, Srivastava successfully synthesized air- and moisture-stable Ru/SiO_2 and Ru/MCM-41 catalysts for the selective hydrogenation of CO_2 to FA [16]. The physiochemical properties of the catalysts were examined through sophisticated analytical techniques, such as N_2 physisorption (BET/BJH methods), XRD, temperature-programmed reduction analysis, H_2 chemisorption, ICP-MS, etc. In the synthesized catalysts, the Ru/MCM-41 catalyst was found to be highly active in terms of FA quantity (TON/TOF). To improve solubility of CO_2 and absorption of FA produced during the reaction, they synthesized and screened a series of functionalized ILs. They determined that [DAMI][$CF_3CF_2CF_2CF_2SO_3$] IL is a promising reaction medium that can accommodate CO_2 at high concentrations. The highest TON value of 17787 for FA was reached using Ru/MCM-41 in a [DAMI][$CF_3CF_2CF_2CF_2SO_3$] medium (Eq. 3.9). Catalyst recycling test indicated that the TON was decreased slightly after 10 cycles.

$$CO_2 \quad + \quad H_2 \quad \xrightarrow[\substack{80\ °C,\ \text{solvent system} \\ NEt_3}]{\text{Ru/Silica or Ru/MCM-41}} \quad HCOOH$$

$$20\ \text{bar} \qquad 20\ \text{bar} \hspace{10em} (3.9)$$
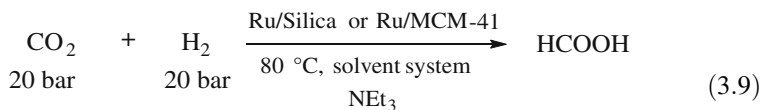
solvent system: $[DAMI][CF_3CF_2CF_2CF_2SO_3] + H_2O$

3.4 Iridium-Based Catalyst

In 2013, Hicks et al. reported that mesoporous silica-tethered iridium complex Ir-PN/SBA-15 (Fig. 3.1) can be used as an effective catalyst for the synthesis of FA through CO$_2$ hydrogenation in aqueous solution in the presence of NEt$_3$ and under mild conditions [60 °C, 4.0 MPa total pressure (H$_2$/CO$_2$ = 1:1)] [17]. The highest activity (1.2 × 10^3 h^{-1}) of the catalyst was obtained at 120 °C, 4.0 MPa, and 2 h. The catalyst was highly recyclable and retained activity even after 10 cycles. In 2014, Hicks et al. developed a new catalyst (PEI-PN/Ir) by modifying a branched polyethyleneimine (PEI) with an iminophosphine ligand coordinated to an Ir pre-catalyst (Fig. 3.1) [18]. By tuning the structure of the PEI-tethered materials, they
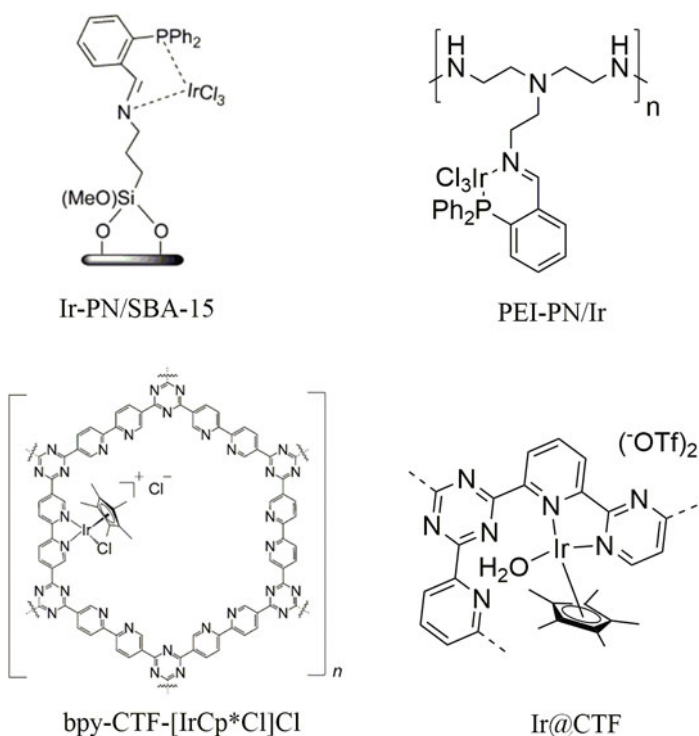
Fig. 3.1 Heterogeneous catalysts used in CO$_2$ hydrogenation to formate

were able to optimize CO_2 capture and the conversion abilities of these materials. Converting 65% of the available primary amines on PEI to PN/Ir active sites yielded the optimal balance between CO_2 capture and conversion, thereby achieving the highest formic acid yields.

In 2015, Yoon et al. developed a novel heterogeneous catalyst (bpy-CTF-[IrCp*Cl]Cl) by immobilizing a {IrCp*} unit onto a covalent triazine framework through coordination bonding (Fig. 3.1) [19]. This catalyst exhibited excellent activities for the hydrogenation of CO_2 to formate in aqueous solution under mild conditions [120 °C, 8 MPa total pressure ($H_2/CO_2 = 1$)]. TON of 5000 and an initial TOF of 5300 h^{-1} were reached, which are the highest values reported to date for a heterogeneous catalytic system for CO_2 hydrogenation.

In 2016, Bavykina et al. developed a new stable heterogeneous catalyst by immobilizing IrCp* through coordination within the covalent triazine framework (CTF) spheres [20]. They found that the shaped catalysts, Ir@CTF spheres (Fig. 3.1), are active and fully recyclable during the direct hydrogenation of CO_2 into FA under mild reaction conditions (20 bar and 50–90 °C). The highest TON (219) was reached at 90 °C under 20 bar H_2/CO_2 (1/1). However, this TON is lower than that of Ir@meso-CTF catalyst (powder solids). Nevertheless, the Ir@CTF sphere catalysts are easy to handle and recycle during the hydrogenation of CO_2 to FA.

3.5 Gold-Based Catalyst

In 2011, Fachinetti et al. prepared a highly stable and robust titania-supported gold (Au/TiO_2) for the formation of $HCOOH/NEt_3$ adducts through the hydrogenation of CO_2 in the presence of neat NEt_3 (Eq. 3.10) [21]. To recover HCOOH, they exploited an amine-exchange method, in which high-boiling tri-n-hexylamine was added to $HCOOH/NEt_3$ adduct with acid/amine molar ratio (AAR) of 1.715 in a $HCOOH/(n\text{-}C_6H_{13})_3N$ molar ratio of 2. A biphasic system was obtained and fractionated under reduced pressure (90 mmHg), and a liquid fraction consisting of pure NEt_3 (90% yield) was collected. At increased temperatures, a fraction consisting of 85 wt% HCOOH contaminated by NEt_3 (11.5 wt%) and (n-C_6H_{13})$_3$N (3.5 wt%) was recovered. Furthermore, pure anhydrous HCOOH was obtained by redistilling the high-boiling fraction at atmospheric pressure. Overall, HCOOH was recovered from the $HCOOH/NEt_3$ adduct with AAR of 1.715 in 83% yield.

$$CO_2 + H_2 \xrightarrow[40\,°C]{NEt_3,\ Au/TiO_2} HCOOH/NEt_3 \qquad (3.10)$$
$$_{90\ bar}\ \ _{90\ bar}$$
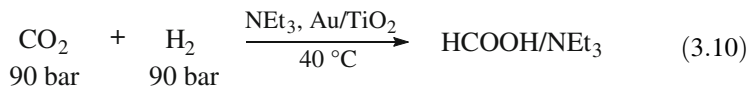
In 2016, Hensen et al. investigated the hydrogenation of CO_2 to FA by using a number of unsupported and supported gold nanoparticle catalysts (Eq. 3.11) [22]. Among the examined catalysts, Au/Al_2O_3 was the most active catalyst. The

catalytic activity depended strongly on the type of support. For example, TON of 110 was obtained using Au/TiO_2 as catalyst for CO_2 dehydrogenation, whereas nearly a twofold increase in TON (215) was observed when Au/Al_2O_3 was employed as catalyst under the same reaction conditions (3 mL EtOH, 0.5 mL NEt_3, 70 °C, 40 bar H_2/CO_2, 20 h). The rate of formate formation, normalized per Au surface atom, was in the range of 118–123 h^{-1}.

$$CO_2 \ + \ H_2 \ \xrightarrow[\text{Base, Ethanol}]{Au/Al_2O_3, \ 70°C} \ \text{Base/HCOOH} \tag{3.11}$$

$$\text{20 bar} \qquad \text{20 bar}$$
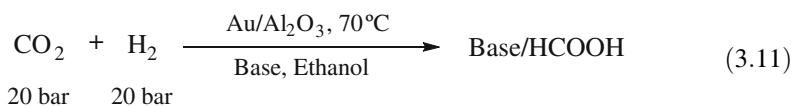
Based on the experimental results, the authors proposed that the reaction occurs at the interface of the Au^0 nanoparticles and alumina support (Fig. 3.2). They also concluded that H_2 heterolytic dissociation occurs at the Au/support interface and then generates surface hydroxyl group and metal hydride. The reaction of surface OH with CO_2 affords bicarbonate, which can be reduced by hydride to produce formate. The key intermediates, surface formate, and bicarbonate were observed by FTIR. This study demonstrated the significant cooperative effect of metals and supports.
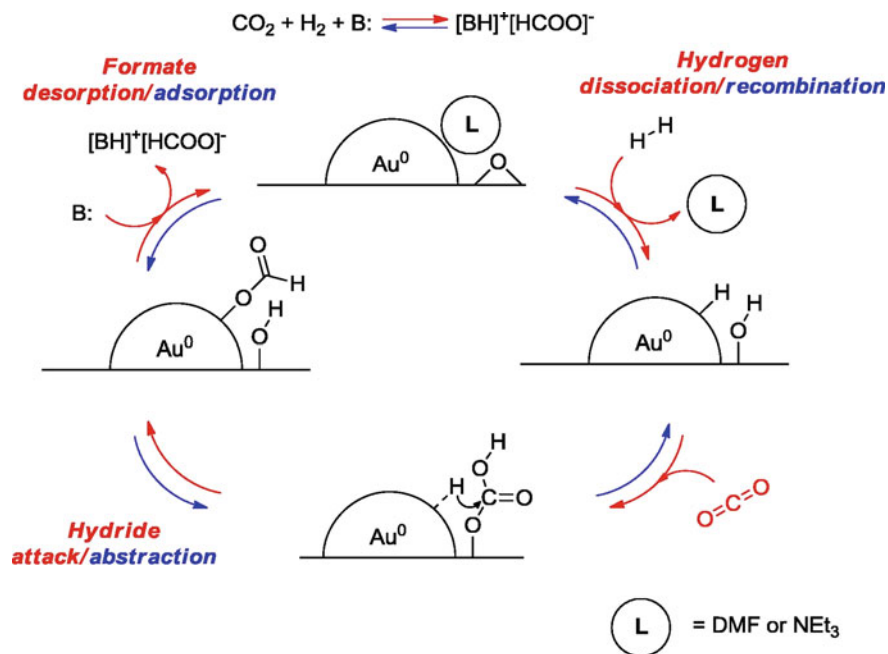
Fig. 3.2 Proposed mechanism for CO_2 hydrogenation over Au/Al_2O_3 catalyst. Reprinted from Ref. [22], Copyright 2015, with permission from Elsevier

References

1. Bredig G, Carter SR (1914) Katalytische Synthese der Ameisensäure unter Druck. Ber Dtsch Chem Ges 47(1):541–545. doi:10.1002/cber.19140470188
2. Gunasekar GH, Park K, Jung K-D, Yoon S (2016) Recent developments in the catalytic hydrogenation of CO_2 to formic acid/formate using heterogeneous catalysts. Inorg Chem Front 3(7):882–895. doi:10.1039/c5qi00231a
3. Farlow MW, Adkins H (1935) The hydrogenation of carbon dioxide and a correction of the reported synthesis of urethans. J Am Chem Soc 57(11):2222–2223
4. Takahashi H, Liu LH, Yashiro Y, Ioku K, Bignall G, Yamasaki N, Kori T (2006) CO_2 reduction using hydrothermal method for the selective formation of organic compounds. J Mater Sci 41(5):1585–1589. doi:10.1007/s10853-006-4649-5
5. Wang T, Ren D, Huo Z, Song Z, Jin F, Chen M, Chen L (2017) A nanoporous nickel catalyst for selective hydrogenation of carbonates into formic acid in water. Green Chem 19(3):716–721. doi:10.1039/c6gc02866g
6. Zhao Y, Zhang Z, Zhao X, Hao R (2016) Catalytic reduction of carbon dioxide by nickel-based catalyst under atmospheric pressure. Chem Eng J 297:11–18. doi:10.1016/j.cej.2016.03.108
7. Klibanov AM, Alberti BN, Zale SE (1982) Enzymatic synthesis of formic acid from H_2 and CO_2 and production of hydrogen from formic acid. Biotechnol Bioeng 24(1):25–36. doi:10.1002/bit.260240104
8. Stalder CJ, Chao S, Summers DP, Wrighton MS (1983) Supported palladium catalysts for the reduction of sodium bicarbonate to sodium formate in aqueous solution at room temperature and one atmosphere of hydrogen. J Am Chem Soc 105(20):6318–6320. doi:10.1021/ja00358a026
9. Wiener H (1988) The heterogeneous catalytic hydrogenation of bicarbonate to formate in aqueous solutions. J Catal 110(1):184–190. doi:10.1016/0021-9517(88)90308-9
10. Su J, Lu M, Lin H (2015) High yield production of formate by hydrogenating CO_2 derived ammonium carbamate/carbonate at room temperature. Green Chem 17(5):2769–2773. doi:10.1039/c5gc00397k
11. Zhang Y, Fei J, Yu Y, Zheng X (2004) Silica immobilized ruthenium catalyst used for carbon dioxide hydrogenation to formic acid (I): the effect of functionalizing group and additive on the catalyst performance. Catal Commun 5(10):643–646. doi:10.1016/j.catcom.2004.08.001
12. Yu Y-M, Zhang Y-P, Fei J-H, Zheng X-M (2005) Silica immobilized ruthenium catalyst for formic acid synthesis from supercritical carbon dioxide hydrogenation ii: effect of reaction conditions on the catalyst performance. Chin J Chem 23(8):977–982. doi:10.1002/cjoc.200590977
13. Zhang Z, Xie Y, Li W, Hu S, Song J, Jiang T, Han B (2008) Hydrogenation of carbon dioxide is promoted by a task-specific ionic liquid. Angew Chem Int Ed 47(6):1127–1129. doi:10.1002/anie.200704487
14. Zhang Z, Hu S, Song J, Li W, Yang G, Han B (2009) Hydrogenation of CO_2 to formic acid promoted by a diamine-functionalized ionic liquid. Chemsuschem 2(3):234–238. doi:10.1002/cssc.200800252
15. Zhang W, Wang S, Zhao Y, Ma X (2016) Hydrogenation of $scCO_2$ to formic acid catalyzed by heterogeneous ruthenium(III)/Al_2O_3 catalysts. Chem Lett 45(5):555–557. doi:10.1246/cl.160013
16. Srivastava V (2016) Active heterogeneous Ru nanocatalysts for CO_2 hydrogenation reaction. Catal Lett 146(12):2630–2640. doi:10.1007/s10562-016-1882-7
17. Xu Z, McNamara ND, Neumann GT, Schneider WF, Hicks JC (2013) Catalytic hydrogenation of CO_2 to formic acid with silica-tethered iridium catalysts. ChemCatChem 5(7):1769–1771. doi:10.1002/cctc.201200839

18. McNamara ND, Hicks JC (2014) CO$_2$ capture and conversion with a multifunctional polyethyleneimine-tethered iminophosphine iridium catalyst/adsorbent. Chemsuschem 7 (4):1114–1124. doi:10.1002/cssc.201301231
19. Park K, Gunasekar GH, Prakash N, Jung KD, Yoon S (2015) A highly efficient heterogenized iridium complex for the catalytic hydrogenation of carbon dioxide to formate. Chemsuschem 8(20):3410–3413. doi:10.1002/cssc.201500436
20. Bavykina AV, Rozhko E, Goesten MG, Wezendonk T, Seoane B, Kapteijn F, Makkee M, Gascon J (2016) Shaping covalent triazine frameworks for the hydrogenation of carbon dioxide to formic acid. ChemCatChem 8(13):2217–2221. doi:10.1002/cctc.201600419
21. Preti D, Resta C, Squarcialupi S, Fachinetti G (2011) Carbon dioxide hydrogenation to formic acid by using a heterogeneous gold catalyst. Angew Chem Int Ed 50(52):12551–12554. doi:10.1002/anie.201105481
22. Filonenko GA, Vrijburg WL, Hensen EJM, Pidko EA (2016) On the activity of supported Au catalysts in the liquid phase hydrogenation of CO$_2$ to formates. J Catal 343:97–105. doi:10.1016/j.jcat.2015.10.002

Chapter 4
Transformation of CO_2 to Methanol with Homogeneous Catalysts

Abstract Homogeneous hydrogenation of carbon dioxide to methanol is highly challenging. Only a few examples using hydrogen as reductant have been reported. Considerable studies employ borane or silane as a reductant. Although these hydrogen sources are expensive, these studies have achieved higher outcomes and are helpful to understand the mechanism of CO_2 reduction. Indirect ways such as catalytic disproportionation of formic acid to methanol and cascade catalysis are also introduced.
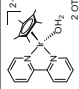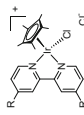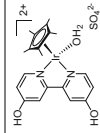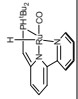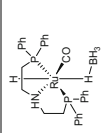
Methanol is an important starting material for the chemical industry. It can be used to produce a variety of chemicals including formaldehyde, methyl *t*-butyl ether, and acetic acid. Moreover, it is an alternative fuel and suitable for internal combustion engine because of its high octane number [1]. The industrial production of methanol is from syngas (CO/H_2) using heterogeneous catalysts at high temperature (200–300 °C) and high pressure (5–20 MPa, Eq. 4.1). Using CO_2 as a feedstock instead of CO attracted increasing attention since it contributes greatly to carbon recycling in methanol economy. The reaction using CO_2 is thermodynamically favorable than using CO due to the generation of H_2O. Meanwhile more H_2 is consumed. But this reaction is meaningful if H_2 is stemmed from renewables.

$$CO + 2H_2 \rightleftharpoons CH_3OH \qquad \Delta H_{298k,5MPa} = -90.7\,\text{kJ mol}^{-1} \qquad (4.1)$$

$$CO_2 + 3H_2 \rightleftharpoons CH_3OH + H_2O \qquad \Delta H_{298k,5MPa} = -40.9\,\text{kJ mol}^{-1} \qquad (4.2)$$
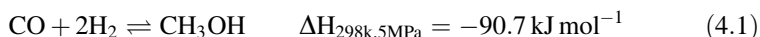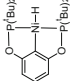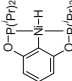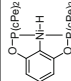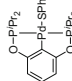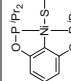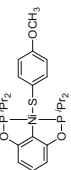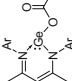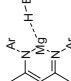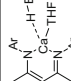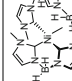
Homogeneous catalytic hydrogenation of CO_2 to generate methanol is rather difficult. Most of the CO_2 hydrogenation to methanol is performed using heterogeneous catalysts as discussed in Chap. 5. However, significant progress has been achieved recently either using metal complexes or organocatalysts. The most important results are summarized in Table 4.1.

Table 4.1 Transformation of CO_2 to methanol or methoxide

Catalyst precursor	Solvent	Additive	T/°C	Reaction time/h	TON[c]	TOF[c]/h^{-1}	Yield/%	References
Formic acid disproportionation								
	D_2O	–	80	24	156	6.5	7[a]	[2]
	THF	MSA	150	1	–	–	50.2	[3]
	H_2O	–	60	21	–	0.91 ± 0.04	1.17 ± 0.30[a]	[4]
	D_2O	H_2SO_4	50	72	–	–	96 ± 1[a]	[5]
	CD_3CN	$iPr_2Et_3NH^+$	130	4.5	–	–	50	[6]
Cascade hydrogenation								
	Dioxane, CH_3OH	NEt_3	135	16	21	–	–	[7]
CO_2 reduction								
	THF	$HNTf_2$	140	24	442	–	–	[8, 9]
	THF	Pentaethylenehexamine	95–155	18	450	–	–	[10]
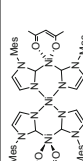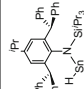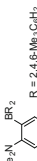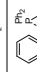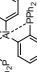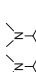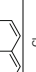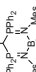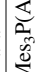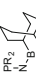
(continued)

Table 4.1 (continued)

Catalyst precursor	Solvent	Additive	T/°C	Reaction time/h	TON[c]	TOF[c]/h^{-1}	Yield/%	References
(structure)	C_6D_6	–	25	1	495	495	–	[11]
(structure)	C_6D_6	–	25	2	100	–	–	[12]
(structure)	C_6D_6	–	25	12	30	–	–	[12]
(structure)	C_6D_6	–	25	0.25–0.42	445	1780	89	[13]
(structure)	C_6D_6	–	25	12	490	2400	99	[14]
(structure)	THF benzene	NH_3BH_3	60 60	2 18	–	–	33–43	[15]
(structure)	THF	–	60	144	10	0.07	–	[16]
(structure)	THF	–	60	96	10	0.1	–	[16]
(structure)	THF	H_2O	25	336	72,000	400	–	[17]
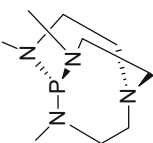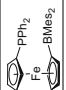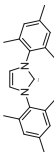
(continued)

Table 4.1 (continued)

Catalyst precursor	Solvent	Additive	T/°C	Reaction time/h	TON[c]	TOF[c]/h⁻¹	Yield/%	References
	THF	H₂O	25	336	143,000	220	–	[17]
	C₆D₆	–	20	0.08	–	1188	–	[18]
	C₆D₆	–	80	216	0.1	–	–	[19]
	C₆D₆	–	70	4	>2950	>737	–	[20]
	C₆D₆	–	60	4	30	–	–	[21]
	C₆D₆	–	80	1	64	64	–	[22]
	C₆D₆	–	80	4	2646	661	–	[23]
Mes₃P(AlX₃)[b]	C₆H₅Br	–	25	0.25	–	–	37–51	[24]
	C₆H₅Br	–	60	11	240	–	–	[25]
	THF	–	25	20	648	31	–	[26]
	CDCl₃	–	25	7	298	42.6	–	[27]

(continued)

Table 4.1 (continued)

Catalyst precursor	Solvent	Additive	T/°C	Reaction time/h	TON[c]	TOF[c]/h^{-1}	Yield/%	References
	THF	–	20	192	6043	33	–	[28]
	d$_8$-THF	–	70	20	1980	99	–	[29]
NaBH$_4$	THF	–	25	12	249	21	87	[30]
	DMF	–	25	24	1840	25.5	–	[31]

[a]Methanol selectivity. [b]Mes = mesityl, X = Cl, Br. [c]Insignificant digits are rounded

4.1 Catalytic Disproportionation of Formic Acid to MeOH

Direct synthesis of methanol from CO$_2$ is highly challenging under homogeneous conditions. Some indirect methods have been reported by catalytic hydrogenation of urea derivatives, alkyl or cyclic carbonates, carbamates, and formats [32, 33]. Compared to the above-mentioned compounds, formic acid is relatively easy to obtain from CO$_2$ as described in Chaps. 2 and 3. Therefore, methanol generation from formic acid attracted considerable attention.

In 2013, Miller and Goldberg et al. first reported disproportionation of formic acid to methanol [2]. It is well known that decomposition of FA releases H$_2$ and CO$_2$ by dehydrogenation or generates CO and H$_2$O by dehydration. Their study demonstrated that FA could be converted to MeOH using [Cp*Ir(bpy)(OH$_2$)](OTf)$_2$ as a catalyst in aqueous solution at 80 °C. The thermodynamics of FA disproportionation were estimated using electrochemical standard potentials. They found that disproportionation of FA to formaldehyde (Eq. 4.3) and direct formation of MeOH (Eq. 4.4) are both possible [2].

$$2\,HCO_2H(aq) \rightarrow H_2CO(aq) + H_2O(aq) + CO_2 \quad \Delta G^\circ_{298} = -11.9\,kcal\,mol^{-1}$$
(4.3)

$$3\,HCO_2H(aq) \rightarrow CH_3OH(aq) + H_2O(aq) + 2CO_2(g) \quad \Delta G^\circ_{298} = -23.5\,kcal\,mol^{-1}$$
(4.4)
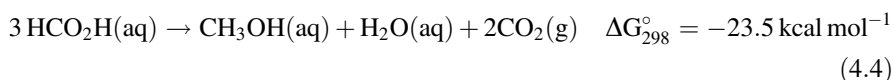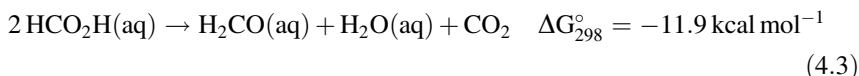
As shown in Scheme 4.1, a mechanism was proposed. Iridium complex reacts with formic acid to give iridium hydride via β-hydride elimination. Reduction of protonated formic acid by Ir-H affords formaldehyde, which is further reduced to generate methanol. Mechanistic investigations using HCO$_2$H in D$_2$O and DCO$_2$D in H$_2$O showed that the existing C–H (or C–D) bond of formic acid is preserved during the reduction. This result supports the formaldehyde path. Under optimized conditions (12.5 mM Cat., 60 °C, pH 0.4, 12 M FA), they obtained the highest MeOH selectivity of 12% and a TON of 70. The highest TON for methanol was
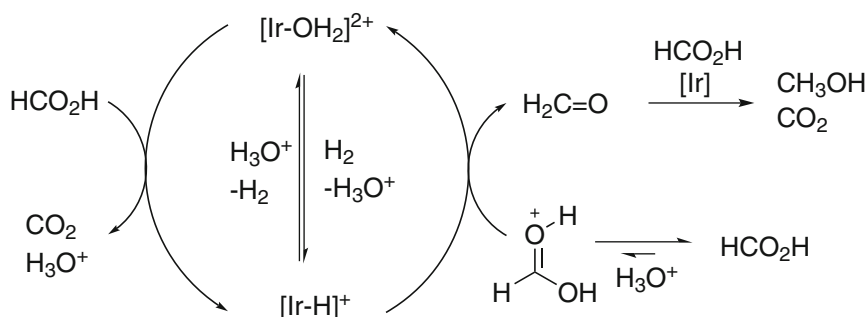
Scheme 4.1 Proposed mechanism of FA disproportionation to methanol with [Cp*Ir(bpy)(OH$_2$)]$^{2+}$ in water. Redrawn based on Ref. [2]

only 200 after 120 h, nevertheless, this study provided a new approach to MeOH generation directly from FA.

Subsequently, Cantat et al. reported significant improvement in MeOH yields from FA disproportionation with ruthenium catalysts [3]. Using [Ru(cod)(methyllallyl)$_2$], an triphos (CH$_3$C(CH$_2$PPh$_2$)$_3$) ligand, and MSA (methanesulfonic acid), they achieved the highest selectivity of 50% for FA disproportionation to MeOH in a THF solution at 150 °C. They isolated an important intermediate [Ru(triphos)(κ^1-HCO$_2$)(κ^2-HCO$_2$)] which liberated CH$_3$OH, H$_2$, and CO$_2$ after treated with 2 equivalents FA. This result indicates that MeOH is generated by transfer hydrogenation of FA but not from hydrogenation of CO$_2$, which is consistent with Miller's report. These two reports suggested that complexes, which are inactive for FA dehydrogenation, are potential to be effective for MeOH production through FA disproportionation.

Kubiak et al. synthesized a series of complexes **1–5**, [Cp*Ir(R-bpy)Cl]Cl, for the catalytic disproportionation of formic acid to methanol (Scheme 4.2) [4]. A TOF of 0.91 ± 0.04 h^{-1} and MeOH selectivity of 1.17 ± 0.30% were achieved by [Cp*Ir (bpy)Cl]Cl under acidic conditions. The research on the effect of the electron-donating ability of the bipyridine substituent indicated that the stronger electron-donating group in ligand is not necessary to improve the activity and selectivity for the disproportionation of FA.

Based on their earlier study of Ir-catalyzed hydrogenation of bicarbonate to formate and dehydrogenation of formic acid, Himeda et al. developed a CO$_2$ to MeOH conversion system, which go through first hydrogenation of CO$_2$ to FA and then disproportionation of FA into MeOH. This conversion can be realized at ambient temperature in acidic aqueous solution by using catalyst [Cp*Ir(4DHBP) (OH$_2$)]SO$_4$ **6** (4DHBP = 4,4′-dihydroxy-2,2′-bi-pyridine, Cp* = pentamethylcyclopentadienyl) [5]. At present, most of the complex catalytic hydrogenation of CO$_2$ to HCOOH required basic additives, however, they discovered that catalyst **6** can catalyze the hydrogenation of CO$_2$ to formic acid in acidic aqueous media without using any additives. In this system, using catalyst **6** and H$_2$SO$_4$, FA
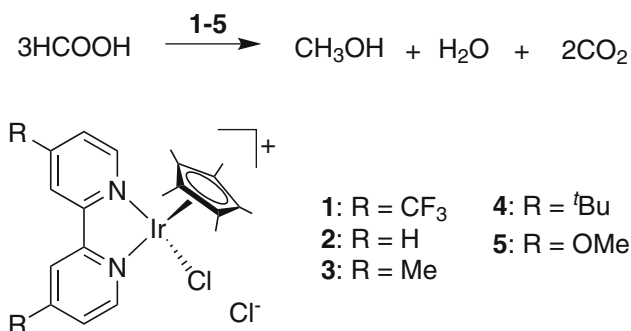
Scheme 4.2 The disproportionation of formic acid to methanol catalyzed by complexes [Cp*Ir (R-bpy)Cl]Cl **1–5**
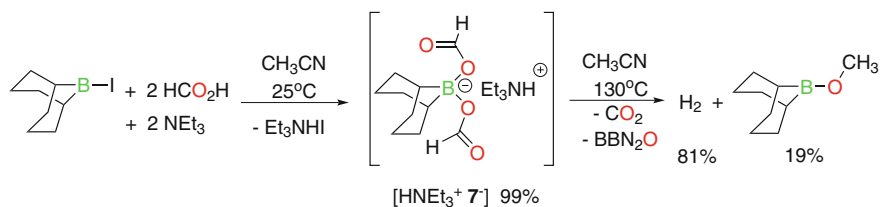
Scheme 4.3 The disproportionation of formic acid to methanol in metal-free condition. Redrawn based on Ref. [6]

disproportionation gave an unprecedented selectivity of 96% for MeOH and FA conversion up to 98% at 50 °C under 50 bar H_2. The authors demonstrated that MeOH originated from formic acid disproportionation instead of direct CO_2 hydrogenation.

In 2016, Cantat et al. reported the first metal-free disproportionation of formate using stoichiometric dialkylborane reagents (9-Iodo-9-borabicyclo[3.3.1]nonane, BBN–I) and bases without any external reductants (Scheme 4.3) [6]. Organic base (Et_3N) was used to prepare the starting bis(formoxy)borate, 7^-. Heating the borate [Et_3NH^+, 7^-] to 130 °C led to the generation of H_2/CO_2 and CH_3OBBN, $(BBN)_2O$. It suggests that formate anions can disproportionate to methoxides in the coordination sphere of boron, with the release of CO_2 and diboroxane $(BBN)_2O$. The
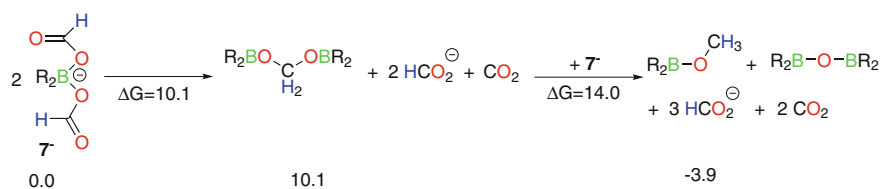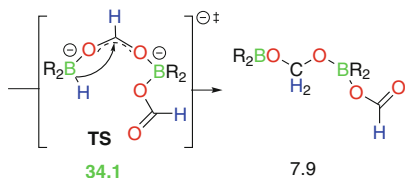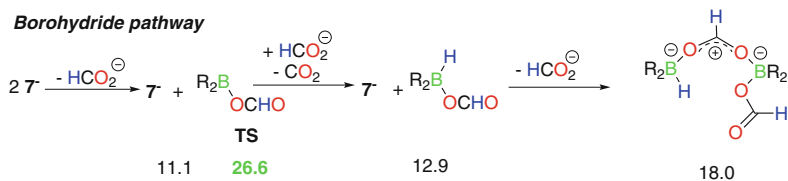
Scheme 4.4 Computed mechanism for the disproportionation of bis(formoxy)borate 7^-. Redrawn based on Ref. [6]

spectroscopy studies indicated that H_2, released by dehydrogenation, played no significant role in disproportionation. The parallel formation of H_2 and CH_3OBBN during reactions indicated that the disproportionation and dehydrogenation of formic acid are competing in this reaction. The nature of the base was found to affect the efficiency of the disproportionation. The bulky tertiary amines, such as $^iPr_2EtN$, improved selectivity of the formation of methoxyboranes. It might originate in the decreased affinity of the bulky amine for the boron center.

A subsequent mechanistic study combining experimental results and DFT calculations demonstrated two pathways are possible (Scheme 4.4). In borohydride pathway, the important role of transient borohydride, which generated from decarboxylation of formate ligands, is to promote the disproportionation of formates to formaldehyde and methanol scaffolds, and the reduction of aldehydes.

4.2   Cascade Catalysis of CO_2 to MeOH

The indirect transformation of CO_2 to MeOH via methyl formate, dimethyl carbonate, methyl carbamate, urea derivatives, formamides, and ethylene carbonate has been developed by Milstein and Ding group [32–35]. Sanford et al. approached the challenge of MeOH synthesis from CO_2 using a one-pot cascade reaction [7]. Their strategy applied several catalysts to promote a three-step cascade catalysis sequence including: (a) FA generation from CO_2 and H_2; (b) formate ester formation from FA; and (c) MeOH production by hydrogenation of the ester (Scheme 4.5). Under optimized conditions for each step, CO_2 hydrogenation/esterification occurred with 40 TONs, while the hydrogenation of the ester yielded methanol quantitatively at 135 °C. In the one-pot reaction using three catalysts, only the low TON of 2.5 for MeOH was obtained. This is attributed to the incompatibility of the three catalysts. A vapor transfer method was then employed to improve the performance. Catalysts **8** and **9** in an inner vessel were separated from catalyst **10** in an outer vessel. The deactivation of catalyst **10** by $Sc(OTf)_3$ could be avoided. The generated methyl formate was transferred into the outer vessel simply by elevating the reaction temperature to 135 °C. The hydrogenation of the ester in the outer vessel proceeded smoothly. The overall TON for MeOH was improved to 21. The distinct advantage of this approach was that the rate and selectivity of each step were tunable simply by changing the catalyst, while special equipment has to be employed to prevent catalyst deactivation due to the incompatibility of the catalysts.

In 2015, the same group reported CO_2 hydrogenation to MeOH using similar strategy [36]. In the presence of $HNMe_2$, DMF was found to be an important intermediate, which is further reduced to MeOH. Using a pincer Ru complex **11**, a TON of 550 for MeOH was obtained under 2.5 bar CO_2 and 50 bar H_2 at 155 °C for 36 h, DMF and formate are also detected as coproducts (Scheme 4.6).

$$3H_2 + CO_2 \xrightarrow{\substack{\textbf{\textit{Homogeneous}}\\ \textbf{\textit{Catalysis}}}} CH_3OH + H_2O$$

Cat. 8   H$_2$ (a)   (c) 2 H$_2$ -ROH Cat. 10

(b)
ROH
-H$_2$O
Cat. 9

Fe(BF$_4$)$_2$• 6H$_2$O/
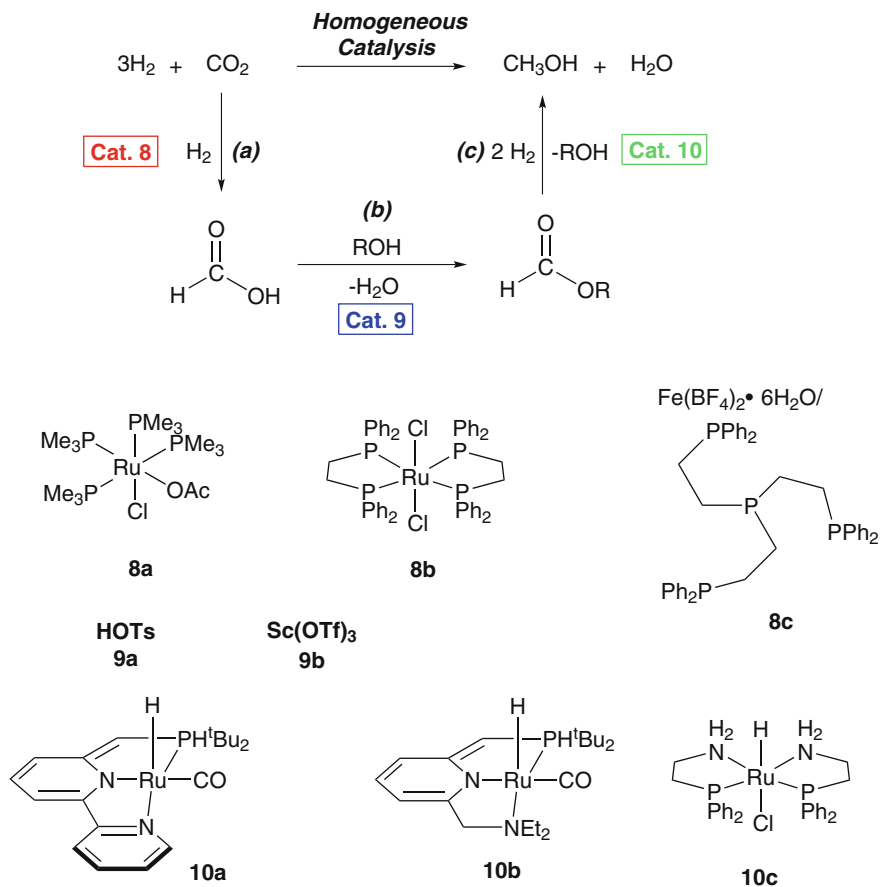
Scheme 4.5 Hydrogenation of CO$_2$ to MeOH with a strategy of cascade catalysis and catalysts used

$$CO_2 + H_2 \xrightarrow[-H_2O]{+HNMe_2} HCONMe_2 \xrightarrow[-HNMe_2]{+2\ H_2} CH_3OH$$

11
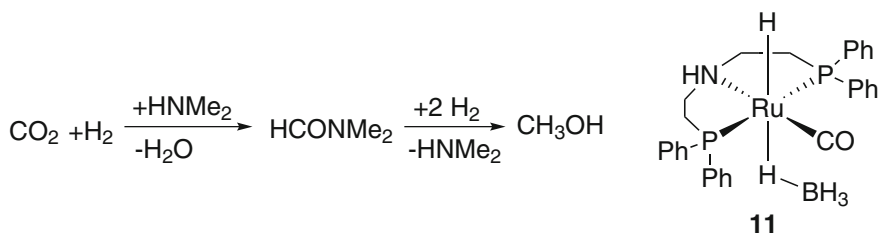
Scheme 4.6 Hydrogenation of CO$_2$ to MeOH using **11** in the presence of amines

4.3 Direct Reduction of CO$_2$ to MeOH with Metal Complexes

Although direct hydrogenation of CO$_2$ to MeOH is highly challenging, considerable efforts have been devoted to this transformation. Great progress has been achieved very recently either using H$_2$ gas or organosilane and borane as reductants [37, 38].

4.3.1 Hydrogen as Reductant

In 2015, Leitner et al. demonstrated direct hydrogenation of CO$_2$ to MeOH using [Ru (triphos)(TMM)] **12** (TMM = trimethylenemethane) [8]. As shown in Scheme 4.7, the Ru complex with one equivalent of bis(trifluoromethane)sulfonimide (HNTf$_2$) gave an initial TOF of 70 h^{-1} under CO$_2$/H$_2$ (20/60 bar at room temperature) at 140 °C. A TON of 603 for MeOH was obtained after recharging the H$_2$/CO$_2$ three times (Scheme 4.7). This result indicated that the catalytic activity was comparable to the most effective heterogeneous system. Mechanistic study revealed that a formate complex, [Ru(triphos)(η^2-O$_2$CH)(solvent)]$^+$ was the resting state, while other complexes isolated from the reaction mixture ([Ru(triphos)(H)(CO)$_2$]$^+$, [Ru$_2$(μ-H)$_2$(triphos)$_2$], and [Ru(triphos)(H)(CO)(Cl)]) were inactive catalysts. According to the mechanism study, the Ru-formate complex is further reduced by one equivalent of H$_2$ to give the Ru-hydroxymethanolate species, which is then converted to the Ru-methanolate complex by consumption of another equivalent of H$_2$. Hydrogenolysis of Ru-OMe liberates the MeOH product and Ru-H. A theoretical mechanism suggested that hydride migration from Ru to the formic acid ligand in [Ru(triphos)(H)(H$_2$)(HCO$_2$H)]$^+$ is a crucial step in the formation of a Ru-hydroxymethanolate species with an energy barrier of 15.5 kcal mol^{-1}.

In 2016, Kothandaraman et al. reported a highly efficient homogeneous catalyst system, which can directly convert various sources of CO$_2$ including CO$_2$ in the air to CH$_3$OH, using pentaethylenehexamine (PEHA) and Ru-Macho-BH (**11**) at 125–165 °C [10]. The amount of PEHA was found to be important for the high TON. After the reaction, CO was detected in the gas mixture. Decreasing the CO$_2$/H$_2$ ratio and (or) lowering the reaction temperature reduced the CO generation and finally to the undetectable amount by GC. Ethereal solvents including THF, 1,4-dioxane, diglyme, and triglyme were examined, triglyme provided the highest TON under the same conditions. Using the high boiling point solvent is also favorable for product separation as well as the catalyst reuse. MeOH can be easily distilled off, the residual triglyme solution of catalyst and PEHA can be reused for next run directly. The catalyst can be recycled for five runs without significant loss of activity (75% activity remained) and afforded a high overall TON of 2150. Moreover, for the first time, they demonstrated that CO$_2$ captured from the air can be directly converted to CH$_3$OH with 79% yield using a homogeneous catalytic system (Scheme 4.8).

$$CO_2 \ + \ 3H_2 \xrightarrow[\substack{140\ ^\circ C,\ 24\ h \\ P_{H_2/CO_2} = 6/2\ MPa \\ THF,\ EtOH,\ HNTf_2}]{\substack{(Triphos)Ru(TMM) \\ (6.3\ \mu mol)}} MeOH \ + \ H_2O$$

TON = 603

+ acid
(Triphos)Ru(TMM) **12**
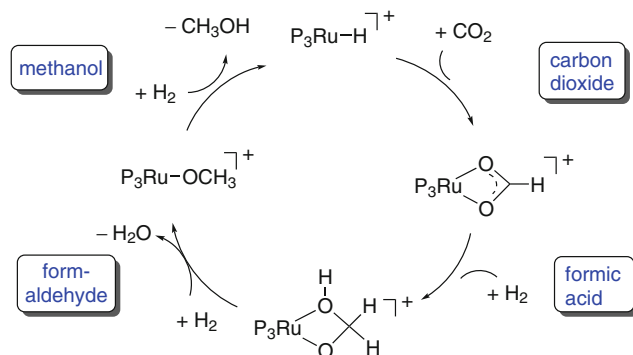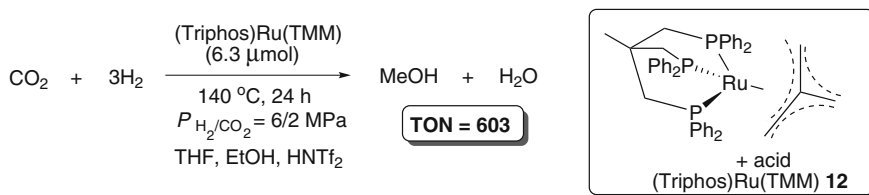
Scheme 4.7 MeOH production from direct catalytic hydrogenation of CO_2 and proposed mechanism based on Ref. [8]

Air
(400 ppm CO_2)
+

11

CO₂ Capture

In-situ
hydrogenation

$CH_3OH \ + \ H_2O$

+ H_2N〜NH₂
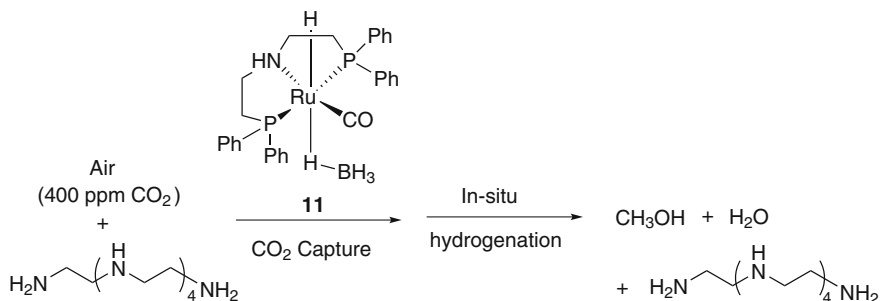
Scheme 4.8 CO_2 capture from air and conversion to MeOH with catalyst **11**. Reprinted with permission from Ref. [10]. Copyright (2016) American Chemical Society

4.3.2 Borane as Reductant

H_2 is an economic and most commonly used reductant. One drawback of H_2 is the potential safety problem due to its gas phase and flammable characters. In addition, using H_2 as a reductant for direct transformation of CO_2 to MeOH is rather difficult because of the unfavorable thermodynamics. Only two catalysts are reported to be effective, moreover, high temperature and pressure are required as above

mentioned. Other reducing agents such as organosilanes and borane have also been explored. The generated methoxide can liberate MeOH easily by hydration. The reduction is favorable due to the formation of stable Si–O or B–O bond. The reaction is feasible even under very mild conditions (ambient temperature or pressure). More importantly, complexes with non-precious metals even organocatalysts (see Sect. 4.4) are capable to promote CO_2 reduction to methanol level using these hydrogen sources. Therefore, using organosilane or borane as alternative hydrogen sources have attracted increasing attention albeit their relatively high cost. In this section, we mainly introduce the metal complexes-catalyzed CO_2 reduction to MeOH using borane as a reductant.

In 2010, Guan et al. reported the first catalytic hydroboration of CO_2 to methoxide level with catecholborane (HBCat) as reductant by using a PCP-pincer nickel hydride ^{tBu}PCPNiH **13a** (Scheme 4.9) [11]. A high TOF of 495 h^{-1} for methoxide (corresponding to a yield of 61% based on HBCat) were achieved at room temperature in C_6D_6. A CatBOBCat by-product was also observed.

Guan and co-workers further investigated other nickel bis(phosphinite) pincer complex [2,6-$(R_2PO)_2C_6H_3$]NiH (L^RNiH, **13b** R = isopropyl, **13c** R = cyclopentyl) which was synthesized from [2,6-$(R_2PO)_2C_6H_3$]NiCl with LiAlH$_4$ [12]. The reaction of L^RNiH (R = ^{t}Bu, ^{i}Pr, and cPe) with CO_2 at room temperature gave respectively the $L^RNiOCHO$ **14** (R = ^{t}Bu, ^{i}Pr, and cPe) as the sole products. The formato complexes **14** reacted with HBCat to form L^RNiH, CH$_3$OCat, and CatBOBCat. The reaction of $L^RNiOCHO$ (R = ^{t}Bu) **14a** is faster than reactions of other formate derivatives, which indicated that the reaction of formate derivatives bearing bulky substitutes had a better performance on the formation of CH$_3$OCat. It was supposed that complex bearing a smaller substituent is favorable for the interaction of L^RNiH and HBCat, resulting in concentration decrease of active L^RNiH. To investigate the scope of reducing reagents for reduction of CO_2, the reaction of $L^RNiOCHO$ (R = ^{t}Bu) **14a** with 9-borabicyclo[3.3.1]nonane (9-BBN), pinacolborane (HBpin) or PhSiH$_3$, was carried out respectively under the same conditions (Scheme 4.10). They found that the reducing reagent significantly affects the reaction outcome. 9-BBN provided a methoxide, while HBpin gave only formate species even large excess of HBpin was used. No reaction was observed when PhSiH$_3$ was employed.
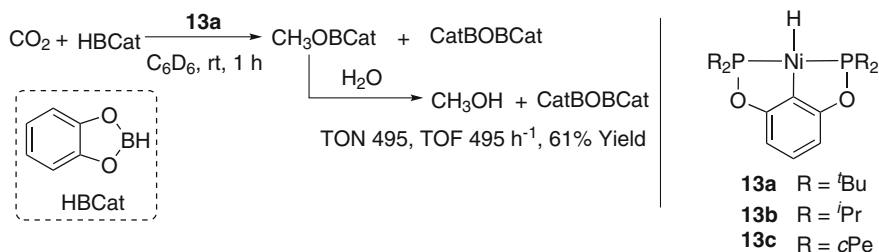
Scheme 4.9 The reaction of catalytic hydroboration of CO_2 by ^{tBu}PCPNiH **13a**
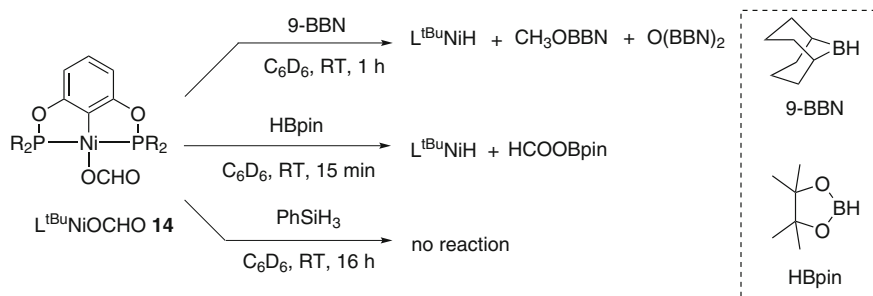
Scheme 4.10 Reaction of L^{R}NiOCHO (R = ^{t}Bu) **14** with 9-BBN, HBpin or PhSiH$_3$

Subsequently, Guan et al. studied the reaction mechanism of hydroboration of CO$_2$ with the Ni complexes using a computational method [39]. Based on the calculation they proposed a mechanism as summarized in Scheme 4.11. The reduction of CO$_2$ goes through three steps. First, CO$_2$ insertion into the [Ni]-H gives a formato complex, which reacts with HBCat to afford HCOOBCat and regenerate the active species [Ni]-H. HCOOBCat was further reduced by [Ni]-H to give an intermediate of [Ni]OCH$_2$OBCat, which is decomposed to [Ni]OBCat and formaldehyde. Although HCHO was not detected experimentally, it is indeed an important intermediate according to their calculations. It can be readily reduced by [Ni]-H to [Ni]OCH$_3$, which reacts with the third equivalent of HBCat to give CH$_3$OBCat and regenerate [Ni]-H. The direct CO$_2$ reduction with HBCat is highly unfavorable. The important role of [Ni]-H is demonstrated to shuttle hydridic H from the borane to CO$_2$, HCOOBCat, and HCHO.

In 2016, they reported a series of pincer Pd thiolate complexes for CO$_2$ reduction with HBCat (Scheme 4.12) [13]. Complex **15** achieved a TOF as high as 1780 h^{-1} at room temperature under atmospheric pressure. Although the mechanism is not
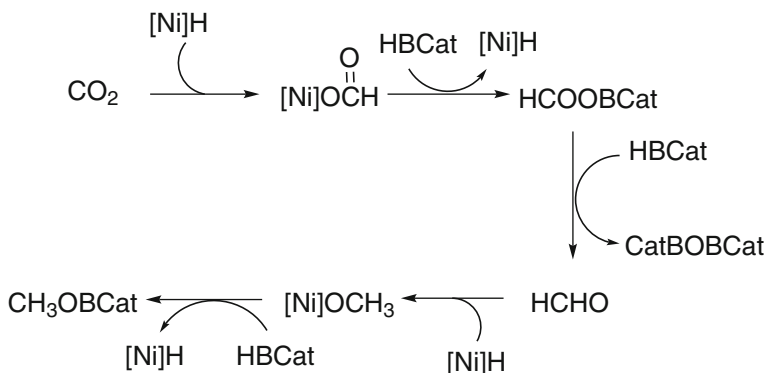
Scheme 4.11 The proposed mechanism of hydroboration of CO$_2$ into methanol. Reprinted with permission from Ref. [39]. Copyright (2011) American Chemical Society
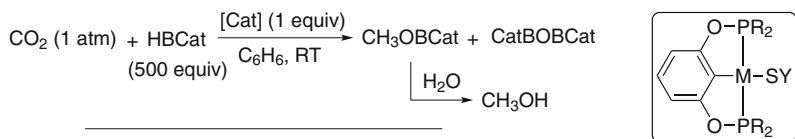
[Cat]	time (min)	TON	TOF (h^{-1})
15	15	445	1780
16	20	447	1341
17	25	449	1078
18	12	490	2400
19	13	470	2100
20	15	460	1800
21	25	480	1100
22	13	460	2100

15 M = **Pd** (R = ^{i}Pr, Y = Ph)
16 M = **Pd** (R = ^{t}Bu, Y = Ph)
17 M = **Pd** (R = ^{i}Pr, Y = CH$_2$Ph)
18 M = **Ni** (R = ^{i}Pr, Y = Ph-p-OCH$_3$)
19 M = **Ni** (R = ^{t}Bu, Y = Ph-p-CH$_3$)
20 M = **Ni** (R = ^{i}Pr, Y = Ph)
21 M = **Ni** (R = ^{i}Pr, Y = Ph-p-CF$_3$)
22 M = **Ni** (R = ^{t}Bu, Y = CH$_2$Ph)

Scheme 4.12 Pincer complexes for CO$_2$ reduction to methanol level

clear yet, it is confirmed that palladium hydride [2,6-(^{t}Bu$_2$PO)$_2$C$_6$H$_3$]PdH is not the main active species. Soon after that, they developed the pincer Ni thiolate analogous [14]. It was found that complexes with electron-rich sulfur ligands and less bulky groups (i.e., isopropyl) on the phosphorus donors are more active. When complex **18** was used for hydroboration of CO$_2$ with HBCat at room temperature under an atmospheric pressure of CO$_2$, an unprecedented TOF of 2400 h^{-1} was achieved and the methoxide products were obtained in a quantitative yield.

In 2010, John and co-workers reported the CO$_2$ reduction to FA and MeOH catalyzed by germanium(II) hydride **24** using ammonia borane as the hydrogen source under mild conditions [15]. Complex **24** was generated from the reaction of germanium(II) chloride **23** with LiNH$_2$BH$_3$ and was found to be an effective catalyst for CO$_2$ reduction to formate. Addition of LiNH$_2$BH$_3$ gave lithium formate and re-formed germanium(II) hydride **24** (Scheme 4.13). The yields of lithium formate were ranged from 85 to 95%. The formato complex **25** was further reduced with 3 equivalent of NH$_3$BH$_3$ using THF or benzene as solvents at 60 °C. After workup with D$_2$O, CH$_3$OD was obtained in yield of 33–43% and complex **24** was regenerated. It is noteworthy that complex **24**, which is stable toward water, can be
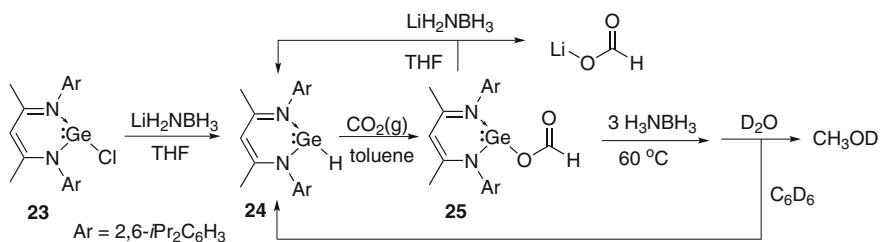
Scheme 4.13 CO$_2$ reduction to methanol with germanium(II) hydride and ammonia borane

easily separated from the products by extraction with benzene. The mechanism study suggests that the Ge–O bond was cleaved prior to reduction of the –OC(O)H group. B–OCH_3 derivatives were observed by NMR. This study provided an effective route for the hydrogenation of carbon dioxide to methanol using germanium(II) hydride as a mediator.

In 2012, Bontemps et al. studied CO_2 reduction with HBpin and a Ru polyhydrides [$RuH_2(H_2)_2(PCy_3)_2$] (Cy = cyclohexyl). Although the reaction was completed in 30 min, CH_3OBpin was detected by NMR in a relatively low selectivity (12%) [40]. Subsequently, Michael and Stephan developed a Ru complex with a tripodal ligand N-(($CH_2)_2NHP^iPr_2)_3$ [41]. The Lewis basic P and Lewis acidic Ru can cooperatively activate CO_2. However, the catalytic reaction only provided a low TON of 9 for MeOBpin after 96 h at 50 °C under ambient pressure of CO_2. In 2014, Tan et al. reported a labile Ge(II) hydride bearing a 2-iminocyclohexylidenebenzylamine ligand for the transformation of CO_2 to formato complex which was further reduced with $AlH_3 \cdot NMe_3$ to provide methanol after hydration [42]. Soon after that, Anker et al. reported two $B(C_6F_5)_3$-activated alkaline earth (Mg and Ca) catalysts, which were effective in selective reduction of CO_2 to a methanol equivalent CH_3OBpin [16]. The alkaline earth catalysts, **27** and **28**, were synthesized from amidoborane derivatives **26** and **29** with $B(C_6F_5)_3$ (Scheme 4.14).

Catalytic hydroboration of $^{13}CO_2$ with 3 equivalents of HBpin was conducted in the presence of **27** and **28** at 60 °C in THF. The borane was completely consumed within 6 and 4 days respectively. In this reaction, the products were found to be $(pinB)_2O$ and $^{13}CH_3OBpin$, while the latter one was identified as the sole ^{13}C-containing product of CO_2 reduction. In addition, small quantities of [HB$(C_6F_5)_3$]$^-$ anion, pinBO^{13}CHO (**30**), and pinBO$^{13}CH_2OBpin$ (**31**) were identified throughout the reaction by in situ NMR monitor. Based on the experimental study, a possible reaction mechanism was proposed (Scheme 4.15). First, CO_2 inserts into the M–H bond to form LM–O(CHO), which is then converted into pinBO^{13}CHO (**30**) with one equivalent of HBpin. **30** is further reduced with LM–HB($C_6F_5)_3$ to form LMO(CH_2)OBpin, which reacts with HBpin to provide pinBOCH$_2$OBpin **31**. During the alkaline earth-centered reductive processes, the electrophilic borane acts as a reagent for the delivery of a hydridic H. Product CH_3OBpin may be formed via two pathways. In pathway A, complex **31** goes through spontaneous or
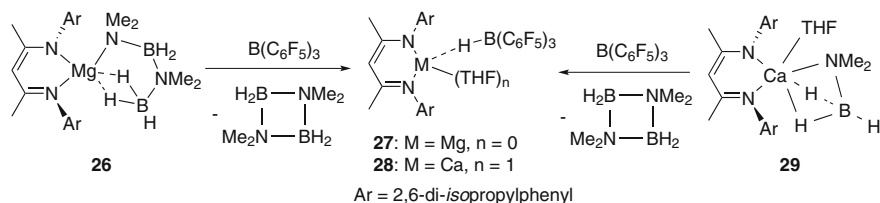
Scheme 4.14 Synthesis of alkaline earth catalysts **27** and **28**. Reprinted with permission from Ref. [16]. Copyright (2014) Royal Society of Chemistry
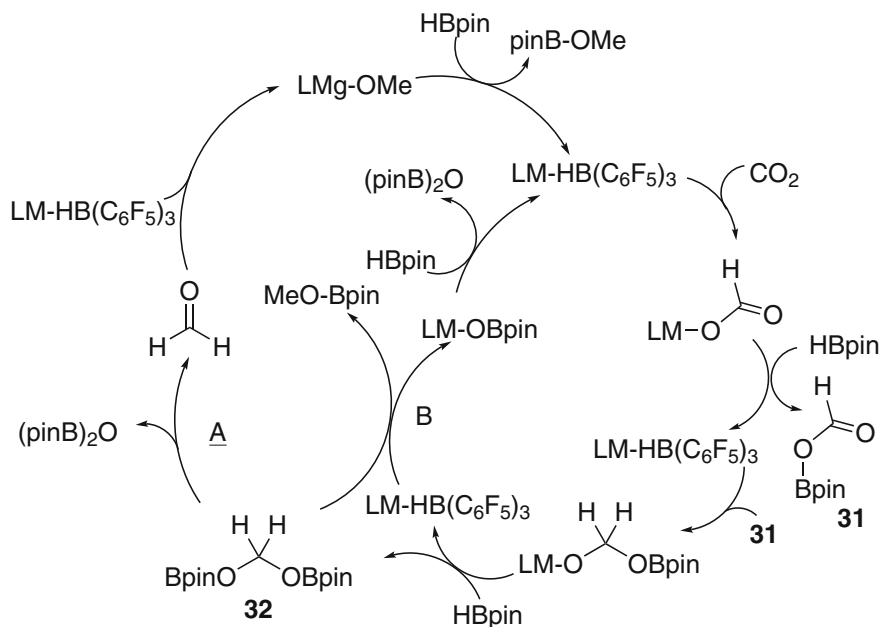
Scheme 4.15 Proposed mechanism for CO_2 reduction with complexes **31** and **32**. Reprinted with permission from Ref. [16]. Copyright (2014) Royal Society of Chemistry

metal-centered breakdown to form $(pinB)_2O$ and formaldehyde, which further reduced to provide CH_3OBpin. In pathway B, CH_3OBpin is directly formed by the reaction of **31** with another equivalent of $LM\text{-}HB(C_6F_5)_3$.

Very recently, Jones group reported that bulky amido − germanium(II) **33** and −tin(II) hydride complexes **34**, as extremely efficient and highly selective catalysts for the reduction of CO_2 to methanol level using HBCat or HBpin as the hydrogen source (Scheme 4.16) [18]. Importantly, Sn complex **34** was demonstrated to be the most active non-transition metal catalyst yet reported, yielding TOF up to 1188 h^{-1} at room temperature.

In the subsequent mechanistic study, it was identified that two thermodynamically and kinetically viable catalytic pathways are viable for these reductions (Scheme 4.17). In both cycles, the first two steps are identical. A germa-/bora-acetal intermediate **38** was generated via the first hydrogermylation of CO_2, followed by cycloaddition reaction with HBpin across one GeO bond. In route A, intermediate **38** undergoes a σ-bond metathesis reaction with HBpin to regenerate **35** and gives $(pinBO)_2CH_2$ **37**. Further reaction of **37** with **35** yielding MeOBpin and the experimentally observed germanium(II) borate ester **39** is the rate-determining step. Intermediate **39** readily reacts with the final equivalent of HBpin to regenerate catalyst **35**. In alternative route B, elimination of formaldehyde from **38** to give **39** is found to be the rate-determining step. In the same way, intermediate **39**

$$CO_2 + 3\ HBCat \xrightarrow{\text{LMH 33 or 34}} H_3COBCat + (CatB)_2O$$

L =

33 M = Ge

34 M = Sn   TOF = 1188 h^{-1}
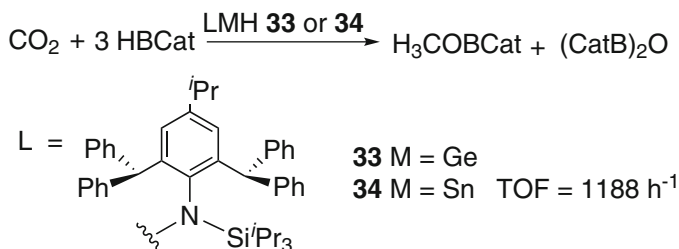
Scheme 4.16 CO_2 hydroboration with **33** and **34**
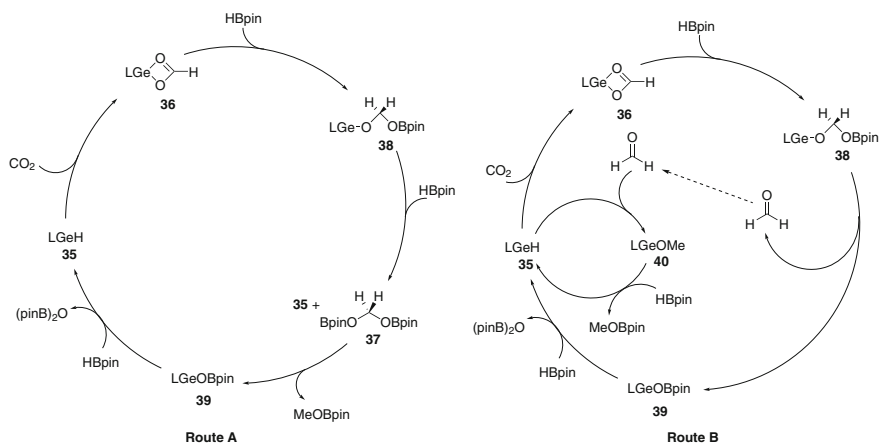
Scheme 4.17 Two possible pathways for the reduction of CO_2 to MeOBpin, catalyzed by **35**. Reprinted with permission from Ref. [18]. Copyright (2017) American Chemical Society

undergoes a σ-bond metathesis reaction with HBpin to give **35** and $(pinB)_2O$. Hydrogermylation of formaldehyde with **35** gives the germanium methoxide **40**. A subsequent spectroscopic study indicates that route A predominates in the experimental situation through identifying intermediates germanium(II) and −tin(II) borate esters. However, the involvement of the second reaction pathway cannot be ruled out as suggested by a series of related stoichiometric reactions. This study indicates that relatively cheap main group complexes are viable alternatives to transition metal-based systems in the catalytic reduction of CO_2 with boranes.

In 2016, Lu and Williams investigated di(carbene)-ligated nickel complexes **41** and **42** for reduction of CO_2 to methanol in the presence of inexpensive and easily handled sodium borohydride at room temperature [17]. The NHC ligands can lead to high catalytic activity of the complex due to their strong electron-donating character. They obtained a high TON of 1.1 million over 2 months. The authors observed that >90% of the hydridic H in $NaBH_4$ were converted to C–H bonds in this reaction, resulting in sodium borate. Furthermore, the complexes are highly
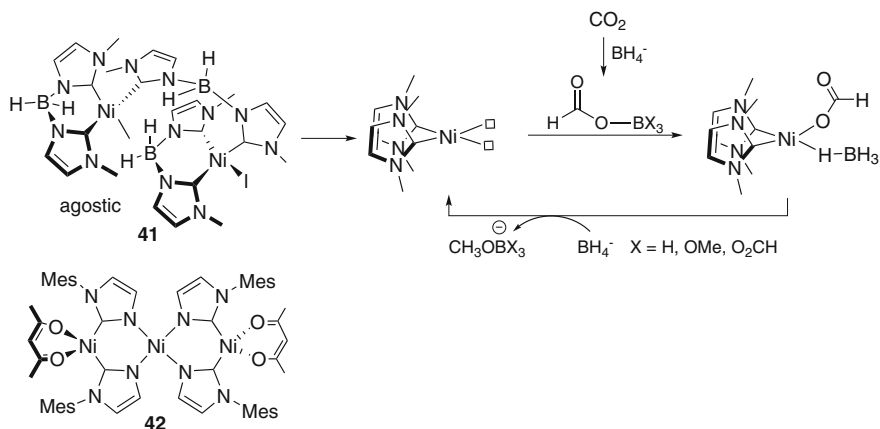
Scheme 4.18 Mechanistic speculation for CO$_2$ reduction by **41**

stable to air and water. In NMR experiments direct production of methanol, instead of boron methoxides was achieved in the presence of 1 vol.% H$_2$O. NMR and X-ray diffraction experiments have been carried out to study the reaction mechanism. Two monomeric Ni carbene species were isolated and their structures were determined by single crystal X-ray diffraction method. NMR experiments suggested that a Ni–H species was formed with **41** in the presence of NaBH$_4$. The speculated catalytic cycle was illustrated in Scheme 4.18. Dimer complex **41** cleaves to give monomer species which reacts with borohydride and CO$_2$ to generate an active hydride. The Ni–H species further reacts with borohydride to give methoxide and regenerates the Ni monomer complex.

4.4 Transformation of CO$_2$ to MeOH with Organocatalysts or FLPs

FLPs as defined by Stephan are combinations of a Lewis acid and base that are not mutually quenched as a result of steric or geometric constraints [43]. Initially developed FLPs usually employ metal Al as Lewis acid. Recently reported FLPs based on B/N, B/P couple are metal-free and belongs to organocatalysts. It should be noted that either metal-based or metal-free FLPs are introduced in this section. The concept of FLPs contributes greatly to the metal-free CO$_2$ reduction. Organocatalysts or FLPs accompanied with organosilanes and borane as reducing agents offers the possibility of CO$_2$ reduction to MeOH under very mild conditions. Most recently, some FLPs are even demonstrated to be active in the reduction of CO$_2$ to MeOH with H$_2$. This strategy attracted much attention due to its use of only low cost and earth-abundant reagents [43–45].

4.4.1   Borane as Reductant

In 2010, Stephan developed the first frustrated Lewis pairs system, Al-based FLPs **43** for reduction of CO$_2$ with ammonia borane (AB) to methanol (Scheme 4.19) [24]. **44** were prepared respectively from the reaction of **43** with CO$_2$ and their structures were confirmed by NMR and X-ray crystallography. The stoichiometric reaction of **44** with ammonia borane proceeded rapidly at room temperature affording average extracted yields of 37–51%.

In 2011, Paul and co-workers investigated mechanistic details by DFT calculation for the CO$_2$ reduction with FLPs **43** to methanol using ammonia borane as the hydrogen source [46]. Unlike CO$_2$ reduction by AB to formic acid through a six-membered transition state (Scheme 4.20a), the computational study revealed that the reduction pathway by the FLP-CO$_2$ complex through a hydride transfer from the borane end of AB (Scheme 4.20b).

To explore the role of the Lewis acid and base in the reduction of CO$_2$, Lim and co-workers examined the reaction of CO$_2$ and AB catalyzed by FLPs through quantum chemical calculations [47]. It was found that hydride transfer was promoted by LA (AlCl$_3$), while LB (2,4,6-trimesitylenephosphine, PMes$_3$) exhibited a negative effect, namely hindered hydride transfer. Based on computational data, the reaction in presence of LB showed a higher hydride transfer barrier than that exclusively catalyzed by LA by ~ 8 kcal/mol. However, LB played a significant role in the stabilization of the active FLP·CO$_2$ complex. The reaction rate is promoted greatly by increasing the concentration of FLP·CO$_2$.

Stephan et al. further investigated the mechanism for reduction of CO$_2$ catalyzed by Al-based FLP o-tol$_3$P/Al(C$_6$F$_5$)$_3$ (Scheme 4.21) [48]. In the reaction, ammonia boranes bearing larger steric hindrance substitutes were employed to increase their solubility in a solvent and slow the reaction rate. FLP (o-tol)$_3$P/Al(C$_6$F$_5$)$_3$ reacted
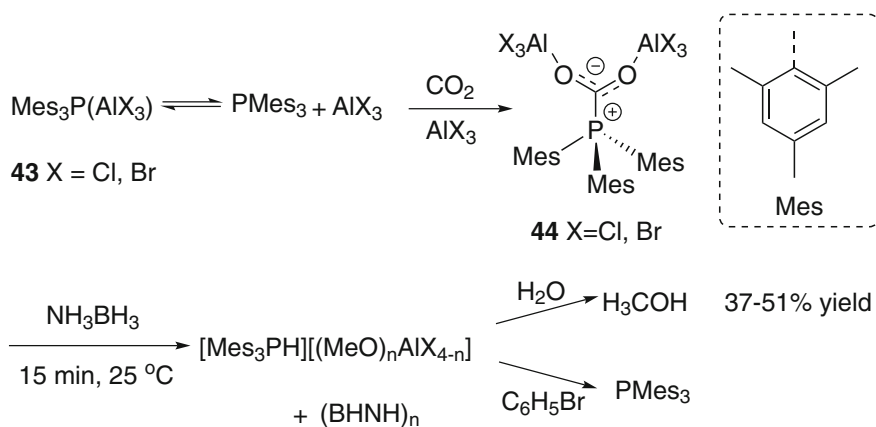
Scheme 4.19   Stoichiometric reduction of **43** or **44** to CH$_3$OH

(a)

(b)
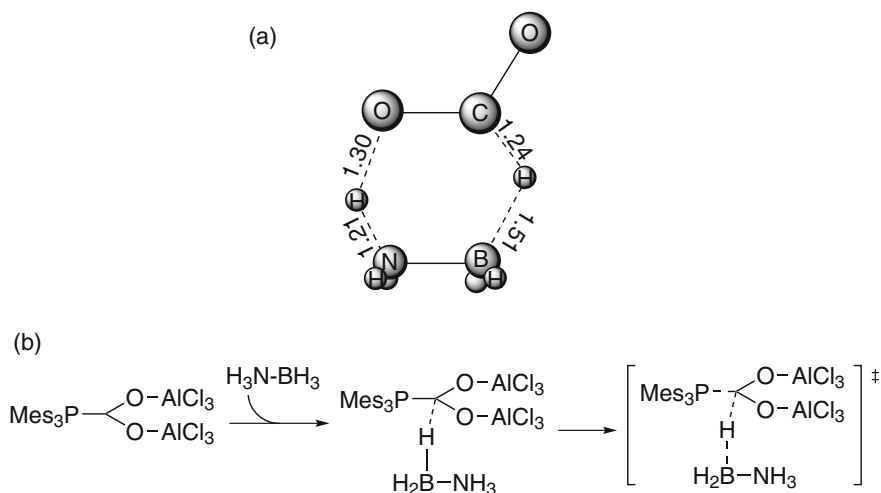
Scheme 4.20 a CO_2 reduction by ammonia borane to formic acid through a six-membered transition state. **b** The reduction of the trapped CO_2 through a hydride transfer from the borane end of ammonia borane
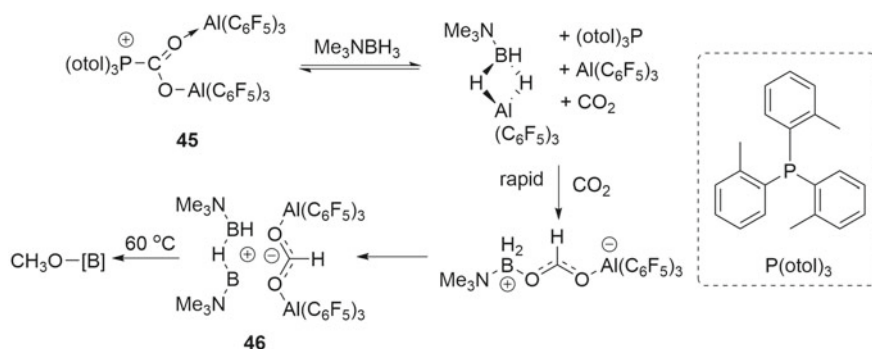
Scheme 4.21 Reaction of **45** with Me_3NBH_3 to give methoxide

with CO_2 to give $(o\text{-tol})_3PC(OAl(C_6F_5)_3)_2$ **45**, which generated formate-bridged species in the presence of H_3BNMe_3. The experiments demonstrated that **45** reacted with Me_3NBH_3 to methoxide level via **46**.

In 2013, Fontaine et al. reported the first organocatalyst 1-BCat-2-PPh$_2$-C$_6$H$_4$ **47** (Cat = catechol) for reduction of CO_2 to CH_3OBR_2 or $(CH_3OBO)_3$ in presence of hydroboranes including HBCat, HBpin, 9-BBN, $BH_3 \cdot SMe_2$, and $BH_3 \cdot THF$ (Scheme 4.22) [20]. A 99% yield for MeOH was obtained in the reaction of CO_2 and $BH_3 \cdot SMe_2$ catalyzed by **47** under atmospheric pressure at 70 °C, with a TOF of 853 h^{-1} and TON of 2950. It is notable that the catalyst exhibited "living" behavior that addition of hydroboranes could restart the reaction when it was consumed.
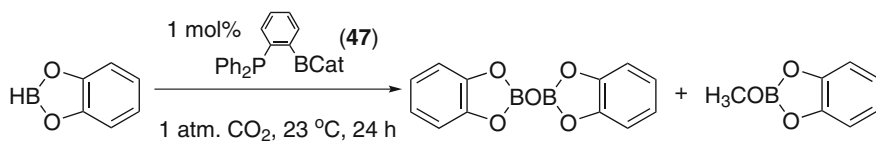
Scheme 4.22 Reduction of CO₂ in presence of HBCat and Catalyst **47**. Reprinted with permission from Ref. [20]. Copyright (2013) American Chemical Society

To expand the scope of the FLP system, they synthesized a novel triphosphine-organoalane $Al(C_6H_4(o\text{-}PPh_2))_3$ **48** to catalyze the reduction of CO_2 with HBCat (Scheme 4.23) [21]. The X-ray diffraction of **48** illustrated that two Al–P interactions resulted in pseudo-bipyramidal-trigonal geometry. The labeling experiment indicates that each molecule **48** can capture one CO_2 to form ambiphilic CO_2 adduct under ambient conditions. Induction period was observed when the reaction of CO_2 and HBCat underwent with precatalyst **48** under atmosphere pressure at 60 °C. Species **47** was isolated from the reaction between **48** and HBCat under atmospheric pressure at 70 °C. However, HBCat cannot react with the adduct of $BH_3 \cdot SMe_2$ and **48** to generate **47**. The reaction between CH_3OBCat and **48** can produce **47** as well, accompanied by the formation of **49**. The species $Al(\kappa^2\text{–}O, O\text{–}(MeO)_2BCat)_3$ **49** can be readily hydrolyzed in methanol.

On the basis of previous work, Fontaine et al. investigated the mechanism of hydroboration of CO_2 promoted by $1\text{–}B(OR)_2\text{-}2\text{-}PR'_2\text{–}C_6H_4$ **50** and **51** by experimental and computational methods (Scheme 4.24) [49]. Phosphine-boranes **50** and **51** were readily converted to formaldehyde adducts **50b·CH₂O** and **51b·CH₂O** respectively in the presence of CO_2 and HBCat. The ^{13}C labeling experiments indicated that **50b·CH₂O** and **51b·CH₂O** are the active catalysts for hydroboration of CO_2. Three possible transition states for the hydroboration of CO_2 were proposed according to the DFT calculation. The CH_2O moiety in catalyst takes part in activating CO_2 or reducing agent (pathways A-C), instead of being hydrogenated into the CH_3OH.

In 2014, Fontaine and co-workers described a Lewis base catalyst 1,8-bis (dimethylamino)naphthalene (**52**) for the transformation of CO_2 to methanoboranes $(CH_3OBO)_3$ with a TOF of 108 h^{-1} at room temperature (Scheme 4.25) [22]. It was
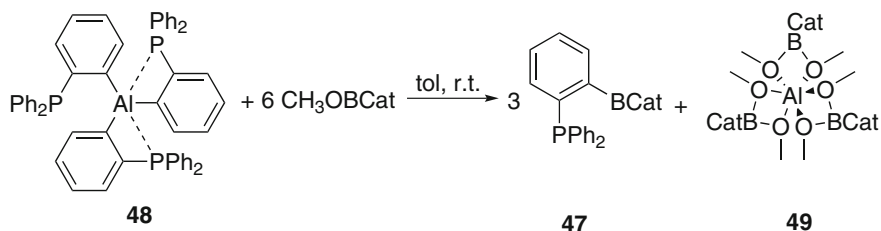
Scheme 4.23 Generation of **47** in reaction of **48** and CH₃OBCat. Reprinted with permission from Ref. [21]. Copyright (2013) American Chemical Society
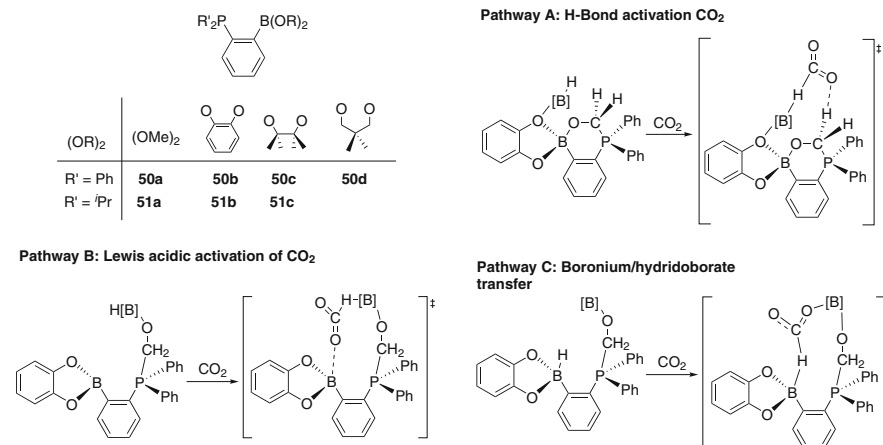
Scheme. 4.24   Structures of **50** and **51**, and transition states for the hydroboration of CO$_2$
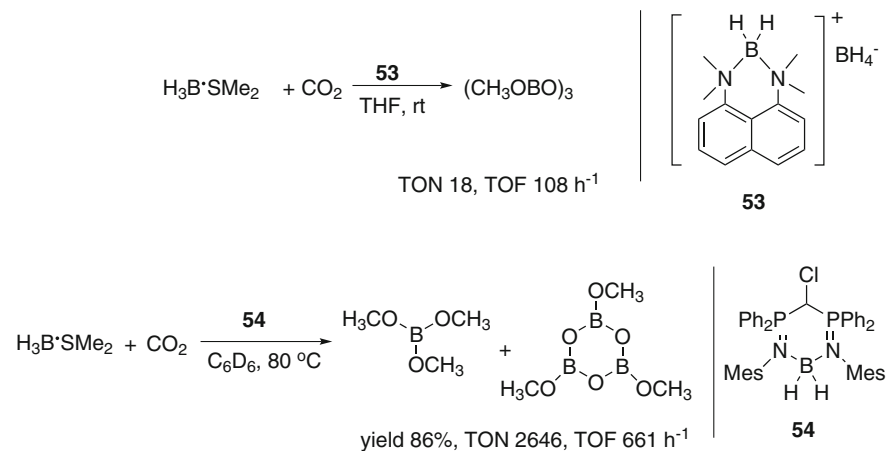
Scheme 4.25   Catalytic activity of **53** and **54** for the reduction of CO$_2$ by BH$_3$·SMe$_2$

discovered that Lewis base catalyst **52** activates the BH$_3$·SMe$_2$ to produce a borenium species **53**, which is an active species for reduction of CO$_2$. The reaction of BH$_3$·SMe$_2$ with CO$_2$ in presence of catalyst **52** monitored by NMR indicated that formation of **53** is rate limiting in the catalytic cycle (Scheme 4.26). Following this report, Mézailles et al. synthesized a zwitterionic boronium species **54**, similar to **53** in structure [23]. Calculation of charges at the "BH$_2$" fragment in **54** indicated a hydridic character as strong as borohydride. **54** was employed to catalyzed the reaction of BH$_3$·SMe$_2$ and CO$_2$ giving methoxyborane and methoxyboroxine at 80 °C with a brilliant TON and TOF.
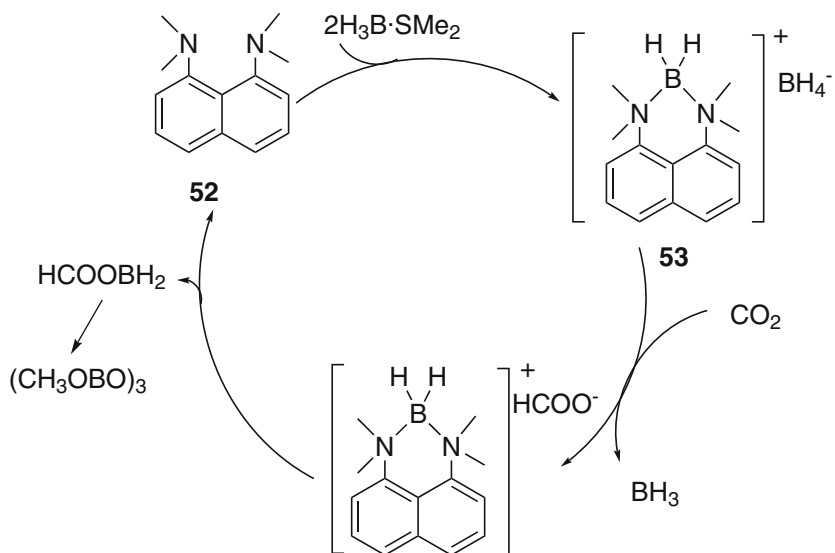
Scheme 4.26 Proposed mechanism for the reduction of CO₂ to methoxyboranes with **52**. Reprinted with permission from Ref. [51]. Copyright (2014) Royal Society of Chemistry

Based on the work that the NHC adduct of 9-BBN activates H_2 in presence of $P(^tBu)_3$, [50]. Wang and Stephan developed two novel intramolecular frustrated Lewis pairs by ring-expansion reaction between phosphine-derived carbenes $C_3H_2(NPR_2)_2$ (R = ^tBu, N^iPr_2) with 9-BBN [25]. These FLPs catalyzed the reduction of CO_2 to methanol in presence of boranes and achieved a moderate TON of 100 at room temperature under 5 atm CO_2. Interestingly, the reactions with different boranes afforded different products. A mixture of HCOOBpin, $CH_2(OBpin)_2$, and CH_3OBpin were obtained when HBpin was used as a reductant. However, the HBCat were completely converted into CH_3OBpin, and only $(MeOBO)_3$ were observed in the presence of $BH_3 \cdot SMe_2$.

Subsequently, they conducted phosphine catalyzed CO_2 reduction with 9-BBN [51]. It was found that $P(^tBu)_3$ can activate CO_2 in presence of 9-BBN by forming an adduct. When the reaction was carried out under catalytic conditions, a TON of 5556 (TOF of 176 h^{-1}) and yield of 98% were achieved after 31.5 h at 60 °C (Scheme 4.27a). An induction period was observed when PPh₃ or $P(p\text{-}MeC_6H_4)_3$ were used instead of $P(^tBu)_3$. The period span decreased to a half when the concentration of the phosphines increased twice.

In 2014, Cantat et al. exploited guanidines and amidines derivatives, such as 1,5,7-triazabicyclo[4.4.0]dec-5-ene (TBD), 7-methyl-1,5,7-triazabicyclo[4.4.0] dec-5-ene (Me-TBD), 1,8-diazabicycloundec-7-ene (DBU) to catalyze the reduction of CO_2 to methanol with hydroboranes [26]. A TON of 648 and TOF of 33 h^{-1} were achieved by Me-TBD with 9-BBN at room temperature (Scheme 4.27b). The formation of formoxyborane intermediate HCOOBR₂ was found to be the

(a)   CO$_2$ + 9-BBN $\xrightarrow[\text{60 °C}]{\text{P(^{t}Bu)}_3}$ CH$_3$OBBN + O(BBN)$_2$

TON 5556, TOF 176 h^{-1}

9-BBN

(b)   CO$_2$ + 9-BBN $\xrightarrow[\text{25 °C}]{\text{Me-TBD}}$ CH$_3$OBBN + O(BBN)$_2$

TON 648, TOF 33 h^{-1}

(c) CO$_2$ + 9-BBN $\xrightarrow[\text{20-70 °C}]{\textbf{56}}$ CH$_3$OBBN + O(BBN)$_2$

TON 6043 (25 °C), TOF 287 h^{-1} (70 °C)   **56**
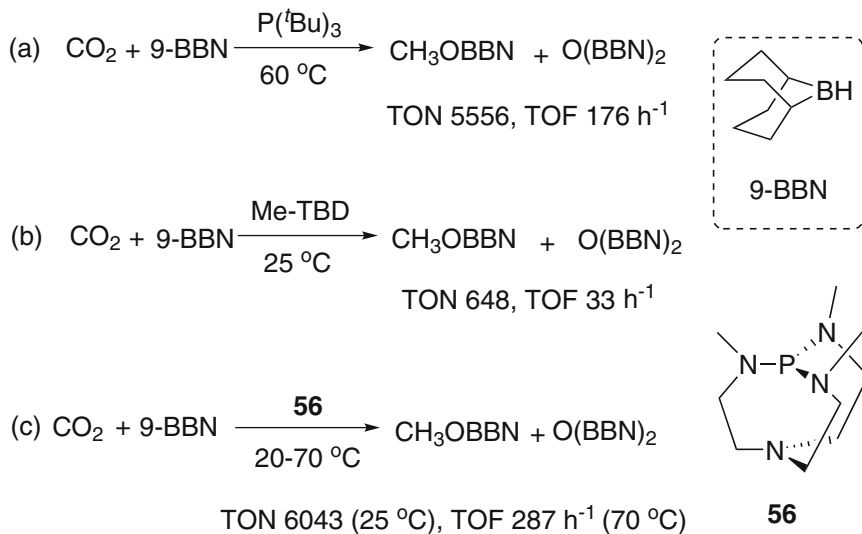
Scheme 4.27 Reaction of CO$_2$ with 9-BBN catalyzed by **a** P(^{t}Bu)$_3$, **b** Me-TBD, and **56**

rate-determining step. Interestingly, experimental and computational studies indicated that TBD and Me-TBD catalyzed the hydrogenation of CO$_2$ in different pathways. Me-TBD catalyzed hydrogenation of CO$_2$ by activating hydroboranes in priority, while TBD was first transformed into active frustrated Lewis pairs which subsequently catalyzed the reduction of CO$_2$ (Scheme 4.28).
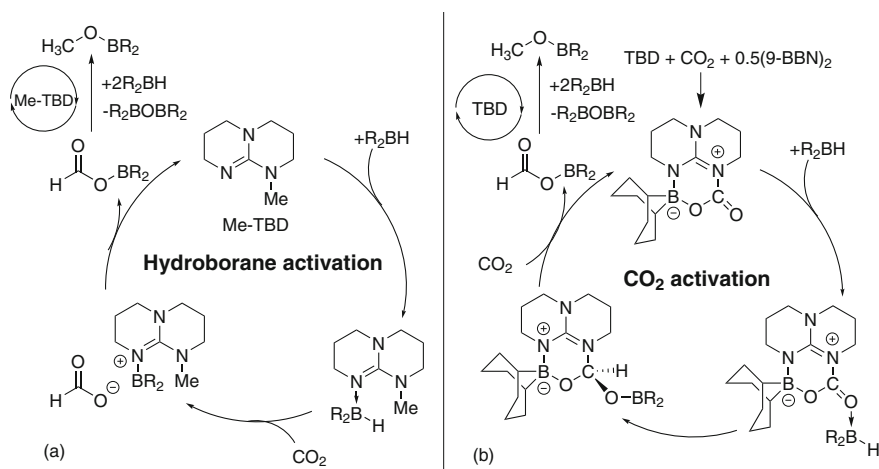
Scheme 4.28 Proposed different pathways for the catalytic hydroboration of CO$_2$ to formoxyborane HCOOBR$_2$ with **a** Me-TBD and **b** TBD
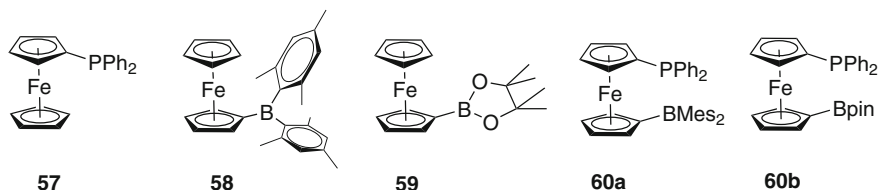
Fig. 4.1 Ferrocene-based phosphinoborane catalysts for the hydroboration of CO$_2$. Reprinted with permission from Ref. [29]. Copyright (2016) Royal Society of Chemistry

In the same year, Cantat et al. reported a highly efficient catalyst proazaphosphatrane superbases **56** for hydroboration of CO$_2$ with 9-BBN to methanol [28]. A high TON of 6043 was achieved with **56** at room temperature (Scheme 4.27c). Notably, this catalyst also enables the catalytic methylation of amines from CO$_2$ with hydroboranes.

In 2016, Cantat et al. developed a series of ferrocene-based phosphine, borane, and phosphinoborane derivatives as catalysts for the hydroboration of CO$_2$ (Fig. 4.1) [29]. **57–59** exhibited no apparent catalytic activity while a TON of 41 were achieved with the mixture of **57** and **58** at room temperature. The results demonstrated the synergistic effects of the mixture of Lewis base and Lewis acid. High catalytic performance was obtained with **60a** at 70 °C under atmospheric pressure. The reaction afforded a TON of 1980 and TOF of 99 h^{-1} with a catalyst loading of 0.05 mol% for 20 h.

Inspired by NHCs catalyzed hydrosilylation of CO$_2$, Song et al. investigated *N*-methyl-4,5-diazafluorenide (**61**) and a two ring analogues **62** for CO$_2$ hydroboration using various of boranes (Fig. 4.2) [27]. After a screening of boranes, BH$_3$·SEt$_2$ was demonstrated to be most effective. Under 1.5 atm CO$_2$ at room temperature, **61** afforded a TON of 294 after 44 h, while **62** provided a TON of 298 only after 7 h.

In 2014, Mizuta explored commercially available THF solution of BH$_3$, containing a small amount NaBH$_4$ to react with CO$_2$ to trimethoxyboroxine with 87% yield at room temperature [30]. NaBH$_4$ was found to act as a catalyst in hydroboration of CO$_2$ through the formation of HCOOBH$_3$ and (HCOO)$_2$BH$_2^-$. Based on the experiments and literature, the author proposed a mechanism for the reaction of BH$_3$ with CO$_2$ promoted by NaBH$_4$ (Scheme 4.29). Replacing NaBH$_4$ with HCOONa, 78% yield was obtained, which supported the proposed mechanism.

Fig. 4.2 Organocatalysts **61** and **62** with carbon-centered activity for CO$_2$ hydroboration
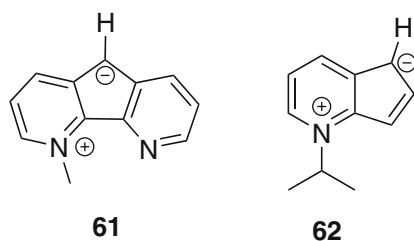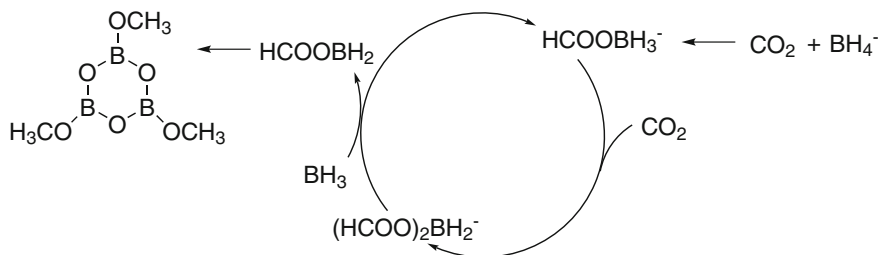
Scheme 4.29 Proposed mechanism for hydroboration of CO_2 promoted by $NaBH_4$

4.4.2 Silane as Reductant

Hydrosilane is a commonly used reductant in organic synthesis. The Si-H bond can be readily activated to give active hydride. More importantly, the inherent affinity of the silicon atom to oxygen is favorable for CO_2 activation. It has been employed in CO_2 reduction to formate, acetal, methoxide, methane levels, and other CO_2 involved reaction. [31, 52–71]. Reduction to formate or methane level is readily accessible, while controlled reduction to methanol is particularly challenging. In 1989, Eisenschmid and Eisenberg reported the first CO_2 reduction with alkylsilanes including Me_3SiH, Me_2SiH_2, and Et_2SiH_2 to methoxide level using a complex [Ir (CN)(CO)dppe] (dppe = 1,2-bis(diphenylphosphino)ethane) albeit with a low TON of 2.28 [66]. Another example of CO_2 reduction to methoxy level with a Ru complex using organosilane as reducing agents was reported in 2014 [72]. Except for metal complexes, organocatlaysts are also explored and will be discussed in this section.

N-Heterocyclic carbenes (NHC) bearing a lone pair of carbene electron can severe as nucleophiles and have been widely used as organocatalysts and ligands. In 2009, Ying and Zhang et al. reported the first organocatalyst catalyzed hydrosilylation of CO_2 to methanol under mild conditions using NHC (Scheme 4.30) [31]. 1,3-Bis(2,4,6-trimethylphenyl)imidazolium carboxylate (IMes-CO_2) and silane were treated with CO_2 in DMF and monitored by $^{13}C\{^1H\}$ NMR spectroscopy. The formation of formoxysilanes and silylacetal intermediates and methoxide product were identified. It was found that the reaction is sensitive to steric hindrance.
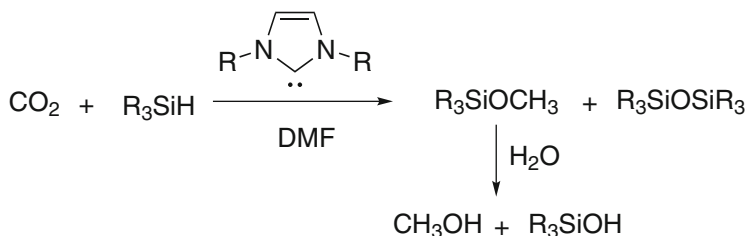
Scheme 4.30 The reduction of CO_2 with R_3SiH by NHCs to methanol

Disubstituted silanes are effective reductants, while trisubstituted ones are inactive. NHCs with bulky substituents resulted in higher efficiency. With low catalyst loading (0.05 mol%) of mesitylimidazolylidene, diphenylsilane was fully consumed and transformed to $Ph_2Si(OMe)_2$ typically in 90% yield. TON and TOF up to 1840 and 25.5 h^{-1} were reached respectively. It is noteworthy that the catalytic system is resistant to oxygen; the reaction with mixed CO_2/O_2 (1:1) offered the same result as that with pure CO_2. This study provides an efficient and selective method for CO_2 reduction to methanol.

Soon after that a series of mechanistic studies was reported [39, 73, 74]. The calculations by Wang predicted that formaldehyde is an inevitable intermediate. On the contrary, Ying and Zhang et al. demonstrated with experiments that hydrosilylation of formaldehyde is not feasible. Primary activation involves formation of NHC-CO_2 adduct from NHC and CO_2. Further reduction of CO_2 to give a formoxysilane intermediate is established as rate limiting. NHC catalyst shows electronic effect to promote hydridic H transfer from silane to the adduct and generates a methoxide end product.

In 2012, Muller et al. reported reduction of CO_2 to formic acid and methanol with trialkylsilanes by stoichiometric amount of trityl borate $[Ph_3C][B(C_6F_5)_4]$ under ambient conditions [75]. The reaction pathway was established according to the experimental results and DFT calculations (Scheme 4.31). The reaction of R_3SiH and $[Ph_3C][B(C_6F_5)_4]$ in PhCl generated chloronium species 63, which was treated with CO_2 and trialkylsilane to produce the formate derivative 65 via an intermediate 64. When triisopropylsilane was used, 65a is the sole product. However, replacement of triisopropylsilane with less bulky triethylsilane led to a mixture of 65b and 67b which can provide FA and MeOH by simple hydrolysis.
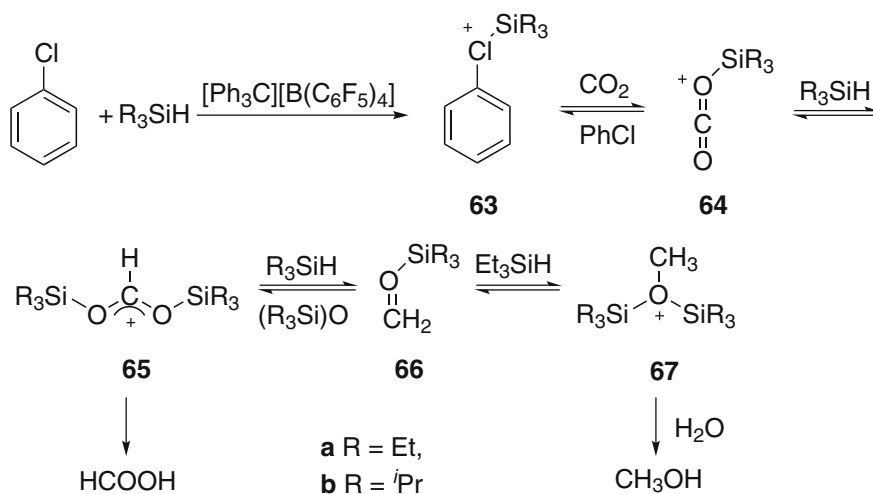
Scheme 4.31 Reduction of CO_2 by $[Ph_3C][B(C_6F_5)_4]$ in PhCl

$$\text{Ph}_2\text{SiH}_2 \xrightarrow[\text{1.25 mol\% } \textbf{68}, \text{ DMF}]{\text{5 atm CO}_2,\ 2\text{h}} \begin{array}{c} \text{HCOO[Si] (97\%)} \\ + \\ \text{[Si]OCH}_2\text{O[Si] (2\%)} \\ + \\ \text{CH}_3\text{O[Si] (1\%)} \end{array} \xrightarrow[\text{36 h}]{\text{Ph}_2\text{SiH}_2} \begin{array}{c} \text{CH}_3\text{O[Si]} \\ \\ 99\% \end{array}$$

68   **69**   **70**
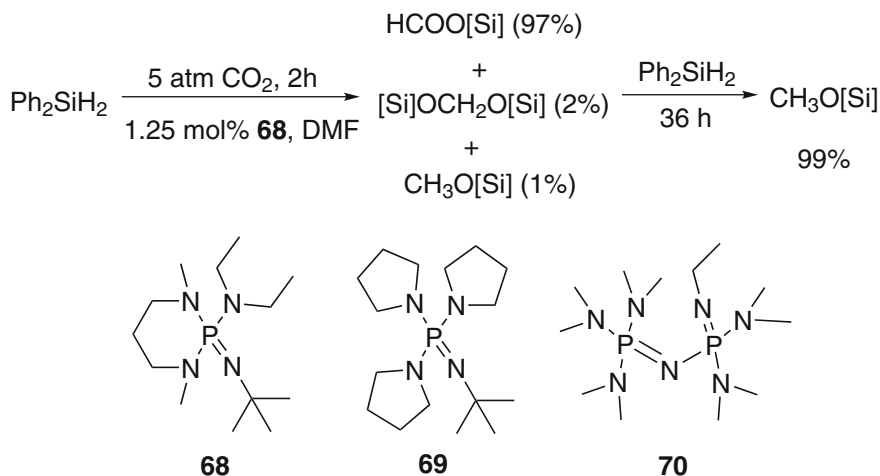
Scheme 4.32 Reduction of CO_2 with silane in the presence of phosphazene superbases

In 2015, Fontaine et al. reported a series of commercially available phosphazene superbases **68–69** for reduction of CO_2 with silanes to methanol [76]. The mixture of formylsilanes, acetalsilanes and methoxysilanes were formed when Ph_2SiH_2 reacted with 5 atm CO_2 in presence of 1.25 mol% **68** in DMF after 2 h (Scheme 4.32). Addition of Ph_2SiH_2 led the further reduction of formylsilanes and acetalsilanes to methoxysilanes after 36 h. An approximate TON of 76 for MeOH were obtained in CH_3CN solvent after 24 h. Interestingly, it was found that *N,N*-dimethylformamide (DMF) can acts as a catalyst for the hydrosilylation of CO_2.

4.4.3 Hydrogen as Reductant

Compared to the relatively high cost boranes and silanes, H_2 is a more attractive reducing agent since it is more potential for industry application. However metal complex catalyzed direct CO_2 hydrogenation to MeOH is rather difficult as above mentioned. FLP are reported to be effective to cleave H_2 heterolytically [77–81]. FLP mediated CO_2 hydrogenation using H_2 as a reductant is an attractive and challenging method for CO_2 hydrogenation to MeOH.

In 2009, Ashley, O'Hare, and co-workers reported the first MeOH production from H_2/CO_2 under metal-free conditions [82]. Heterolytic cleavage of H_2 by an equimolar mixture of 2,2,6,6-tetramethylpiperidine (TMP) and $B(C_6F_5)_3$ gave a salt [TMPH][HB(C_6F_5)$_3$] (**71**). The reaction of CO_2 and **71** in toluene at 100 °C generated a formatoborate complex [TMPH][HCO$_2$B(C_6F_5)$_3$] (**72**) in quantitative yield. Based on the NMR and MS studies, a mechanism was proposed. $B(C_6F_5)_3$ attacks
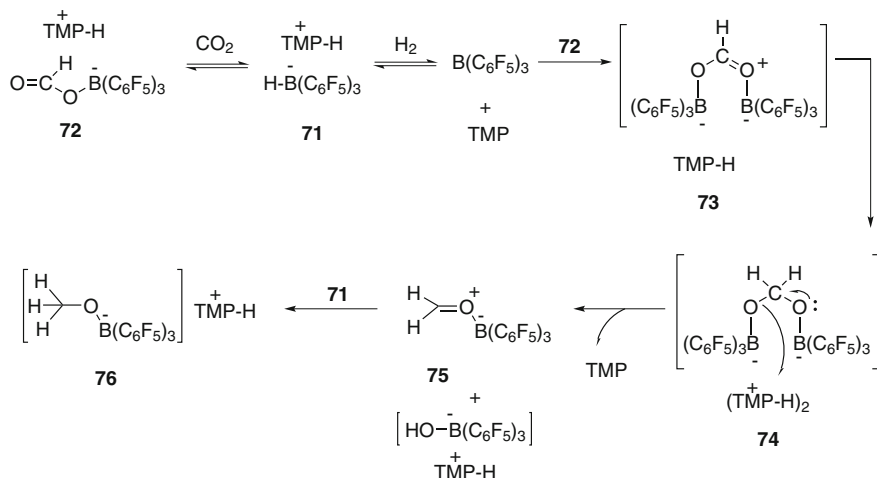
Scheme 4.33 CO_2 hydrogenation to methoxide with TMP/B(C_6F_5)$_3$

on the acyl oxygen atom of **72** resulting in an intermediate A (Scheme 4.33). Further reduction of the activated formate **73** by an equivalent of **71** affords the formaldehyde acetal (intermediate **74**) which cleaves by [TMPH]$^+$ to give intermediate **75**. Final hydride reduction of **75** by **71** forms [TMPH][(MeO)B(C_6F_5)$_3$] **76**. MeOH may forms by reaction of $CH_3OB(C_6F_5)_2$ with TMP or its conjugate acid. The conversion of **73–74** is supposed to be rate-determining. The reduction of CO_2 (1 equiv) by a 1:1 mixture of TMP/B(C_6F_5)$_3$ (4 equiv) in toluene-d_8 under an H_2 atmosphere led to quantitative conversion into $CH_3OB(C_6F_5)_2$ after 6 days at 160 °C. Remarkably, CH_3OH was isolated in 17–25% yield by direct vacuum distillation of the solvent at 100 °C with no requirement of hydrolysis.

In 2015, Stephan and Fontaine et al. synthesized two intramolecular B/N frustrated Lewis pairs **77** and **78** for hydrogenation of CO_2 to methanol level [19]. According to experimental study and DFT calculation, both **77** and **78** can be converted into a stable dimer **80** in the presence of H_2 through two consecutive steps of H_2 splitting and protodeborylation (Scheme 4.34). **80** exhibited no reactivity in the CO_2 reduction due to its dimeric nature, while the reaction using **78** exclusively generated acetal species $BOCH_2OB$ at room temperature. Therefore, the first protodeborylation step is believed to be required prior to CO_2 reduction. The reaction of **77** and **78** with 1 atm H_2 and 4 atm CO_2 afforded formate, acetal, and methoxide derivatives at 80 °C. The author also investigated the hydrogenation of CO_2 with **77** by DFT calculation. It was found that the reaction of **79** and CO_2 undergoes concerted transfer proton and hydride from N–H and B–H to O and C of CO_2, respectively. This TS is reminiscent of bifunctional metal-based complex for CO_2 activation.
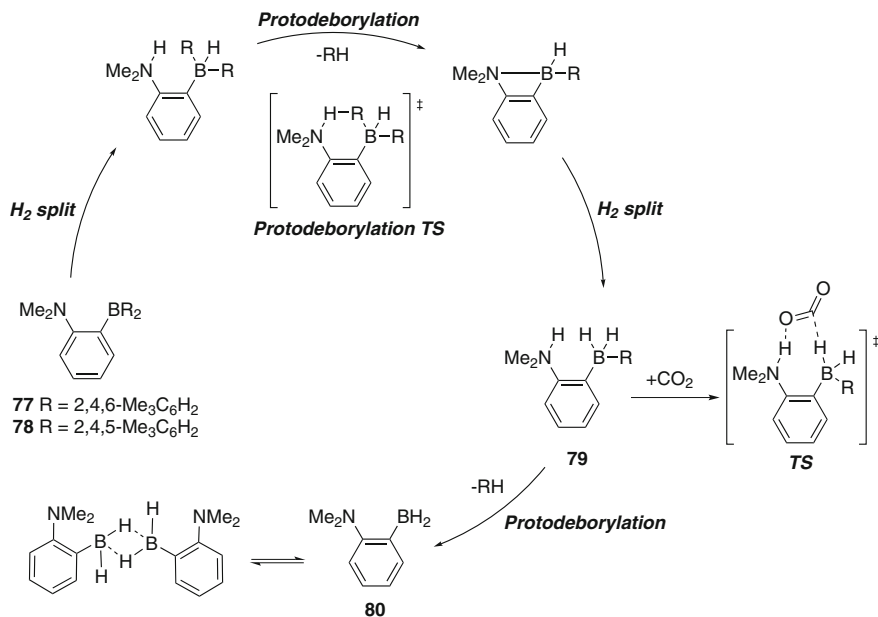
Scheme 4.34 Proposed mechanism of H$_2$ activation and protodeborylation

References

1. Olah GA, Goeppert A, Prakash GKS (2009) Chemical recycling of carbon dioxide to methanol and dimethyl ether: from greenhouse gas to renewable, environmentally carbon neutral fuels and synthetic hydrocarbons. J Org Chem 74(2):487–498. doi:10.1021/jo801260f
2. Miller AJ, Heinekey DM, Mayer JM, Goldberg KI (2013) Catalytic disproportionation of formic acid to generate methanol. Angew Chem Int Ed 52(14):3981–3984. doi:10.1002/anie.201208470
3. Savourey S, Lefevre G, Berthet J-C, Thuery P, Genre C, Cantat T (2014) Efficient disproportionation of formic acid to methanol using molecular ruthenium catalysts. Angew Chem Int Ed 53(39):10466–10470. doi:10.1002/anie.201405457
4. Sasayama AF, Moore CE, Kubiak CP (2016) Electronic effects on the catalytic disproportionation of formic acid to methanol by [Cp*Ir(III)(R-bpy)Cl]Cl complexes. Dalton Trans 45 (6):2436–2439. doi:10.1039/c5dt04606h
5. Sordakis K, Tsurusaki A, Iguchi M, Kawanami H, Himeda Y, Laurenczy G (2016) Carbon dioxide to methanol: the aqueous catalytic way at room temperature. Chem—Eur J 22 (44):15605–15608. doi:10.1002/chem.201603407
6. Chauvier C, Thuéry P, Cantat T (2016) Metal-free disproportionation of formic acid mediated by organoboranes. Chem Sci 7(9):5680–5685. doi:10.1039/c6sc01410k
7. Huff CA, Sanford MS (2011) Cascade catalysis for the homogeneous hydrogenation of CO$_2$ to methanol. J Am Chem Soc 133(45):18122–18125. doi:10.1021/ja208760j
8. Wesselbaum S, Moha V, Meuresch M, Brosinski S, Thenert KM, Kothe J, Tv Stein, Englert U, Holscher M, Klankermayer J, Leitner W (2015) Hydrogenation of carbon dioxide to methanol using a homogeneous ruthenium-triphos catalyst: from mechanistic investigations to multiphase catalysis. Chem Sci 6(1):693–704. doi:10.1039/C4SC02087A

9. Krocher O, Koppel RA, Baiker A (1997) Highly active ruthenium complexes with bidentate phosphine ligands for the solvent-free catalytic synthesis of *N,N*-dimethylformamide and methyl formate. Chem Commun (5):453–454. doi:10.1039/A608150I

10. Kothandaraman J, Goeppert A, Czaun M, Olah GA, Prakash GK (2016) Conversion of CO$_2$ from air into methanol using a polyamine and a homogeneous ruthenium catalyst. J Am Chem Soc 138(3):778–781. doi:10.1021/jacs.5b12354

11. Chakraborty S, Zhang J, Krause JA, Guan H (2010) An efficient nickel catalyst for the reduction of carbon dioxide with a borane. J Am Chem Soc 132(26):8872–8873. doi:10.1021/ja103982t

12. Chakraborty S, Patel YJ, Krause JA, Guan H (2012) Catalytic properties of nickel bis (phosphinite) pincer complexes in the reduction of CO$_2$ to methanol derivatives. Polyhedron 32(1):30–34. doi:10.1016/j.poly.2011.04.030

13. Ma Q-Q, Liu T, Li S, Zhang J, Chen X, Guan H (2016) Highly efficient reduction of carbon dioxide with a borane catalyzed by bis(phosphinite) pincer ligated palladium thiolate complexes. Chem Commun 52(99):14262–14265. doi:10.1039/C6CC07987C

14. Liu T, Meng W, Ma Q-Q, Zhang J, Li H, Li S, Zhao Q, Chen X (2017) Hydroboration of CO$_2$ catalyzed by bis(phosphinite) pincer ligated nickel thiolate complexes. Dalton Trans 46 (14):4504–4509. doi:10.1039/C7DT00490G

15. Jana A, Tavcar G, Roesky HW, John M (2010) Germanium(II) hydride mediated reduction of carbon dioxide to formic acid and methanol with ammonia borane as the hydrogen source. Dalton Trans 39(40):9487–9489. doi:10.1039/c0dt00921k

16. Anker MD, Arrowsmith M, Bellham P, Hill MS, Kociok-Köhn G, Liptrot DJ, Mahon MF, Weetman C (2014) Selective reduction of CO$_2$ to a methanol equivalent by B(C$_6$F$_5$)$_3$-activated alkaline earth catalysis. Chem Sci 5(7):2826–2830. doi:10.1039/c4sc00885e

17. Lu Z, Williams TJ (2016) Di(carbene)-supported nickel systems for CO$_2$ reduction under ambient conditions. ACS Catal 6(10):6670–6673. doi:10.1021/acscatal.6b02101

18. Hadlington TJ, Kefalidis CE, Maron L, Jones C (2017) Efficient reduction of carbon dioxide to methanol equivalents catalyzed by two-coordinate amido–germanium(II) and –Tin(II) hydride complexes. ACS Catal 7(3):1853–1859. doi:10.1021/acscatal.6b03306

19. Courtemanche MA, Pulis AP, Rochette E, Legare MA, Stephan DW, Fontaine FG (2015) Intramolecular B/N frustrated Lewis pairs and the hydrogenation of carbon dioxide. Chem Commun 51(48):9797–9800. doi:10.1039/c5cc03072b

20. Courtemanche MA, Legare MA, Maron L, Fontaine FG (2013) A highly active phosphine-borane organocatalyst for the reduction of CO$_2$ to methanol using hydroboranes. J Am Chem Soc 135(25):9326–9329. doi:10.1021/ja404585p

21. Courtemanche M-A, Larouche J, Légaré M-A, Bi W, Maron L, Fontaine F-G (2013) A Tris (triphenylphosphine)aluminum ambiphilic precatalyst for the reduction of carbon dioxide with catecholborane. Organometallics 32(22):6804–6811. doi:10.1021/om400645s

22. Legare MA, Courtemanche MA, Fontaine FG (2014) Lewis base activation of borane-dimethylsulfide into strongly reducing ion pairs for the transformation of carbon dioxide to methoxyboranes. Chem Commun 50(77):11362–11365. doi:10.1039/c4cc04857a

23. Ho SY, So CW, Saffon-Merceron N, Mezailles N (2015) Formation of a zwitterionic boronium species from the reaction of a stable carbenoid with borane: CO$_2$ reduction. Chem Commun 51(11):2107–2110. doi:10.1039/c4cc09239b

24. Menard G, Stephan DW (2010) Room temperature reduction of CO$_2$ to methanol by Al-based frustrated Lewis pairs and ammonia borane. J Am Chem Soc 132(6):1796–1797. doi:10.1021/ja9104792

25. Wang T, Stephan DW (2014) Carbene-9-BBN ring expansions as a route to intramolecular frustrated Lewis pairs for CO$_2$ reduction. Chem–Eur J 20(11):3036–3039. doi:10.1002/chem.201304870

26. Das Neves Gomes C, Blondiaux E, Thuery P, Cantat T (2014) Metal-free reduction of CO$_2$ with hydroboranes: two efficient pathways at play for the reduction of CO$_2$ to methanol. Chem–Eur J 20(23):7098–7106. doi:10.1002/chem.201400349

27. Yang Y, Xu M, Song D (2015) Organocatalysts with carbon-centered activity for CO_2 reduction with boranes. Chem Commun 51(56):11293–11296. doi:10.1039/C5CC04337A

28. Blondiaux E, Pouessel J, Cantat T (2014) Carbon dioxide reduction to methylamines under metal-free conditions. Angew Chem Int Ed 53(45):12186–12190. doi:10.1002/anie.201407357

29. Tlili A, Voituriez A, Marinetti A, Thuery P, Cantat T (2016) Synergistic effects in ambiphilic phosphino-borane catalysts for the hydroboration of CO_2. Chem Commun 52(48):7553–7555. doi:10.1039/c6cc02809h

30. Fujiwara K, Yasuda S, Mizuta T (2014) Reduction of CO_2 to trimethoxyboroxine with BH_3 in THF. Organometallics 33(22):6692–6695. doi:10.1021/om5008488

31. Riduan SN, Zhang Y, Ying JY (2009) Conversion of carbon dioxide into methanol with silanes over N-heterocyclic carbene catalysts. Angew Chem Int Ed 48(18):3322–3325. doi:10.1002/anie.200806058

32. Balaraman E, Gunanathan C, Zhang J, Shimon LJW, Milstein D (2011) Efficient hydrogenation of organic carbonates, carbamates and formates indicates alternative routes to methanol based on CO_2 and CO. Nat Chem 3(8):609–614. doi:10.1038/nchem.1089

33. Han Z, Rong L, Wu J, Zhang L, Wang Z, Ding K (2012) Catalytic hydrogenation of cyclic carbonates: a practical approach from CO_2 and epoxides to methanol and diols. Angew Chem Int Ed 51(52):13041–13045. doi:10.1002/anie.201207781

34. Balaraman E, Gnanaprakasam B, Shimon LJW, Milstein D (2010) Direct hydrogenation of amides to alcohols and amines under mild conditions. J Am Chem Soc 132(47):16756–16758. doi:10.1021/ja1080019

35. Balaraman E, Ben-David Y, Milstein D (2011) Unprecedented catalytic hydrogenation of urea derivatives to amines and methanol. Angew Chem Int Ed 50(49):11702–11705. doi:10.1002/anie.201106612

36. Rezayee NM, Huff CA, Sanford MS (2015) Tandem amine and ruthenium-catalyzed hydrogenation of CO_2 to methanol. J Am Chem Soc 137(3):1028–1031. doi:10.1021/ja511329m

37. Ren DZ, Song ZY, Fu J, Huo ZB (2015) Application of diverse hydrogen sources to methanol synthesis from CO_2. In: Advances in CO_2 capture, sequestration, and conversion, vol 1194, pp 109–122. doi:10.1021/bk-2015-1194.ch004

38. Li Y-N, Ma R, He L-N, Diao Z-F (2014) Homogeneous hydrogenation of carbon dioxide to methanol. Catal Sci Tech 4(6):1498–1512. doi:10.1039/c3cy00564j

39. Huang F, Zhang C, Jiang J, Wang ZX, Guan H (2011) How does the nickel pincer complex catalyze the conversion of CO_2 to a methanol derivative? A computational mechanistic study. Inorg Chem 50(8):3816–3825. doi:10.1021/ic200221a

40. Bontemps S, Vendier L, Sabo-Etienne S (2012) Borane-mediated carbon dioxide reduction at ruthenium: formation of C_1 and C_2 compounds. Angew Chem Int Ed 51(7):1671–1674. doi:10.1002/anie.201107352

41. Sgro MJ, Stephan DW (2012) Frustrated lewis pair inspired carbon dioxide reduction by a ruthenium tris(aminophosphine) complex. Angew Chem Int Ed 51(45):11343–11345. doi:10.1002/anie.201205741

42. Tan G, Wang W, Blom B, Driess M (2014) Mechanistic studies of CO_2 reduction to methanol mediated by an N-heterocyclic germylene hydride. Dalton Trans 43(16):6006–6011. doi:10.1039/c3dt53321b

43. Fontaine F-G, Stephan DW (2017) Metal-free reduction of CO_2. Curr Opin Green and Sustain Chem 3:28–32. doi:10.1016/j.cogsc.2016.11.004

44. Fontaine FG, Courtemanche MA, Legare MA (2014) Transition-metal-free catalytic reduction of carbon dioxide. Chem–Eur J 20(11):2990–2996. doi:10.1002/chem.201304376

45. Sordakis K, Tang C, Vogt LK, Junge H, Dyson PJ, Beller M, Laurenczy G (2017) Homogeneous catalysis for sustainable hydrogen storage in formic acid and alcohols. Chem Rev doi:10.1021/acs.chemrev.7b00182

46. Roy L, Zimmerman PM, Paul A (2011) Changing lanes from concerted to stepwise hydrogenation: the reduction mechanism of frustrated Lewis acid-base pair trapped CO$_2$ to methanol by ammonia-borane. Chem–Eur J 17(2):435–439. doi:10.1002/chem.201002282

47. Lim CH, Holder AM, Hynes JT, Musgrave CB (2013) Roles of the lewis acid and base in the chemical reduction of CO$_2$ catalyzed by frustrated lewis pairs. Inorg Chem 52(17):10062–10066. doi:10.1021/ic4013729

48. Menard G, Stephan DW (2013) CO$_2$ reduction via aluminum complexes of ammonia boranes. Dalton Trans 42(15):5447–5453. doi:10.1039/c3dt00098b

49. Declercq R, Bouhadir G, Bourissou D, Légaré M-A, Courtemanche M-A, Nahi KS, Bouchard N, Fontaine F-G, Maron L (2015) Hydroboration of carbon dioxide using ambiphilic phosphine-borane catalysts: on the role of the formaldehyde adduct. ACS Catal 5 (4):2513–2520. doi:10.1021/acscatal.5b00189

50. Farrell JM, Hatnean JA, Stephan DW (2012) Activation of hydrogen and hydrogenation catalysis by a borenium cation. J Am Chem Soc 134(38):15728–15731. doi:10.1021/ja307995f

51. Wang T, Stephan DW (2014) Phosphine catalyzed reduction of CO$_2$ with boranes. Chem Commun 50(53):7007–7010. doi:10.1039/C4CC02103G

52. González-Sebastián L, Flores-Alamo M, García JJ (2015) Selective N-methylation of aliphatic amines with CO$_2$ and hydrosilanes using nickel-phosphine catalysts. Organometallics 34(4):763–769. doi:10.1021/om501176u

53. Motokura K, Kashiwame D, Miyaji A, Baba T (2012) Copper-catalyzed formic acid synthesis from CO$_2$ with hydrosilanes and H$_2$O. Org Lett 14(10):2642–2645. doi:10.1021/ol301034j

54. Motokura K, Naijo M, Yamaguchi S, Miyaji A, Baba T (2015) Reductive transformation of CO$_2$ with hydrosilanes catalyzed by simple fluoride and carbonate salts. Chem Lett 44 (9):1217–1219. doi:10.1246/cl.150510

55. Ren X, Zheng Z, Zhang L, Wang Z, Xia C, Ding K (2017) Rhodium-complex-catalyzed hydroformylation of olefins with CO$_2$ and hydrosilane. Angew Chem Int Ed 56(1):310–313. doi:10.1002/anie.201608628

56. Riduan SN, Zhang Y, Ying JY (2009) Conversion of carbon dioxide into methanol with silanes over N-heterocyclic carbene catalysts. Angew Chem 121(18):3372–3375. doi:10.1002/ange.200806058

57. Mukherjee D, Sauer DF, Zanardi A, Okuda J (2016) Selective metal-free hydrosilylation of CO$_2$ catalyzed by triphenylborane in highly polar, aprotic solvents. Chem–Eur J 22(23):7730–7733. doi:10.1002/chem.201601006

58. Jansen A, Gorls H, Pitter S (2000) Trans-[Ru^{II}Cl(MeCN)$_5$][Ru^{III}Cl$_4$(MeCN)$_2$]: a reactive intermediate in the homogeneous catalyzed hydrosilylation of carbon dioxide. Organometallics 19(2):135–138. doi:10.1021/om990654k

59. Ken Motokura DK, Miyaji Akimitsu, Baba Toshihide (2012) Copper-catalyzed formic acid synthesis from CO$_2$ with hydrosilanes and H$_2$O. Org Lett 14(10):2642–2645. doi:10.1021/ol301034j

60. Lalrempuia R, Iglesias M, Polo V, Sanz Miguel PJ, Fernandez-Alvarez FJ, Perez-Torrente JJ, Oro LA (2012) Effective fixation of CO$_2$ by iridium-catalyzed hydrosilylation. Angew Chem Int Ed 51(51):12824–12827. doi:10.1002/anie.201206165

61. Itagaki S, Yamaguchi K, Mizuno N (2013) Catalytic synthesis of silyl formates with 1 atm of CO$_2$ and their utilization for synthesis of formyl compounds and formic acid. J Mol Catal A-Chem 366:347–352. doi:10.1016/j.molcata.2012.10.014

62. Park S, Bezier D, Brookhart M (2012) An efficient iridium catalyst for reduction of carbon dioxide to methane with trialkylsilanes. J Am Chem Soc 134(28):11404–11407. doi:10.1021/ja305318c

63. Scheuermann ML, Semproni SP, Pappas I, Chirik PJ (2014) Carbon dioxide hydrosilylation promoted by cobalt pincer complexes. Inorg Chem 53(18):9463–9465. doi:10.1021/ic501901n

64. Berkefeld A, Piers WE, Parvez M, Castro L, Maron L, Eisenstein O (2013) Decamethylscandocinium-hydrido-(perfluorophenyl)borate: fixation and tandem tris

(perfluorophenyl)borane catalysed deoxygenative hydrosilation of carbon dioxide. Chem Sci 4(5):2152–2162. doi:10.1039/C3SC50145K

65. LeBlanc FA, Piers WE, Parvez M (2014) Selective hydrosilation of CO_2 to a bis(silylacetal) using an anilido bipyridyl-ligated organoscandium catalyst. Angew Chem Int Ed 53(3):789–792. doi:10.1002/anie.201309094

66. Eisenschmid TC, Eisenberg R (1989) The iridium complex catalyzed reduction of carbon-dioxide to methoxide by alkylsilanes. Organometallics 8(7):1822–1824. doi:10.1021/om00109a041

67. Matsuo T, Kawaguchi H (2006) From carbon dioxide to methane: homogeneous reduction of carbon dioxide with hydrosilanes catalyzed by zirconium-borane complexes. J Am Chem Soc 128(38):12362–12363. doi:10.1021/ja0647250

68. Berkefeld A, Piers WE, Parvez M (2010) Tandem frustrated lewis Pair/Tris(pentafluorophenyl)borane-catalyzed deoxygenative hydrosilylation of carbon dioxide. J Am Chem Soc 132(31):10660–10661. doi:10.1021/ja105320c

69. Khandelwal M, Wehmschulte RJ (2012) Deoxygenative reduction of carbon dioxide to methane, toluene, and diphenylmethane with $[Et_2Al]^+$ as catalyst. Angew Chem Int Ed 51 (29):7323–7326. doi:10.1002/anie.201201282

70. Mitton SJ, Turculet L (2012) Mild reduction of carbon dioxide to methane with tertiary silanes catalyzed by platinum and palladium silyl pincer complexes. Chem–Eur J 18 (48):15258–15262. doi:10.1002/chem.201203226

71. Koinuma H, Kawakami F, Kato H, Hirai H (1981) Hydrosilylation of carbon-dioxide catalyzed by ruthenium complexes. Chem Commun 5:213–214. doi:10.1039/C39810000213

72. Metsänen TT, Oestreich M (2015) Temperature-dependent chemoselective hydrosilylation of carbon dioxide to formaldehyde or methanol oxidation state. Organometallics 34(3):543–546. doi:10.1021/om501279a

73. Riduan SN, Ying JY, Zhang Y (2013) Mechanistic insights into the reduction of carbon dioxide with silanes over N-heterocyclic carbene catalysts. ChemCatChem 5(6):1490–1496. doi:10.1002/cctc.201200721

74. Huang F, Lu G, Zhao L, Li H, Wang Z-X (2010) The catalytic role of N-heterocyclic carbene in a metal-free conversion of carbon dioxide into methanol: a computational mechanism study. J Am Chem Soc 132(35):12388–12396. doi:10.1021/ja103531z

75. Schäfer A, Saak W, Haase D, Muller T (2012) Silyl cation mediated conversion of CO_2 into benzoic acid, formic acid, and methanol. Angew Chem Int Ed 51(12):2981–2984. doi:10.1002/anie.201107958

76. Courtemanche MA, Legare MA, Rochette E, Fontaine FG (2015) Phosphazenes: efficient organocatalysts for the catalytic hydrosilylation of carbon dioxide. Chem Commun 51 (31):6858–6861. doi:10.1039/c5cc01282a

77. Welch GC, San Juan RR, Masuda JD, Stephan DW (2006) Reversible, metal-free hydrogen activation. Science 314(5802):1124–1126. doi:10.1126/science.1134230

78. Welch GC, Stephan DW (2007) Facile heterolytic cleavage of dihydrogen by phosphines and boranes. J Am Chem Soc 129(7):1880–1881. doi:10.1021/ja067961j

79. Chase PA, Stephan DW (2008) Hydrogen and amine activation by a frustrated lewis pair of a bulky N-heterocyclic carbene and $B(C_6F_5)_3$. Angew Chem Int Ed 47(39):7433–7437. doi:10.1002/anie.200802596

80. Sumerin V, Schulz F, Atsumi M, Wang C, Nieger M, Leskelä M, Repo T, Pyykkö P, Rieger B (2008) Molecular tweezers for hydrogen: synthesis, characterization, and reactivity. J Am Chem Soc 130(43):14117–14119. doi:10.1021/ja806627s

81. Sumerin V, Schulz F, Nieger M, Leskelä M, Repo T, Rieger B (2008) Facile heterolytic H_2 activation by amines and $B(C_6F_5)_3$. Angew Chem Int Ed 47(32):6001–6003. doi:10.1002/anie.200800935

82. Ashley AE, Thompson AL, O'Hare D (2009) Non-metal-mediated homogeneous hydrogenation of CO_2 to CH_3OH. Angew Chem Int Ed 48(52):9839–9843. doi:10.1002/anie.200905466

Chapter 5
Transformation of CO_2 to Methanol Over Heterogeneous Catalysts

Abstract Hydrogenation of CO_2 to methanol over heterogeneous catalysts usually requires hash conditions. Various heterogeneous catalysts based on Cu, Pd, Ni, Ag, Au, In, and other metals have been recently developed and investigated. Cu doped by other metals or metal oxides are the preferred selection. Besides metal itself, catalyst morphology, which is generally influenced by the method of preparation and calcination, is crucial for reaction conversion and selectivity. The relationship between catalyst characteristics and catalyst performance is discussed.

Keywords CO_2 hydrogenation · Heterogeneous catalyst · Methanol · Support Co-precipitation · Calcination · Specific surface area · Morphology

Methanol synthesis through CO_2 hydrogenation over heterogeneous catalysts has been extensively investigated since it was first established in the 1960s given its high industrial relevance. Several excellent reviews on the catalytic hydrogenation of CO_2 over heterogeneous catalysts have been published [1–4]. Over the past few decades, various heterogeneous catalysts have been prepared and used for the hydrogenation of CO_2 to methanol. The state of the art of the hydrogenation of CO_2 to methanol over heterogeneous catalysts is presented in this chapter.

5.1 Cu-Based Catalysts

The hydrogenation of CO_2 to methanol over Cu-based catalysts has been widely reported (Table 5.1). Sun et al. prepared a ZrO_2-doped CuZnO catalyst (Zr–Cu/ZnO) through a successive precipitation method. They found that the presence of ZrO_2 increases the dispersion of copper in a manner distinctive from that of CuZnO [5]. Using Zr–CuO/ZnO as a catalyst under 250 °C, 5 MPa, space velocity (SV) of 4000 h^{-1} and 3:1 molar ratio of H_2/CO_2 provide 26.4% CO_2 conversion and 0.22 g mL^{-1} h^{-1} methanol yield. By contrast, under the same conditions, only 16% CO_2 conversion and 0.14 g mL^{-1} h^{-1} methanol yield are achieved when CuO/ZnO

Table 5.1 Transformation of CO_2 to methanol with Cu-based heterogeneous catalysts

Catalyst	Pressure/ MPa	SV/[mL/(h g) or h^{-1}]	Flow rate/ (mL/min)	T/°C	Selectivity/%			Conversion/%	MeOH yield	H$_2$/CO$_2$	References
					CO	CH$_3$OH	CH$_4$				
ZrO$_2$ doped CuZnO	5.0	4000	–	250	39.55	60.45	0.01	26.41	0.22 g mL^{-1} h^{-1}	3	[5]
12Cu10Zr/γ-Al$_2$O$_3$	3.0	1800	–	240	77.40	17.10	5.50	14.30	–	3	[6]
Cu/ZnO/ZrO$_2$	3.0	–	50	250	–	29.30	–	19.40	–	3	[7]
Cu/Zn/Al/Zr	4.0	9742		240	38.99	61.01	–	20.51	0.435 g mL^{-1} h^{-1}	3	[8]
Cu–ZnO/ZrO$_2$	3.0	4400	–	240	–	48.40	–	17.50	–	3	[9]
Cu–V/γ-Al$_2$O$_3$	3.0	3600	–	240	63.50	24.80	11.70	14.10	–	3	[10]
Cu/ZnO(Al$_2$O$_3$)	5.0	–	20	170	27.10	72.90	0	25.90	–	3	[11]
Cu–ZnO/ZrO$_2$	1.0	8800	–	200	–	64.70	–	3.20	–	3	[12]
CuO/ZnO/ZrO$_2$ (CZZ)	3.0	3600	–	240	–	56.20	–	17.00	9.6%	3	[13]
CuO/ZnO/ZrO$_2$ (CZZ)	3.0	3600	–	220	–	71.10	–	12.00	8.5%	3	[14]
Cu/ZrO$_2$	2.0	5400	–	250	16.52	83.48	0	13.60	1.76 mmol g^{-1} h^{-1}	3	[15]
Cu/ZnO/Al$_2$O$_3$	–	–	50	220	–	–	–	–	–	1	[16]
Cu/ZnAl$_2$O$_4$	4.0	–	–	260	–	93.00	–	–	233 g g$_{cat}^{-1}$ h^{-1}	3	[17]
Cu/ZnO/ZrO$_2$	3.0	3600	–	240	–	58.00	–	15.70	9.1%	3	[18]
Cu/ZnO/Al$_2$O$_3$	3.0	12,000	–	240	–	41.00	–	12.00	212 g L$_{cat}^{-1}$ h^{-1}	3	[19]
La-Cu/ZrO$_2$	3.0	3600	–	220	34.00	66.00	–	6.20	4.3%	3	[20]
5% Au–20% Cu/Cr$_2$O$_3$:3Al$_2$O$_3$	4.0	–	–	260	–	93.00	–	–	66 g kg$_{cat}^{-1}$ h^{-1}	3	[21]
ZnOCu/CeZrO$_2$	3.0	8800	–	240	–	51.00	–	16.90	–	3	[22]
2 wt% SiO$_2$–TiO$_2$/ CuO–ZnO–Al$_2$O$_3$	2.6	3600	–	260	58.83	41.17	–	40.70	16.8%	3	[23]
Cu/ZnO	0.7	2400	–	140–160	–	100	–	–	–	9	[24]

(continued)

Table 5.1 (continued)

Catalyst	Pressure/MPa	SV/[mL/(h g) or h⁻¹]	Flow rate/(mL/min)	T/°C	Selectivity/%			Conversion/%	MeOH yield	H₂/CO₂	References
					CO	CH₃OH	CH₄				
Cu/Zn/Al/Y	5.0	12,000	–	250	52.40	47.10	–	26.90	$0.52\ \mathrm{g\ g_{cat}^{-1}\ h^{-1}}$	3	[25]
Cu–ZnO/ZrO₂	5.0	8800–55,000	–	240	–	64.00	–	22.40	14.3%	3	[26]
Cu–ZnO–ZrO₂	7.0	1500	–	250	28.00	72.00	–	22.00	$22\ \mathrm{mol\ kg_{cat}^{-1}\ h^{-1}}$	3	[27]
Cu/ZnO/Al₂O₃	36	182.000	–	260	–	77.30	–	65.80	$7.7\ \mathrm{g\ g_{cat}^{-1}\ h^{-1}}$	10	[28]
Cu–ZrO₂/CNF	3.0	–	–	170	–	–	–	–	$4.28\ \mathrm{g\ kg_{cat}^{-1}\ h^{-1}}$	3	[29]
Cu/ZnO/Al₂O₃/Y₂O₃	9.0	10,000	–	230	–	89.70	–	29.90	$0.57\ \mathrm{g\ g_{cat}^{-1}\ h^{-1}}$	73/24	[30]
Cu/CrCuO₄ and Cu/Mo₂C	4.0	–	–	135	–	77.00	–	–	–	3 (V:V)	[31]
Cu–ZnO–ZrO₂–MgO/Al₂O₃	2.0	1400	–	250	61.61	35.98	2.41	12.12	$31\ \mathrm{g\ kg_{cat}^{-1}\ h^{-1}}$	3	[32]
CuO/ZnO-filament	3.0	0.54 mol/(g_cat h)	–	240	–	78.20	–	16.50	$0.55\ \mathrm{g\ g_{cat}^{-1}\ h^{-1}}$	3	[33]
CuO–ZnO	3.0	2400	30	240	–	43.80	–	17.40	7.6%	3	[34]
Cu/HAl	3.0	–	60	280	–	21.70	–	15.00	–	3	[35]
CuO–ZnO–ZrO₂	3.0	3600	–	240	–	54.10	–	12.10	6.5%	3	[36]
(CuZnGa)ₘw	3.0	3000	–	270	69.80	29.70	0.54	15.90	$4241\ \mathrm{mmol\ kg_{cat}^{-1}\ h^{-1}}$	3	[37]
Cu₂Zn₁Al₁.₂Zr₀.₁	9.0	4000	–	250	–	84.60	–	36.50	$0.45\ \mathrm{g\ g_{cat}^{-1}\ h^{-1}}$	73/24	[38]
Cu/ZnO/Al₂O₃	3.0	–	100	250	–	–	–	–	–	–	[39]
Cu–ZnO	3.0	18,000	150	250	–	–	–	–	–	3	[40]
core-shell Cu/ZnO@m-SiO₂	5.0	6000	–	270	23.00	61.80	5.2	11.90	$153.9\ \mathrm{g\ kg_{cat}^{-1}\ h^{-1}}$	73/24	[41]
Cu/β-Mo₂C	2.0	–	30	300	35.00	26.00	27.00	28.00	–	5	[42]

(continued)

Table 5.1 (continued)

Catalyst	Pressure/ MPa	SV/[mL/(h g) or h^{-1}]	Flow rate/ (mL/min)	T/°C	Selectivity/%			Conversion/%	MeOH yield	H$_2$/CO$_2$	References
					CO	CH$_3$OH	CH$_4$				
Pd/Mo$_2$C	4.0	–	–	200	9.60	68.00	7.60	97.00	–	3	[43]
Cu-ZrO$_2$	3.0	–	60	250	–	–	–	–	–	3	[44]
Cu-ZnO/Al$_2$O$_3$(i)	5.0	–	–	270	–	100.00	–	9.00	–	3	[45]
Cu/Zn/Al/Zr fibrous	5.0	6000	–	250	–	17.80	–	25.50	–	3	[46]
Cu/ZnO/ZrO$_2$	5.0	4600	–	270	43.20	56.80	–	23.00	0.21 g mL^{-1} h^{-1}	3	[47]
CuZn/rGO	1.5	2400	–	250	33.90	5.10	7.1	26.00	424 mg g$_{cat}^{-1}$ h^{-1}	3	[48]
CuO–ZnO–ZrO$_2$	2.0	–	–	240	–	32.30	–	13.20	219.7 g kg$_{cat}^{-1}$ h^{-1}	3	[49]
Cu/ZnO/Al$_2$O$_3$	44.2	100,000	–	280	–	91.90	–	65.30	15.3 g g$_{cat}^{-1}$ h^{-1}	3	[50]
Cu-ZnO	3.0	18,000	150	250	–	100.00	–	–	–	3	[51]

is used as a catalyst. Zhang et al. investigated the effect of modifying Cu-based catalysts with zirconia on γ-Al_2O_3 supports [6]. They found that Zr addition improves the catalytic activity and methanol selectivity of the catalyst. They obtained the highest methanol yield with the 12Cu10Zr/γ-Al_2O_3 catalyst under 240 °C, 3.0 MPa, 3:1 molar ratio of H_2/CO_2, and SV of 1800 h^{-1}.

Raudaskoski et al. investigated the effect of aging time on coprecipitated Cu/ZnO/ZrO_2 catalysts [7]. They found that extending aging time during the preparation of Cu–ZnO/ZrO_2 benefits the activity of the Cu–ZnO/ZrO_2 catalysts in the hydrogenation of CO_2 to methanol. The sodium content of the catalyst decreases and finer crystallite structures are formed with increasing aging time. Wang et al. utilized a coprecipitation method to prepare a series of Cu/Zn/Al/Zr catalysts containing different Al/Zr ratios [8]. The catalysts comprise Cu/Zn crystallites in a fibrous structure. The researchers reported that the dispersion and stability of the crystallites in the coprecipitated catalysts are better than that of the commercial catalyst. These properties consequently enhance CO_2 hydrogenation. Moreover, the addition of 5% Zr increases the methanol space-time yield (STY) of the catalysts to 80%, which is higher than that of the commercial catalyst. Arena et al. prepared Cu–ZnO/ZrO_2 catalysts (Zn_{at}/Cu_{at}, 0–3; ZrO_2, 42–44 wt%) through a novel synthesis route based on reverse coprecipitation under ultrasound irradiation [9]. The synthesis method significantly improves the total surface exposure, dispersion, and surface area of the active metal phase in the catalyst, and ZnO strongly promotes catalyst texture. The hydrogenation reaction over the coprecipitated catalysts is structurally sensitive, resulting in the changes in turnover frequency (TOF) with metal dispersion. The activity of the Cu–ZnO/ZrO_2 catalyst in methanol synthesis under 160–260 °C and 1.0–3.0 MPa was compared with that of a commercial Cu–ZnO/Al_2O_3 catalyst under the same conditions. The thermodynamic analysis of the reaction revealed the formation of methanol. The performance of the conventional alumina-based catalyst is poorer than that of zirconia-based catalysts because water negatively affects the rate of methanol formation. Zhang et al. investigated the effect of vanadium addition to a Cu/γ-Al_2O_3 catalyst [10]. The efficacy of Cu–V/γ-Al_2O_3 was higher than that of Cu/γ-Al_2O_3 in the hydrogenation of CO_2 to methanol. The researchers also investigated the influence of reaction conditions, including reaction temperature, SV, and the molar ratio of H_2 to CO_2, on the performance of 12% Cu–6%V/γ-Al_2O_3 catalyst. They reported that the optimum conditions for CO_2 hydrogenation are as follows: 240 °C, 3600 h^{-1}, and 3:1 molar ratio of H_2 to CO_2. Tsubaki et al. used a novel low-temperature route for the efficient conversion of CO_2 to methanol in a semi-batch autoclave [11]. The researchers reported 25.9% CO_2 conversion and 72.9% methanol selectivity under a low temperature of 443 K and pressure of 5 MPa with Cu/ZnO (Al_2O_3) and alcohol as the catalyst and solvent, respectively.

Arena et al. investigated the solid-state interactions, adsorption sites, and functionality of Cu–ZnO/ZrO_2 catalysts (ZrO_2 loading, 43 wt%; Zn/Cu (at/at), 0.0–2.8) in the hydrogenation of CO_2 to methanol [12]. Characterization data indicated that the strong Cu–ZnO interaction effectively promotes the dispersion and reactivity of metal copper to oxygen. The interaction of metal Cu particles with ZnO and ZrO_2
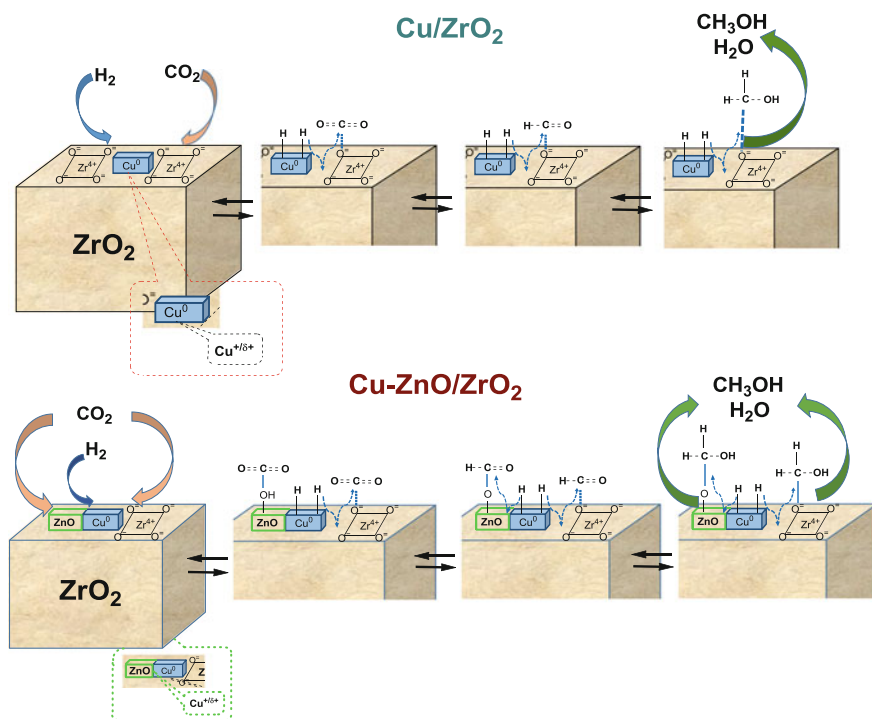
Fig. 5.1 Sketch of the catalysts surface and functionality of the various surface sites under CO_2 hydrogenation conditions. Reprinted from Ref. [12]. Copyright (2008), with permission from Elsevier

stabilizes $Cu^{\delta+}$ sites at the metal/oxides interface, whereas a "mix" of Cu^0, $Cu^{\delta+}$, and oxide basic sites interact to promote the adsorption/activation of H_2, CO, and CO_2. The effects of the metal/oxide interface on the functionality of Cu–ZnO/ZrO_2 catalysts have a fundamental role in hydrogenation of CO_2 to methanol. The dual-site nature of the reaction path explains the formal structure-insensitive character of CO_2 hydrogenation over Cu–ZnO/ZrO_2 catalysts (Fig. 5.1).

Lu et al. synthesized a series of $CuO/ZnO/ZrO_2$ (CZZ) catalysts through a urea–nitrate combustion method [13]. The catalysts were synthesized with 40–150% stoichiometric amount of urea. The researchers then investigated the performance of the synthesized catalysts in the hydrogenation of CO_2 to methanol and the effects of the urea/nitrate ratio on catalyst properties. The catalyst prepared with 50% of the stoichiometric amount of urea exhibited the optimum performance. The use of this catalyst for methanol synthesis from CO_2 hydrogenation under 240 °C, 3.0 MPa, 3:1 H_2/CO_2 molar ratio, and 3600 h^{-1} SV provided 17% CO_2 conversion, 56.2% methanol selectivity, and 9.6% methanol yield.

Lu et al. synthesized a series of CZZ catalysts through the glycine–nitrate combustion method with 50–150% stoichiometric amount of glycine [14]. Characterization data indicated that the physicochemical properties of the catalysts

are strongly influenced by the fuel content used in the combustion process. CuO dispersion exhibited an inverse-volcano variation trend as glycine amount was increased from 50 to 150%. The researchers then evaluated the catalytic performance of CZZ catalysts in CO_2 hydrogenation to methanol and found that the 50-CZZ catalyst prepared with 50% stoichiometric amount of glycine exhibits the maximum activity. ZrO_2 transforms from the tetragonal (t-ZrO_2) to the monoclinic (m-ZrO_2) phase with changing glycine content, and the selectivity of methanol over m-ZrO_2 is higher than that over t-ZrO_2. The catalytic activity of CZZ depends on the surface properties of metallic copper and the phase state of ZrO_2. These results indicated that the glycine–nitrate combustion method is a simple, fast, and effective method for the preparation of CZZ catalysts.

Liu et al. utilized fractional precipitation, impregnation–precipitation (IP), and solid-state reaction methods to synthesize Cu/ZrO_2 catalysts for methanol synthesis through CO_2 hydrogenation [15]. The physical structure and reducibility, as well as interaction between CuO and ZrO_2, of the Cu/ZrO_2 catalysts are greatly affected by the preparation methods and determine the performances of the catalysts in methanol synthesis from CO_2/H_2. The catalytic performance of Cu/ZrO_2 is mainly determined by the interaction between Cu and ZrO_2 rather than by its surface area. Compared with the catalysts prepared through other methods, the Cu/ZrO_2 catalyst prepared through the IP method exhibits higher CuO dispersion and stronger interaction between Cu and ZrO_2. When used to catalyze methanol synthesis through CO_2 hydrogenation, the Cu/ZrO_2 prepared through the IP method exhibits higher CO_2 conversion and higher methanol yield than catalysts prepared through other methods.

Li et al. investigated the reaction mechanism of methanol synthesis from CO_2/H_2 using an in situ IR (Infrared Spectroscopy) technique [16]. They confirmed that methanol could be formed through CO_2 hydrogenation. The strong adsorbability of CO_2 on Cu suppresses the dissociation of H_2 on Cu, thus decelerating the formation rate of methanol. The researchers also proposed a scheme for methanol synthesis in which HCOO–Zn and HCOO–Cu intermediates are present, whereas CH_3O–Cu is absent (Fig. 5.2). In this scheme, HCOO–Zn is the key intermediate, and the hydroxylation of CH_3O–Zn is the rate-limiting step.
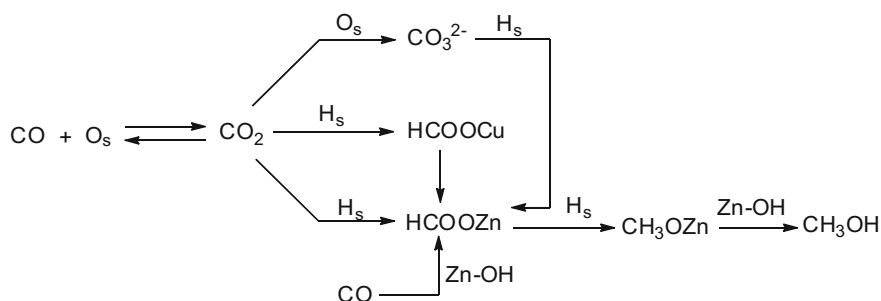
Fig. 5.2 Scheme for the mechanism of methanol synthesis from CO/H_2 and CO_2/H_2 over Cu/ ZnO/Al_2O_3 catalyst. Reprinted from Ref. [16]. Copyright (2010), with permission from Springer

Maniecki et al. comparatively studied the physicochemical properties of different Cu-support catalysts (support = ZnO, Al_2O_3, Cr_2O_3, $ZnAl_2O_4$, $FeAlO_3$, or $CrAl_3O_6$) and their catalytic activity in methanol synthesis through CO_2 hydrogenation [17]. The researchers then investigated the influence of different supports on the activity of the copper catalyst in methanol synthesis through CO_2 hydrogenation. They reported that the 20% $Cu/ZnAl_2O_4$ catalyst is the most suitable catalyst system for methanol synthesis given its high selectivity (93%) and activity. By contrast, the 20% $Cu/FeAlO_3$ catalyst is the most unsuitable catalyst system for methanol synthesis given its low selectivity (21%) for methanol.

Mao et al. investigated the hydrogenation of CO_2 to methanol over $Cu/ZnO/ZrO_2$ catalysts prepared through solid-state reaction [18]. They investigated the effects of calcination temperature on the physicochemical properties of the catalysts and found that Cu dispersion decreases with increasing calcination temperature. Moreover, they found that ZrO_2 transforms from the tetragonal to the monoclinic phase when the calcination temperature exceeds 600 °C. They reported that the catalyst that was calcined at 400 °C exhibits the highest activity and achieves 15.7% CO_2 conversion, 58% methanol selectivity, and 9.1% yield under 240 °C, 3 MPa, 3600 h^{-1}, and 3:1 molar ratio of H_2/CO_2.

Chou et al. synthesized $Cu/ZnO/Al_2O_3$ catalysts through the decomposition of M (Cu, Zn)–ammonia complexes (DMAC) under various temperatures and designated the synthesized catalysts as CZA-T (T = decomposition temperature of DMAC) [19]. The researchers then investigated the influences of the complete decomposition temperature of DMAC, reaction temperature, and specific Cu surface area on catalytic performance. The aurichalcite phase in the precursor plays a key role in improving the physiochemical properties and activities of the final catalysts. The catalyst prepared from aurichalcite-rich precursor exhibits small particle size, good Cu dispersion, large specific Cu surface area, and high STY of methanol under 212 g L_{cat}^{-1} h^{-1}, 513 K, 3 MPa, and 12,000 h^{-1}. As confirmed by evolved gas analysis (EGA), the residue of the high-temperature carbonate species helps to inhibit the growth of Cu particles and enhances catalytic activity. The CZA-343 catalyst that contains a high amount of aurichalcite-rich precursor and high-temperature carbonate species upon calcination has remarkably high activity.

Mao et al. synthesized a series of Cu/ZrO_2 catalysts with various La loadings through a urea–nitrate combustion method [20]. They investigated the influence of La loadings on the physicochemical and catalytic properties of the $La–Cu/ZrO_2$ catalysts for methanol synthesis from CO_2 hydrogenation. Results revealed that La^{3+} partially substitutes for Zr^{4+} and that $La_2Zr_2O_7$ is formed with the introduction of La. The surface area of Cu first increases and then decreases with increasing La loading, whereas the amount of basic sites over the catalysts continuously increases. The conversion of CO_2 and the surface area of Cu are linearly related. Methanol selectivity increases linearly with the increase in the fraction of γ basic sites to the total basic sites. These results provide evidence for a dual-site or bifunctional mechanism of methanol synthesis through CO_2 hydrogenation over Cu/ZrO_2-based catalysts (Fig. 5.3). The presence of La favors methanol production, and the
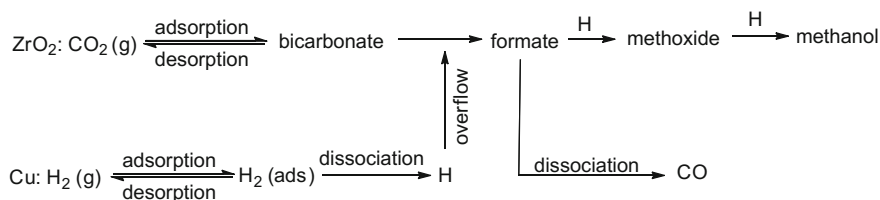
Fig. 5.3 The dual-site or bifunctional mechanism for methanol synthesis from CO_2 hydrogenation over Cu/ZrO_2 catalysts. Reprinted from Ref. [20]. Copyright (2011), with permission from Elsevier

optimum catalytic activity is obtained when the amount of La doping is 5% of the total amount of Cu^{2+} and Zr^{4+}.

Mierczynski et al. compared the physicochemical properties of Cu/$Cr_2O_3 \cdot 3Al_2O_3$ and Au–Cu/$Cr_2O_3 \cdot 3Al_2O_3$-supported catalysts and their catalytic activity in methanol synthesis from H_2 and CO_2 [21]. The researchers proved that the addition of gold to Cu/support catalysts promotes methanol synthesis. The selectivity of copper–gold catalysts in methanol synthesis is mainly determined by alloy formation between Au and Cu during reduction in 5% H_2–95% Ar mixture at 300 °C. XRD analysis confirmed the formation of Au–Cu alloys. Cu/$Cr_2O_3 \cdot 3Al_2O_3$ catalysts are highly active in methanol synthesis. The introduction of gold onto the catalyst surface increases methanol selectivity because metallic gold particles provide nucleation centers for copper crystallization during catalyst reduction.

Arena et al. investigated the effects of ceria promoter and carrier on the functionality of Cu-based catalysts in the hydrogenation of CO_2 to methanol under 453–513 K, 3.0 MPa, and gas hourly space velocity (GHSV) of 8.8 N L g^{-1} h^{-1} [22]. The ceria carrier promotes the surface functionality of the Cu–ZnO system by negatively influencing catalyst texture and metal surface area (MSA). ZnO promotes the dispersion and catalytic functionality of the metal copper phase. The remarkable promoting effect of ceria on the activity of the Cu–ZnO system increases surface methanol yields. Activation in diluted hydrogen enhances the surface functionality of ceria-promoted Cu–ZnO catalysts. The lack of relationship between MSA and catalytic activity substantiates the dual-site nature of the main reaction path, thus confirming the fundamental role of the metal/oxide(s) interface on the CO_2-hydrogenation functionality of the Cu-based catalysts.

Zhang et al. prepared CuO–ZnO–Al_2O_3 catalysts through coprecipitation. They then studied the effect of SiO_2, TiO_2, or SiO_2–TiO_2 promoters on the performance of CuO–ZnO–Al_2O_3 catalysts in methanol synthesis through CO_2 hydrogenation [23]. Under reaction conditions of 533 K, 2.6 MPa, 3:1 volume ratio of H_2/CO_2, and 3600 h^{-1}, the CuO–ZnO–Al_2O_3 catalysts modified with SiO_2, TiO_2, or SiO_2–TiO_2 have better catalytic performances than those without promoters. The addition of promoters increases CO_2 conversion and methanol yield, and the maximum CO_2 conversion and methanol yield are obtained over 2 wt% SiO_2–TiO_2/CuO–ZnO–Al_2O_3. For example, the catalyst promoted with SiO_2–TiO_2 maximized catalytic activity in CO_2 conversion by 40.70% and methanol selectivity by 41.17% as

compared with that without the promoter (15.81% in CO_2 conversion and 23.31% in methanol selectivity). All the promoters, including SiO_2, TiO_2, or SiO_2–TiO_2, improved CuO dispersion in the catalyst body and improved the adsorption/ activation of H_2 on the catalyst, in which the SiO_2–TiO_2 promoter exhibits better performance than SiO_2 or TiO_2.

Karelovic et al. investigated methanol synthesis from CO_2 and H_2 under mild reaction conditions (140–250 °C and 7 bar) over Cu/ZnO catalysts prepared through the citrate method [24]. A wide range in copper particle size (2–12 nm) was obtained by varying copper content and calcination temperature. A total of 100% selectivity to methanol can be achieved under low temperature (lower than 160 °C). The TOFs for methanol formation at 180 °C range from 0.84×10^{-3} to 2.98×10^{-3} s^{-1}. CO formation in reverse water gas–shift reaction is highly favored at higher temperatures. Methanol formation rates exhibit a linear dependence on the amount of exposed copper atoms and the size of copper particles, and the size of copper particles greatly influence the selectivity of methanol formation at constant CO_2 conversion. The Cu/ZnO catalyst with large copper particles (10–12 nm) has a relatively higher selectivity for methanol formation than the Cu/ZnO catalyst with small copper particles (2–3 nm). The activity of mechanically mixed CuO and ZnO is considerably higher than that of pure ZnO and CuO catalysts, suggesting that the activity of the Cu/ZnO catalyst is defined by a good contact between Cu^0 and ZnO, whereas its selectivity is dependent on the morphology of copper nanoparticles.

Zhao et al. synthesized a series of promoted Cu/Zn/Al catalysts from hydrotalcite-like precursors through the coprecipitation method [25]. They investigated the influence of modifiers (Mn, La, Ce, Zr, and Y) on the physicochemical properties of the Cu/Zn/Al catalysts. They found that BET-specific surface area, Cu surface area, and Cu dispersion increase in the order of Cu/Zn/Al < Cu/Zn/Al/ Mn < Cu/Zn/Al/La < Cu/Zn/Al/Ce < Cu/Zn/Al/Zr < Cu/Zn/Al/Y. The total number of basic sites on the Cu/Zn/Al catalysts exhibits a similar trend. The Zr-modified Cu/Zn/Al catalyst exhibits the highest density and proportion of strongly basic sites. The capability of the catalysts for CO_2 conversion is dependent on the exposed Cu surface area, and methanol selectivity linearly increases in the order of Cu/Zn/ Al < Cu/Zn/Al/Mn < Cu/Zn/Al/La < Cu/Zn/Al/Ce < Cu/Zn/Al/Y < Cu/Zn/Al/Zr as the proportion of strongly basic sites to the total basic sites increases. Methanol production is favored by the introduction of Mn, La, Ce, Zr, and Y to the catalysts. The Y- and Zr-modified Cu/Zn/Al catalysts exhibit the highest CO_2 conversion and methanol selectivity, respectively, and the maximum methanol yield is obtained over Cu/Zn/Al/Y catalysts.

Arena et al. investigated the effects of temperature, pressure, and SV on the activity–selectivity patterns of Al_2O_3-, ZrO_2-, and CeO_2-supported Cu–ZnO systems in the synthesis of methanol through CO_2 hydrogenation [26]. Oxide carriers control the catalyst texture and MSA, thus affecting the adsorption properties and catalytic functionality of the Cu–ZnO system. Methanol is the main reaction product under high pressures (>0.1 MPa) and low temperatures (≤ 473 K). The superior performance of the Cu–ZnO/ZrO_2 system could be attributed to the

textural and chemical effects of zirconia. The system could attain a STY of 1.2 kg_{MeOH} kg_{cat}^{-1} h^{-1} at 10% of CO_2 conversion per pass (T = 513 K; P = 5.0 MPa).

Rojas et al. systematically studied the catalytic hydrogenation of CO_2 into methanol over Ga-doped $Cu/ZnO/ZrO_2$ catalysts [27]. The use of Ga-promoted $Cu/ZnO/ZrO_2$ catalysts is highly effective for the selective production of methanol from CO_2 and H_2. Methanol productivity increases with the increasing amount of exposed Cu atoms and with the increasing surface area of Cu^0. Reaction kinetic analysis revealed that the methanol production increases at high temperature with increasing H_2 pressure; however, methanol selectivity decreases at high temperatures.

Urakawa et al. developed an efficient and highly productive process for the synthesis of methanol through the continuous catalytic hydrogenation of CO_2 under high pressures of up to 360 bar over coprecipitated $Cu/ZnO/Al_2O_3$ catalysts [28]. Excellent one-pass CO_2 conversion (>95%) and methanol selectivity (>98%) are achieved under the optimized reaction conditions. Under similar reaction conditions, a commercial catalyst (1.3% MgO; purchased from Alfa Aesar, product ID: 45776) exhibited high methanol productivity at a very high GHSV of 182,000 h^{-1} and the methanol weight time yield (WTY) of 7.7 g_{MeOH} g_{cat}^{-1} h^{-1} with 65.8% CO_2 conversion and 77.3% methanol selectivity. The WTY of the commercial catalyst is best one reported to date for the one-pass yield of methanol through CO_2 hydrogenation.

Shaharun et al. synthesized carbon nanofiber-based $Cu–ZrO_2$ catalysts (Cu–ZrO_2/CNF) through the deposition–precipitation method [29]. The carbon nanofibers were used as a catalyst support after oxidation to CNF–O with 10% (v/v) nitric acid solution. The researchers also investigated the performance of $Cu–ZrO_2$/CNF catalysts with various copper loadings of 10, 15, and 20 wt% for the hydrogenation of carbon dioxide to methanol in a slurry-type reactor under 443 K, 30 bar, and 3:1 molar ratio of H_2/CO_2. They reported that the highest methanol yield and highest activity of 4.28 g kg_{cat}^{-1} h^{-1} were achieved using the catalyst modified with 20 wt% copper loading.

Wei and Sun et al. synthesized a series of Y_2O_3-modified $Cu/ZnO/Al_2O_3$ catalysts ($Cu^{2+}:Zn^{2+}:(Al^{3+} + Y^{3+})$ = 2:1:1) using hydrotalcite-like precursors with Y^{3+}:$(Al^{3+} + Y^{3+})$ atomic ratios between 0 and 0.5 [30]. The introduction of Y_2O_3 into $Cu/ZnO/Al_2O_3$ catalysts increases the surface area and dispersion of Cu. However, the dispersion of Cu and ZnO in the reduced catalysts decreases with the introduction of excess Y, which weakens the interaction between Cu and ZnO. Y_2O_3 and the hydrotalcite-like structure could prevent the aggregation of Cu nanoparticles during reduction and improve the reducibility of Cu^{2+} species. Cu^0 species are the predominant active sites for methanol synthesis through CO_2 hydrogenation. The addition of suitable amounts of Y_2O_3 to $Cu/ZnO/Al_2O_3$ catalysts remarkably enhances their catalytic performance in CO_2 hydrogenation. When Y^{3+}:$(Al^{3+} + Y^{3+})$ > 0.1, CO_2 conversion drastically decreases because of the low Cu surface area and relatively weak interaction between Cu and ZnO. The researchers reported that a maximum methanol yield of 0.57 g_{MeOH} g_{cat}^{-1} h^{-1} with a CO_2
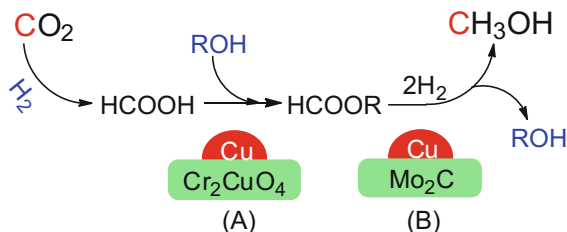
Fig. 5.4 Schematic of proposed reaction pathway for the Cu–Cr and Cu/Mo_2C catalytic cascade system. Reprinted with permission from Ref. [31]. Copyright (2015) American Chemical Society

conversion of 29.9% and a methanol selectivity of 89.7% was obtained over the Cu/ $ZnO/Al_2O_3/Y_2O_3$ catalyst with Y^{3+}:($Al^{3+} + Y^{3+}$) = 0.1 at 503 K and 9.0 MPa.

Thompson et al. developed a novel heterogeneous cascade system for the hydrogenation of CO_2 to methanol through a formate intermediate [31]. They selected a Cu chromite catalyst for the hydrogenation of CO_2 to formate and a Cu/ Mo_2C catalyst for the conversion of formate to methanol. These catalysts work cooperatively in the presence of ethanol, yielding a methanol turnover frequency of 4.7×10^{-4} s^{-1} under 135 °C, 10 bar CO_2, and 30 bar H_2 in 1,4-dioxane. The Cu/ Mo_2C catalyst also catalyzes the hydrogenation of CO_2 to methanol. The deposition of Cu onto the Mo_2C surface enhances methanol formation rates. The hydrogenation of CO_2 to formic acid might be the rate-limiting step for most of the heterogeneous catalysts (Fig. 5.4).

Xu et al. investigated methanol synthesis through CO_2 hydrogenation over Cu/ γ-Al_2O_3 catalysts modified with ZnO, ZrO_2, or MgO [32]. Modification with ZnO, ZrO_2, and MgO increases the dispersion and surface area of metallic Cu^0, as well as promotes the formation of small Cu^0 particles on the Cu/Al_2O_3 catalysts prepared through impregnation. The activation temperature is also an important factor that affects the size of the metallic Cu^0 particle. Methanol is mainly formed through the hydrogenation of activated CO_2 with active hydrogen on Cu^0 particles and the direct CO_2 hydrogenation to methanol is inhibited by high reaction temperature because of the improvements in reverse water–gas shift reaction and methanation.

Lei et al. synthesized a filament-like ZnO and rod-like ZnO through a hydrothermal method [33]. They developed two CuO/ZnO catalysts through an ammonia evaporation synthetic method that involves impregnating filament-like ZnO or rod-like ZnO in $Cu(NH_3)_4^{2+}$ complex cation aqueous solution. The activities of these catalysts in the hydrogenation of CO_2 to methanol are strongly dependent on the morphology of ZnO. The CuO/ZnO catalyst prepared with filament-like ZnO exhibits the best activity and attains 0.55 g_{MeOH} g_{cat}^{-1} h^{-1} STY of methanol with 78.2% selectivity under 3:1 molar ratio of H_2/CO_2, 240 °C, 3.0 MPa, and 0.54 mol g_{cat}^{-1} h^{-1}. The CuO/ZnO catalyst with filament-like ZnO exhibits stronger interaction between ZnO and Cu, more oxygen vacancies, and superior catalytic performance than the CuO/ZnO catalyst prepared through the conventional coprecipitation method. Mao et al. developed CuO–ZnO-based catalysts with various promoters (TiO_2, ZrO_2, or TiO_2–ZrO_2 mixed oxide) through an oxalate

coprecipitation method [34]. They investigated the effect of TiO_2, ZrO_2, and TiO_2–ZrO_2 on the performance of CuO–ZnO catalysts in methanol synthesis through CO_2 hydrogenation. All the additives improve the dispersion of CuO in the catalyst body and increase the surface area of Cu and the adsorption capacities of CO_2 and H_2. The addition of promoters increases CO_2 conversion and methanol yield, and their maximum values are obtained over the TiO_2–ZrO_2 mixed oxide-modified CuO–ZnO catalyst. The methanol yield and the CO_2 adsorption capacity of the catalysts are linearly related, thus substantiating the dual-site mechanism of methanol synthesis through CO_2 hydrogenation.

Witoon et al. investigated the effects of the pore structures of alumina on the catalytic performance of copper catalysts in CO_2 hydrogenation [35]. The activity of the catalysts in methanol synthesis from CO_2 hydrogenation is strongly affected by the pore structure of the catalysts. The Cu-loaded hierarchical meso–macroporous alumina catalyst (Cu/HAl) exhibited higher methanol selectivity and stability than the Cu-loaded unimodal mesoporous alumina catalyst (Cu/UAl). This behavior could be attributed to the inhabitation of undesirable reactions induced by the shortened mesopore diffusion path length (Fig. 5.5).

Mao et al. utilized a surfactant-assisted coprecipitation method to synthesize a series of CuO–ZnO–ZrO_2 catalysts for the synthesis of methanol through CO_2 hydrogenation [36]. They then investigated the effects of calcination temperature on the physicochemical properties of the synthesized catalysts. They found that the size of the copper particles increases with increasing calcination temperature, thus decreasing the TOF for methanol formation. Methanol synthesis through CO_2 hydrogenation is a structure-sensitive reaction in which small Cu particles demonstrate high TOF values. The CuO–ZnO–ZrO_2 catalysts prepared through the novel surfactant-assisted coprecipitation method have significantly higher methanol selectivity than their counterparts prepared through the conventional coprecipitation method. The superior property of the prepared CuO–ZnO–ZrO_2 catalyst can be attributed to the formation of numerous Cu–ZnO_x and/or Cu–ZrO_x species and mesoporous structures.

Homs et al. synthesized a series of CuZnGa catalysts through a microwave-assisted method [37]. They investigated the performance of the synthesized catalysts in the hydrogenation of CO_2 to methanol under a range of reaction conditions (250–270 °C and pressure of up to 4.5 MPa). Characterization indicates that the one-pot microwave-assisted precipitation method used to prepare the $(CuZnGa)_{MW}$ catalysts promotes the dispersion of Cu and Ga_2O_3. The performances of the catalysts in the hydrogenation of CO_2 to methanol are also considerably improved by the MW-assisted preparation methods. $(CuZnGa)_{MW}$ is highly stable and produces 4.87 mol_{MeOH} kg_{cat}^{-1} h^{-1} at 250 °C with a selectivity of approximately 50% under 4.5 MPa, 3000 h^{-1}, and 1:3 molar ratio of CO_2/H_2. The strong interaction between Cu and the support prevents metallic copper sintering, conferring the catalyst with high stability. The good catalytic performance of $(CuZnGa)_{MW}$ in the hydrogenation of CO_2 to methanol is attributed to an intimate association between the highly dispersed copper species and strongly basic ZnO species in the presence of small particles of Ga_2O_3.
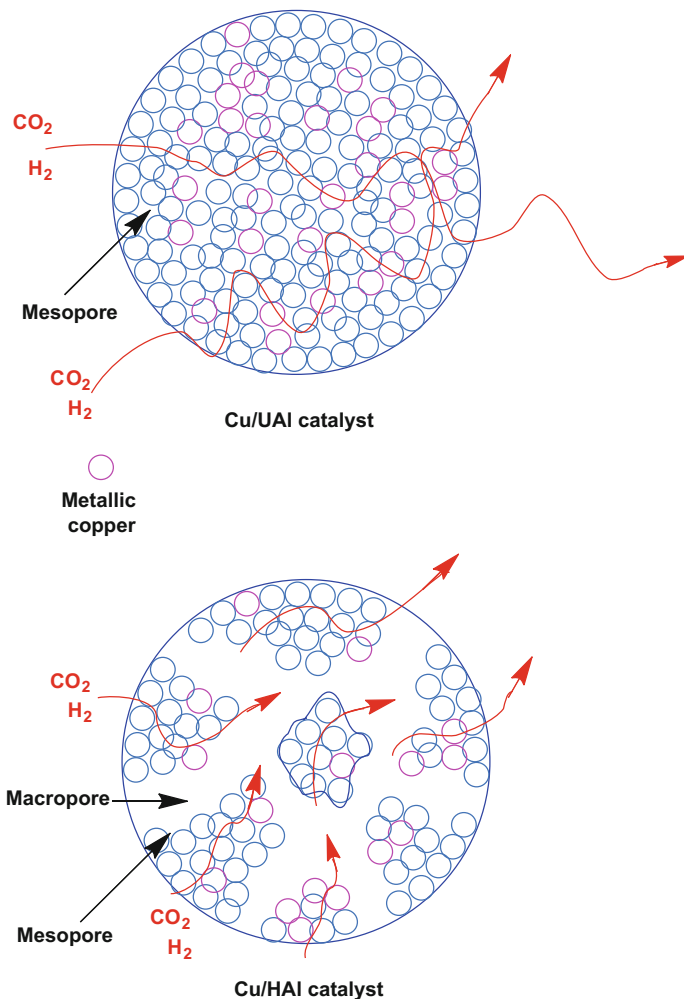
Fig. 5.5 Illustration of gas diffusion inside mesopores of the Cu/UAl and Cu/HAl catalysts. Reprinted from Ref. [35]. Copyright (2015), with permission from Elsevier

Wang et al. synthesized a series of Cu/Zn/Al/Zr hydrotalcite-like catalysts with $Cu^{2+}:Zn^{2+}:Al^{3+}:Zr^{4+} = 2:1:x:0.1$ ($x = 0.6$–1.5) through a simple coprecipitation method [38]. Phase-pure Cu/Zn/Al/Zr hydrotalcite-like compounds are obtained when $x \geq 0.9$, and the yields increase with increasing Al content. The specific surface area and the dispersion of Cu gradually increase with increasing Al content, whereas the specific surface area of Cu decreases when Al content exceeds 27.9 mol %. In CO_2 hydrogenation, the phase-pure hydrotalcite-like Cu/Zn/Al/Zr compounds exhibit better catalytic performance with higher CO_2 conversion and methanol selectivity than the mixed-phase catalyst (hydrotalcite-like and malachite). Cu/Zn/

Al/Zr catalysts with $Cu^{2+}:Zn^{2+}:Al^{3+}:Zr^{4+}$ = 2:1:1.2:0.1 derived from phase-pure hydrotalcite-like precursors exhibit substantial stability and optimal catalytic performance.

Schlögl et al. performed H/D exchange experiments to investigate the hydrogenation of CO_2 to methanol over a $Cu/ZnO/Al_2O_3$ catalyst [39]. Methanol synthesis exhibits a strong thermodynamic isotope effect, which is attributed to differences in the zero-point energy of the deuterated species relative to that of their hydrogen counterparts. H/D substitution exhibits an inverse kinetic isotope effect in the kinetic regime of CO_2 hydrogenation. This effect is stronger for methanol synthesis than for CO formation, suggesting that the two reactions do not share a common intermediate. Similar observations have been obtained for other catalysts, such as Cu/MgO, Cu/SiO_2, and Pd/SiO_2, indicating that methanol formation from CO_2 does not proceed through consecutive reverse water–gas shifts and CO hydrogenation.

Methanol synthesis from CO_2 over industrial catalysts suffers from a lack of selectivity because large amounts of CO are formed as by-products. Valant et al. investigated Cu–ZnO synergy in methanol synthesis from CO_2 [40]. They synthesized a series of Cu–ZnO coprecipitated catalysts, which were tested in methanol synthesis through CO_2 hydrogenation. The Cu–ZnO synergy in the creation of the active sites for methanol and CO formation is the key for the development of catalysts for CO-free methanol synthesis. The coprecipitates exhibit a relationship between migrated Zn and methanol activity as previously observed in mechanical mixtures. However, this correlation is not observed for CO formation, suggesting that the active sites for methanol and CO are different. CO_2 conversion is correlated with the total amount of chemisorbed hydrogen. Hydrogen spillover on two distinct active sites results from Cu–ZnO contacts. The researchers then developed a mathematical model for sphere contact quantification in randomly packed binary mixtures and reported that their theoretical calculations are in complete agreement with their experimental results. Therefore, catalyst based on a core–shell structure is a very promising CO-free methanol synthesis catalyst.

Gao et al. developed a series of core–shell structured $Cu@m–SiO_2$ and $Cu/ZnO@m–SiO_2$ catalysts [41]. Given the confined effect of the silica shell, the Cu nanoparticles are only approximately 5.0 nm in size. The small size of the catalysts promotes high activity for CO_2 conversion. The Cu dispersion of the core–shell nanocatalyst is considerably higher than that of the mesoporous-SiO_2 supported catalyst. The contribution of strongly basic sites to the total basic sites significantly increases with the introduction of ZnO and considerably increases methanol selectivity. The core–shell structure of the nanocomposites endows the entrapped Cu nanoparticles with excellent anti-aggregation properties upon reduction. Therefore, the core–shell $Cu/ZnO@m-SiO_2$ nanocatalyst exhibits the maximum methanol yield with high stability.

Viñes et al. studied the hydrogenation of CO_2 over Cu/Mo_2C (001) surfaces and Cu/Mo_2C powders through a combination of experimental and theoretical models [42]. The addition of Cu to a Mo_2C substrate produces drastic changes in the selectivity of the system for methanol. The methanol yield obtained on a Cu/Mo_2C

(001) surface is substantially higher than that obtained on bare Mo_2C (001), Cu (111), or Cu/ZnO000$\bar{1}$). The deposition of Cu clusters avoids methane formation and increases methanol production. DFT calculations on the surface models of possible C- and Mo-terminations corroborated the experimental observations of the researchers. Calculations for the clean Mo-terminated surface revealed the existence of two possible routes for methane production: $C + 4H \rightarrow CH_4$ and $CH_3O + 3H \rightarrow CH_4 + H_2O$. Both routes compete with methanol synthesis and possess low energy barriers. Moreover, a model for Cu-deposited clusters on the Mo-terminated surface points toward a novel route for methanol and CO production that avoids methane formation. The new route is a direct consequence of the generation of a Mo_2C–Cu interface.

Thompson et al. synthesized a series of M/Mo_2C (M = Cu, Pd, Co, and Fe) catalysts and evaluated their activities in CO_2 hydrogenation at 135–200 °C in liquid 1,4-dioxane solvent [43]. Mo_2C serves as the support and cocatalyst for CO_2 hydrogenation, exhibiting turnover frequencies of $0.6 \times 10^{-4} \text{ s}^{-1}$ and $20 \times 10^{-4} \text{ s}^{-1}$ at 135 and 200 °C, respectively. Methanol is the major product at 135 °C, whereas methanol, C_2H_5OH, and C_{2+} hydrocarbons are produced at 200 °C. The addition of Cu and Pd to Mo_2C with high surface area enhances methanol production. However, the addition of Co and Fe to Mo_2C enhances the production of C_{2+} hydrocarbons. CO_2 is the primary source for methanol in this reaction, whereas CO is the intermediate for hydrocarbon production in CO_2 hydrogenation (Fig. 5.6).

Dumesic et al. investigated the possible active sites on catalysts used for the synthesis of methanol from CO_2 and H_2 [44]. They synthesized Cu/SiO_2 catalysts with different amounts of ZrO_2 through controlled surface reactions and atomic layer deposition. The researchers found that Cu–ZrO_2 interfacial sites, which increase TOF by an order of magnitude in the synthesis of methanol from CO_2 and H_2, are the active sites for the synthesis of methanol from CO_2 and H_2.

Mota et al. developed Al_2O_3- and Nb_2O_5-supported Cu–ZnO catalysts through the precipitation or impregnation of the metal precursors [45]. Characterization results indicated that the atomic ratio of the metals is nearly 1 for the majority of the

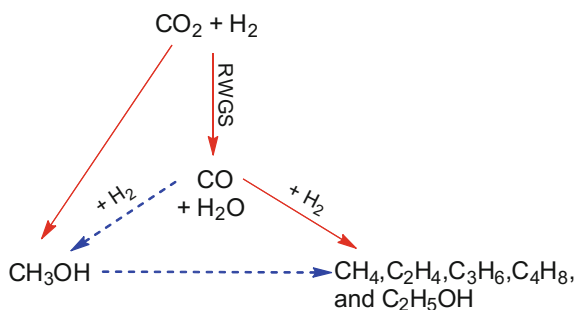**Fig. 5.6** Proposed reaction pathways to produce alcohols and hydrocarbons from CO_2 and H_2. The solid arrows denote major pathways and the dashed arrows denote minor pathways. The pathways are applicable to the following experimental conditions: 200 °C, 10 bar CO_2, and 30 bar H_2 in 1,4-dioxane. Reprinted from Ref. [43]. Copyright (2016), with permission from Elsevier

synthesized catalysts. The choice of the synthetic method affects the activity and selectivity of the catalysts in CO_2 hydrogenation under the conditions used in the study. CO_2 conversion by the catalysts is dependent on temperatures and pressures and being higher at 270 °C and 50 bar. The most active catalyst is $Cu–ZnO/Al_2O_3$ (i), which exhibits 9% conversion under the reaction conditions in the study. $Cu–ZnO/Al_2O_3$ (p) and $Cu–ZnO/Nb_2O_5$ (p) produce only methanol, whereas $Cu–ZnO/Al_2O_3$ (i) and $Cu–ZnO/Nb_2O_5$ (i) produce methanol and DME.

Considerable effort has been devoted to the development of technologies for methanol synthesis through the hydrogenation of CO_2. CO_2 is available from many sources but inexpensive sources of H_2 are rare. Kiss et al. developed an efficient process for methanol synthesis through CO_2 hydrogenation [46]. The process involves the use of wet hydrogen by-products from chloralkali production over a highly active Cu/Zn/Al/Zr fibrous catalyst. A key feature of this novel process is the use of a stripping unit, where the wet hydrogen (saturated with water) flows in countercurrent mode with the condensed methanol–water mixture from the flash separator after reaction. This operation has a double positive effect because it removes CO/CO_2 from the methanol–water mixture, thereby enabling CO_2 to be completely recycled and eliminating its presence from the product. This operation also removes water from the wet hydrogen (initially saturated with water), thus avoiding the negative effect of water on the equilibrium conversion. Moreover, the process is highly energy efficient with an energy consumption of 550 kWh and production of 0.48–1.16 ton steam per ton methanol.

Zhao et al. synthesized a series of $Cu/ZnO/ZrO_2$ catalysts through the precipitation–reduction method and tested its performance in the synthesis of methanol through CO_2 hydrogenation [47]. The precipitation–reduction process influences the average Cu particle size, aggregation state, and interaction among different elements. $NaBH_4$ content affects the exposed Cu surface area and the ratio of Cu^0/Cu^+, thus influencing catalytic performance. The catalysts prepared through the precipitation–reduction method have higher numbers of basic sites and better methanol selectivity than the catalyst prepared through conventional precipitation method. A suitable $NaBH_4$ content improved the catalytic performance of $Cu/ZnO/ZrO_2$ catalysts and a maximum STY of methanol was obtained with B/Cu = 5 at 543 K.

Kongkachuichay et al. synthesized Cu–Zn catalysts supported by graphene oxide (rGO) through an incipient wetness impregnation method and evaluated its performance in the hydrogenation of CO_2 to methanol [48]. They investigated the effects of Cu–Zn metal loading content and reaction temperature on methanol production through CO_2 hydrogenation. The use of the rGO nanosheets as the support greatly enhances catalytic performance and improves the dispersion of bimetallic compound Cu–Zn particles. The 10 wt% CuZn/rGO catalyst yielded the maximum STY of 424 $mg_{MeOH} g_{cat}^{-1} h^{-1}$ under 250 °C and 15 bar.

Witoon et al. synthesized a series of $CuO–ZnO–ZrO_2$ catalysts through a reverse coprecipitation method [49]. They investigated the influence of Zn/Cu ratio and ZrO_2 content on the physicochemical properties of the $CuO–ZnO–ZrO_2$ catalysts, as well as their catalytic performance in the hydrogenation of CO_2 to methanol. The

binary $CuO–ZrO_2$ (67:33) catalyst exhibits the highest methanol selectivity under all reaction temperatures given its strong basic sites and large CuO crystallite size. Its maximum methanol yield (144.5 g_{MeOH} kg_{cat}^{-1} h^{-1}) is achieved at 280 °C. The addition of Zn to the binary $CuO–ZrO_2$ catalyst increases Cu dispersion and the number of active sites for CO_2 and H_2 adsorption. The increase of Zn/Cu ratio also causes a weaker interaction between CO_2 molecules and the catalyst surface, resulting in a lower methanol selectivity compared to the binary $CuO–ZrO_2$ catalyst. However, the weaker interaction between CO_2 molecules and the catalyst surface promotes the formation of methanol at low reaction temperatures (240 and 250 °C). The optimum catalyst composition of Cu–Zn–Zr (38.2:28.6:33.2) exhibits the maximum methanol productivity of 219.7 g_{MeOH} kg_{cat}^{-1} h^{-1} at 240 °C. Results demonstrated the possibility of controlling catalytic CO_2 hydrogenation by tuning catalyst composition.

Urakawa et al. systematically studied the interplay among three important reaction parameters (pressure, temperature, and SV) in the stoichiometric hydrogenation of carbon dioxide ($CO_2:H_2$ = 1:3) over a commercial $Cu/ZnO/Al_2O_3$ catalyst [50]. Under high-pressure conditions and above a threshold temperature, the reaction overcomes kinetic control, entering a thermodynamically controlled regime. Approximately, 90% CO_2 conversion and >95% methanol selectivity are achieved with excellent methanol yield (0.9–2.4 g_{MeOH} g_{cat}^{-1} h^{-1}) under 442 bar. Such high-pressure condition induces the formation of highly dense phases and consequently limits mass transfer. When this limitation is overcome, the advantages of high-pressure conditions can be fully exploited, and high WTY (15.3 g_{MeOH} g_{cat}^{-1} h^{-1}) and high GHSV (100,000 h^{-1}) could be achieved at 442 bar pressure.

Comminges et al. studied the influence of the composition of Cu@ZnOx core–shell catalysts on the formation rate of methanol from CO_2 and H_2 [51]. They inferred structure–reactivity relationships using a reported methodology and from physicochemical and catalytic observations. Zn migration is responsible for the formation of the active $Cu_xZn_{(1-x)}O_y$ phase (Fig. 5.7). The researchers reported a direct correlation between their theoretical and experimental results. The methanol formation rate is a linear function of Zn migration into Cu during the reduction of the catalyst and is independent of the catalyst design, thereby confirming that high Zn migration is necessary to obtain an efficient catalyst for methanol synthesis.

5.2   Pd-Based Catalysts

Pd-based catalysts are also commonly used for the hydrogenation of CO_2 to methanol. These catalysts exhibit considerable activity and selectivity (Table 5.2). Support also exerts a significant effect on the performance of this kind of heterogeneous catalyst.

Zhang et al. developed Pd/ZnO catalysts supported on multi-walled carbon nanotubes (MWCNTs). These catalysts exhibited excellent catalytic performance in

Fig. 5.7 General scheme for methanol synthesis over Cu–ZnO-based catalysts. Reprinted from Ref. [51]. Copyright (2016), with permission from Elsevier
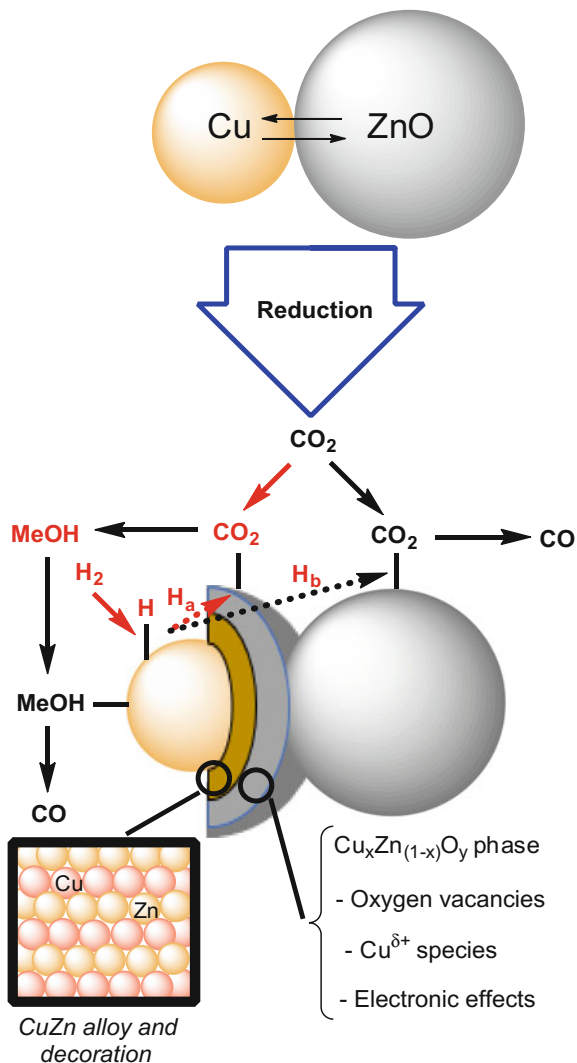
the hydrogenation of CO_2 to methanol [52]. The TOF is 1.15×10^{-2} s^{-1} when 16% $Pd_{0.1}Zn_1$/CNTs (*h*-type) was used as a catalyst for CO_2 hydrogenation under 3.0 MPa and 523 K. CNTs act as the catalyst supporter and promoter. The use of CNTs instead of AC or γ-Al_2O_3 as the catalyst support increases the relative surface concentration of the catalytically active Pd^0 species that are closely associated with methanol generation. The rate of surface hydrogenation increases because the MWCNT-supported Pd–ZnO catalysts reversibly adsorb high amounts of hydrogen, causing high amounts of active H adspecies to concentrate at the surface of the functional catalyst.

Table 5.2 Transformation of CO$_2$ to methanol with Pd-based heterogeneous catalysts

Catalyst	Pressure/MPa	SV/[mL/(h g) or h^{-1}]	Flow rate/mL/min	T/°C	Selectivity/%			Conversion/%	MeOH yield	H$_2$/CO$_2$	References
					CO	CH$_3$OH	CH$_4$				
Pd–ZnO	3.0	1800	–	250	–	99.6	–	6.3	37.1 mg g$_{cat}^{-1}$ h^{-1}	3	[52]
Pd–Ga$_2$O$_3$	5.0	18,000	–	250	–	95.7	0.1	9.8	555 mg g$_{cat}^{-1}$ h^{-1}	3	[53]
Pd–ZnO	5.0	15,000	–	270	–	99.8	–	7.0	343 mg g$_{cat}^{-1}$ h^{-1}	3	[54]
Pd/β–Ga$_2$O$_3$	1.7	27	–	270	–	–	–	12.0	–	7.5	[55]
Pd–Cu/SiO$_2$	4.1	3600	–	250	66	34.0	–	6.6	0.31 μmol g$_{cat}^{-1}$ h^{-1}	3	[56]
Pd@Zn	4.5	–	–	270	–	80.0	–	–	12 g g$_{cat}^{-1}$ h^{-1}	–	[57]
Pd/ZnO	0.1	–	100	150–300	–	15.7	–	4.0	–	9	[58]

Zhang et al. developed Pd-decorated and CNT-promoted Pd–Ga catalysts and reported that these catalysts display excellent performance in the hydrogenation of CO_2 to methanol [53]. Under 5.0 MPa and 523 K, the observed specific reaction rate of CO_2 hydrogenation reached 2.23 µmol s^{-1} (m^2-Pd)$^{-1}$, which is 1.39 times that of the non-promoted Pd–Ga host (1.60 µmol s^{-1} (m^2-Pd)$^{-1}$). The addition of Pd-decorated CNTs not only enhances the molar percentage of catalytically active Pd^0 species but also improves the capability of the catalyst to adsorb/activate H_2. Compared with herringbone-type CNTs, parallel-type CNTs possess a smaller active surface (with less dangling bonds). Parallel-type CNTs thus exhibit a low capacity for H_2 adsorption and a limited promoter effect.

Liang et al. developed a novel Pd-decorated and carbon nanotube-promoted Pd–ZnO catalyst for the hydrogenation of CO_2 to methanol [54]. Under 5.0 MPa, 543 K, V(H_2)/V(CO_2)/V(N_2) of 69/23/8, and GHSV of 15,000 mL g^{-1} h^{-1}, the conversion of hydrogenated CO_2 and the corresponding STY of methanol reached 6.98% and 343 mg g^{-1} h^{-1}, respectively, over the composition-optimized $Pd_{0.1}Zn_1$-10%(5.0%Pd/CNTs) catalyst (Table 5.2). This STY (CH_3OH) value is 1.7 times that (202 mg g^{-1} h^{-1}) of the corresponding (5.0%Pd/CNTs)-free counterpart $Pd_{0.1}Zn_1$ under the same reaction conditions. The addition of a minor amount of Pd-decorated CNTs to the Pd–ZnO host catalyst slightly changes the apparent activation energy for CO_2 hydrogenation. The 5%Pd/CNTs (or simple CNTs) mainly promote catalytic activity by providing sp^2-C surface sites for the adsorption–activation of H_2 while simultaneously enhancing the molar percentage of the catalytically active Pd^0 species in the form of PdZn alloys. Moreover, the 5% Pd/CNTs generate a surface microenvironment with a high concentration of H adspecies in the form of sp^2-C–H on the functional catalyst.

Cardona-Martínez et al. studied methanol production through CO_2 hydrogenation over Pd catalysts supported on α-Ga_2O_3, α-β-Ga_2O_3, and β-Ga_2O_3 polymorphs [55]. Increasing the content of the Pd_2Ga intermetallic compound improves catalytic activity. The Pd_2Ga content of Pd/Ga_2O_3 is dependent on the crystalline Ga_2O_3 phase of the catalyst. The Pd/α-β-Ga_2O_3 catalyst exhibits the highest deactivation. The reduction of the number of basic sites on Ga_2O_3 during the reaction appears to cause catalyst deactivation. The formation of the intermetallic compound Pd_2Ga and the type of Ga_2O_3 polymorph strongly affect the catalytic hydrogenation of CO_2. The content of Pd_2Ga of the Pd/Ga_2O_3 catalysts is a crucial parameter for the hydrogenation of CO_2 to methanol.

Song et al. developed a novel Pd–Cu bimetallic catalyst for the selective hydrogenation of CO_2 to methanol [56]. The synergy between Pd and Cu strongly affects methanol formation over amorphous silica-supported Pd–Cu bimetallic catalysts when the Pd/(Pd + Cu) atomic ratios of the catalysts range from 0.25–0.34. The methanol formation rate over Pd(0.25)–Cu/SiO_2 is twice that of the simple sum of those over monometallic Cu and Pd catalysts. Characterization results indicated that the presence of two well-dispersed Pd–Cu alloy particles (PdCu and PdCu$_3$) is important for methanol formation. The conversion–selectivity profile of the Pd–Cu/SiO_2 catalyst suggested that CO_2 is the primary carbon source

for methanol synthesis at low CO_2 conversion. The CO by-product contributes also to methanol synthesis through CO hydrogenation at high CO_2 conversion.

Tsang et al. synthesized well-dispersed core–shell Pd@Zn nanoparticles with controllable shell thickness from a Pd/CdSe–ZnO precursor in H_2 without the use of a surfactant [57]. The newly formed Pd@Zn surface not only promotes the rate of methanol synthesis but also considerably suppresses RWGS in CO_2 hydrogenation. The PdNPs on the surface of Pd@Zn are electronically modulated by Zn atoms. The core–shell Pd@Zn catalysts produced a TOF and selectivity of 3.3×10^{-1} s^{-1} and 80%, respectively, and a yield twice that of the best-reported value over other Pd-based catalysts.

Díez-Ramírez et al. evaluated the catalytic performance of Pd catalysts supported on zinc oxide (Pd/ZnO) in methanol production through CO_2 hydrogenation under atmospheric pressure [58]. A high reduction temperature increases the formation of PdZn alloy particles. These alloy particles are directly related to a major conversion toward methanol. Moreover, increasing metal loading improves the selectivity of methanol as more PdZn alloy particles are formed. A methanol selectivity of 100% was obtained at 425 K by using the catalyst with a metal content of 18%. However, TOF was low given the large size of PdZn alloy particles and their poor dispersion. Calcination conditions influence the size of the generated metallic palladium particles; slow calcination results in the formation of small metallic palladium particles. The generation of metallic palladium particles is related to CO production. The precursor used to load the Pd on ZnO also remarkably influences the final catalyst structure.

5.3   Ni-Based Catalysts

Kruse et al. investigated CO_2 hydrogenation on metallic Ni under 1 bar by analyzing chemical transients following abrupt changes in reactant composition [59]. CO_2 adsorption is strongly affected by hydrogen co-adsorption and coverage effects. The observed transients suggested that two reaction mechanisms operate in parallel. In the first case, a complex obtained through direct CO_2 hydrogenation suddenly dissociates and further reacts to produce gaseous methane. In the second case, a surface intermediate is obtained (a "formate-derived" species) due to slow hydrogenation and accumulates at the surface of the catalyst. The initial reaction rate involves the fast and direct hydrogenation of CO_2, whereas a low reaction rate was observed under steady-state conditions due to a change in the mechanism that involves the accumulation of an oxygen-containing species at the surface over time.

Chorkendorff et al. investigated the formation of supported intermetallic Ni–Ga catalysts (NiGa and Ni_5Ga_3) for the hydrogenation of CO_2 to methanol [60]. The bimetallic phase is formed during the temperature-programmed reduction of metal nitrates. Supported nanocrystalline intermetallic Ni–Ga particles of the desired phase and composition could be produced through the direct reduction of the corresponding nitrates in hydrogen flow (Fig. 5.8). These intermetallic Ni–Ga
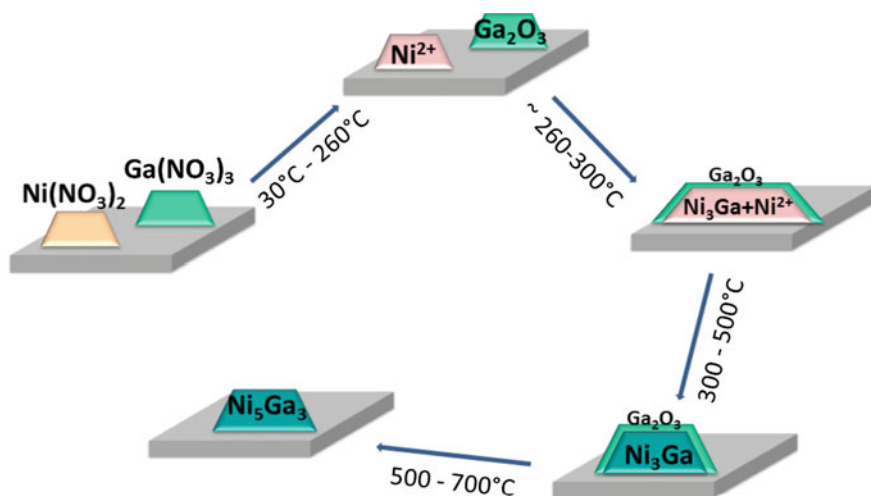
Fig. 5.8 Proposed mechanism of the formation of Ni_5Ga_3 phase during temperature-programmed reduction from nitrates. Reprinted from Ref. [60]. Copyright (2014), with permission from Elsevier

catalysts exhibit high activity and selectivity in the hydrogenation of CO_2 to methanol (Table 5.3). Catalytic activity is intimately dependent on composition and process conditions. Bimetallic Ni–Ga nanoparticles containing 67.5 wt% Ni exhibited the maximum TOF for methanol.

5.4 Ag-Based Catalysts

Grabowski et al. synthesized Ag/ZrO_2 and $Ag/ZrO_2/ZnO$ catalysts through a coprecipitation method [61]. They investigated the influence of polymorphic ZrO_2 phases and the electronic state of silver on the activity of Ag/ZrO_2 catalysts in the hydrogenation of CO_2 to methanol (Fig. 5.9). The selected conditions for catalyst preparation influence the dispersion degree, electronic state, and content of silver in t-ZrO_2 and m-ZrO_2. The presence of oxygen vacancies stabilizes the thermodynamically unstable t-ZrO_2 phase and Ag^+ cations near oxygen vacancies. The catalytic activity to methanol increases with increasing t-ZrO_2 content.

5.5 Au-Based Catalysts

Petrov et al. investigated methanol synthesis through CO_2 hydrogenation over Au/Cu–Zn–Al catalysts [62]. They synthesized the base Cu–Zn–Al with different Cu contents through the rapid precipitation method and subsequently deposited gold

Table 5.3 Transformation of CO_2 to methanol with Ni, Ag, Au, and In-based heterogeneous catalysts

Catalyst	Pressure/MPa	SV/[mL/ (h g) or h^{-1}]	Flow rate/ (mL/min)	T/°C	Selectivity/%			Conversion/%	MeOH yield	H$_2$/CO$_2$	References
					CO	CH$_3$OH	CH$_4$				
Pure Ni	0.1	–	–	290, 360	–	–	–	–	–	0.25–15	[59]
Ni–Ga	0.1	–	100	205	–	98.5	–	–	–	3	[60]
Ag/ZrO$_2$	8.0	3600	–	180–260	–	–	–	–	–	3	[61]
Au/Cu–Zn–Al	6	7000	–	260	–	–	–	28	16.6%	6	[62]
In$_2$O$_3$/ZrO$_2$	1.0–5.0	16,000–48,000	–	100–200	–	100	–	–	–	4	[63]
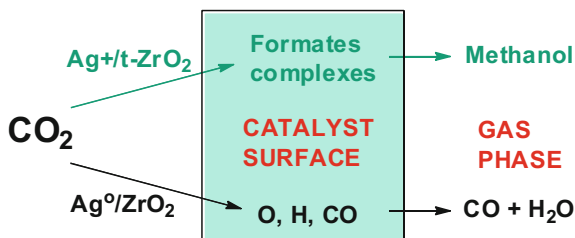
(0.5–3.0 wt%) on the base Cu–Zn–Al through the deposition–precipitation method. Characterization results indicated that the formation of methanol is influenced by the copper content of the base Cu–Zn–Al and by the gold loading. The C_4ZA composition promoted by 1 wt% gold (1 wt% Au deposited on Cu:Zn: Al = 4:1:1 mol ratio) exhibits the maximum methanol yield of 16.6% mass and the highest degree of CO_2 conversion of 28.0% mass at 6:1 H_2:CO_2 and 7000 h^{-1} GHSV (Table 5.3). The optimal amount of gold content in the base catalyst is 1 wt %. Cooperation between copper and gold occurs at the copper–gold interface. Methanol yield is improved by hydrogen spillover and the enhanced adsorption capacities for CO and H_2 at the copper–gold interface. Cu chemically interacts with Zn to form the $Cu_{0.3}Zn_{0.7}$ matrix, whereas Cu and Au do not chemically interact.

5.6 In-Based Catalysts

Pérez-Ramírez et al. developed a ZrO_2-supported In_2O_3 catalyst for methanol synthesis through CO_2 hydrogenation [63]. In_2O_3/ZrO_2 has emerged as a highly efficient catalyst for the hydrogenation of CO_2 to methanol and features 100% selectivity and outstanding activity under the industrially relevant conditions of 473–573 K, 1.0–5.0 MPa, and 16,000–48,000 h^{-1} GHSV (Table 5.3). Compared with the benchmark Cu–ZnO–Al_2O_3 catalyst, the supported In_2O_3/ZrO_2 catalyst is more selective and stable for 1000 h on stream. Characterization results indicated that the creation of oxygen vacancies by thermal desorption and their annihilation constitute the key mechanism of the catalytic cycle.

5.7 Other Heterogeneous Catalysts

Considerable attention has been paid to the use of $AB_{1-x}B_xO_3$ perovskite catalyst, which contains mixed valence ions and catalytic active sites, in hydrogenation. The $AB_{1-x}B_xO_3$ perovskite catalyst was first used for CO hydrogenation to higher alcohol synthesis, Fischer–Tropsch synthesis, and methane reforming with CO_2.

Jia et al. developed a pre-reduced lanthanum chromite perovskite doped with 50% Cu catalyst ($LaCr_{0.5}Cu_{0.5}O_3$) for the conversion of CO_2 to methanol [64]. At

Table 5.4 Transformation of CO$_2$ to methanol with other heterogeneous catalysts

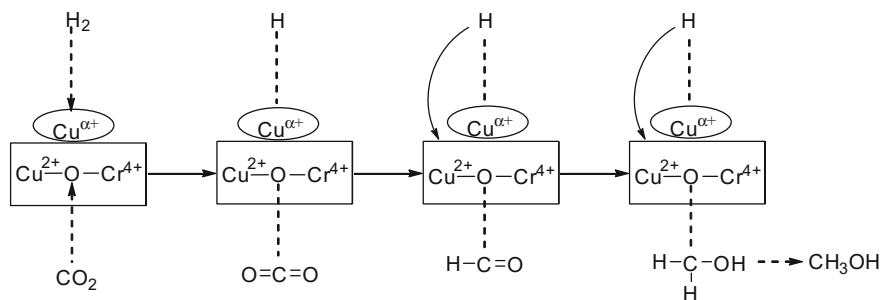| Catalyst	Pressure/MPa	SV/[ml/ (h g) or h^{-1}]	Flow rate/ (mL/min)	T/°C	Selectivity/%			Conversion/%	MeOH yield	H$_2$/CO$_2$	References
					CO	CH$_3$OH	CH$_4$				
Cu–LaCr$_{0.5}$Cu$_{0.5}$O$_3$	2	9000	–	250	5.50	90.8	3.40	10.40	–	3	[64]
LaMn$_{1-x}$Cu$_x$O$_3$	2	2400	–	250	13.83	82.14	4.02	11.33	–	3	[65]

Fig. 5.10 Sketch of the functionality of various surface sites on $LaCr_{0.5}Cu_{0.5}O_3$ for CO_2 hydrogenation. Reprinted from Ref. [64]. Copyright (2009), with permission from Elsevier

250 °C, the catalytic activity (X_{CO_2} = 10.4% and S_{MeOH} = 90.8%, Table 5.4) of the $LaCr_{0.5}Cu_{0.5}O_3$ catalyst is superior to that of the 13% Cu/$LaCrO_3$ catalyst (X_{CO_2} = 4.8% and S_{MeOH} = 46.6%). The high catalytic activity of $LaCr_{0.5}Cu_{0.5}O_3$ could be attributed to the absorption of H_2 on Cu^{a+} sites and the activation of CO_2 on the medium basic sites of the catalyst (Fig. 5.10).

Jia et al. utilized the sol–gel method to synthesize a series of pre-reduced $LaMn_{1-x}Cu_xO_3$ ($0 \leq x < 1$) catalysts for methanol synthesis through CO_2 hydrogenation [65]. The performances of the catalysts are strongly dependent on their copper content. The perovskite structure can be maintained by doping less than 50% of Cu into $LaMnO_3$. In CO_2 hydrogenation, the Cu-doped ($x = 0.5$) $LaMnO_3$ is considerably more active than the other catalysts and exhibits a CO_2 conversion rate of up to 11.33% and a methanol selectivity that is close to 82.14%. H_2 is adsorbed on Cu^+ sites and CO_2 is activated on the medium CO_2 active species in the lattice. The strong interaction between Cu^+ and Mn inhibits the reduction of Cu^+ to Cu^0 and induces the fine dispersion of medium basic sites to adsorb CO_2. However, the Cu-undoped $LaMnO_3$ has no catalytic activity in CO_2 hydrogenation given its poor hydrogen adsorption. The poor catalytic performance of $LaMn_{0.3}Cu_{0.7}O_3$ and $LaMn_{0.1}Cu_{0.9}O_3$ in CO_2 hydrogenation could be attributed to the incomplete perovskite structure and lack of interaction between Cu and Mn.

References

1. Liu X-M, Lu GQ, Yan Z-F, Beltramini J (2003) Recent advances in catalysts for methanol synthesis via hydrogenation of CO and CO_2. Ind Eng Chem Res 42(25):6518–6530. doi:10.1021/ie020979s
2. Wang W, Wang S, Ma X, Gong J (2011) Recent advances in catalytic hydrogenation of carbon dioxide. Chem Soc Rev 40(7):3703–3727. doi:10.1039/c1cs15008a
3. Jadhav SG, Vaidya PD, Bhanage BM, Joshi JB (2014) Catalytic carbon dioxide hydrogenation to methanol: a review of recent studies. Chem Eng Res Des 92(11):2557–2567. doi:10.1016/j.cherd.2014.03.005

4. Ali KA, Abdullah AZ, Mohamed AR (2015) Recent development in catalytic technologies for methanol synthesis from renewable sources: a critical review. Renew Sustain Energy Rev 44:508–518. doi:10.1016/j.rser.2015.01.010

5. Yang C, Ma Z, Zhao N, Wei W, Hu T, Sun Y (2006) Methanol synthesis from CO_2-rich syngas over a ZrO_2 doped CuZnO catalyst. Catal Today 115(1–4):222–227. doi:10.1016/j.cattod.2006.02.077

6. Zhang Y, Fei J, Yu Y, Zheng X (2006) Methanol synthesis from CO_2 hydrogenation over Cu based catalyst supported on zirconia modified γ-Al_2O_3. Energy Convers Manage 47(18–19):3360–3367. doi:10.1016/j.enconman.2006.01.010

7. Raudaskoski R, Niemelä MV, Keiski RL (2007) The effect of ageing time on co-precipitated $Cu/ZnO/ZrO_2$ catalysts used in methanol synthesis from CO_2 and H_2. Top Catal 45(1–4):57–60. doi:10.1007/s11244-007-0240-9

8. An X, Li J, Zuo Y, Zhang Q, Wang D, Wang J (2007) A Cu/Zn/Al/Zr fibrous catalyst that is an improved CO_2 hydrogenation to methanol catalyst. Catal Lett 118(3–4):264–269. doi:10.1007/s10562-007-9182-x

9. Arena F, Barbera K, Italiano G, Bonura G, Spadaro L, Frusteri F (2007) Synthesis, characterization and activity pattern of Cu–ZnO/ZrO_2 catalysts in the hydrogenation of carbon dioxide to methanol. J Catal 249(2):185–194. doi:10.1016/j.jcat.2007.04.003

10. Zhang Y, Fei J, Yu Y, Zheng X (2007) Study of CO_2 hydrogenation to methanol over Cu-V/γ-Al_2O_3 catalyst. J Nat Gas Chem 16(1):12–15. doi:10.1016/s1003-9953(07)60019-x

11. Liu Y, Zhang Y, Wang T, Tsubaki N (2007) Efficient conversion of carbon dioxide to methanol using copper catalyst by a new low-temperature hydrogenation process. Chem Lett 36(9):1182–1183. doi:10.1246/cl.2007.1182

12. Arena F, Italiano G, Barbera K, Bordiga S, Bonura G, Spadaro L, Frusteri F (2008) Solid-state interactions, adsorption sites and functionality of Cu-ZnO/ZrO_2 catalysts in the CO_2 hydrogenation to CH_3OH. Appl Catal A Gen 350(1):16–23. doi:10.1016/j.apcata.2008.07.028

13. Guo X, Mao D, Wang S, Wu G, Lu G (2009) Combustion synthesis of CuO–ZnO–ZrO_2 catalysts for the hydrogenation of carbon dioxide to methanol. Catal Commun 10(13):1661–1664. doi:10.1016/j.catcom.2009.05.004

14. Guo X, Mao D, Lu G, Wang S, Wu G (2010) Glycine–nitrate combustion synthesis of CuO–ZnO–ZrO_2 catalysts for methanol synthesis from CO_2 hydrogenation. J Catal 271(2):178–185. doi:10.1016/j.jcat.2010.01.009

15. H-d Zhuang, S-f Bai, X-m Liu, Z-f Yan (2010) Structure and performance of Cu/ZrO_2 catalyst for the synthesis of methanol from CO_2 hydrogenation. J Fuel Chem Tech 38(4):462–467. doi:10.1016/s1872-5813(10)60041-2

16. Wang X, Zhang H, Li W (2010) In situ IR studies on the mechanism of methanol synthesis from CO/H_2 and CO_2/H_2 over Cu-ZnO-Al_2O_3 catalyst. Korean J Chem Eng 27(4):1093–1098. doi:10.1007/s11814-010-0176-9

17. Maniecki TP, Mierczyński P, Jóźwiak WK (2010) Copper-supported catalysts in methanol synthesis and water gas shift reaction. Kinet Catal 51(6):843–848. doi:10.1134/s0023158410060108

18. Guo X, Mao D, Lu G, Wang S, Wu G (2011) CO_2 hydrogenation to methanol over Cu/ZnO/ZrO_2 catalysts prepared via a route of solid-state reaction. Catal Commun 12(12):1095–1098. doi:10.1016/j.catcom.2011.03.033

19. Wang D, Zhao J, Song H, Chou L (2011) Characterization and performance of $Cu/ZnO/Al_2O_3$ catalysts prepared via decomposition of M(Cu, Zn)-ammonia complexes under sub-atmospheric pressure for methanol synthesis from H_2 and CO_2. J Nat Gas Chem 20(6):629–634. doi:10.1016/s1003-9953(10)60246-0

20. Guo X, Mao D, Lu G, Wang S, Wu G (2011) The influence of La doping on the catalytic behavior of Cu/ZrO_2 for methanol synthesis from CO_2 hydrogenation. J Mol Catal A Chem 345(1–2):60–68. doi:10.1016/j.molcata.2011.05.019

21. Mierczynski P, Maniecki TP, Maniukiewicz W, Jozwiak WK (2011) Cu/Cr$_2$O$_3$·3Al$_2$O$_3$ and Au–Cu/Cr$_2$O$_3$·3Al$_2$O$_3$ catalysts for methanol synthesis and water gas shift reactions. React Kinet Mech Catal 104(1):139–148. doi:10.1007/s11144-011-0336-x

22. Bonura G, Arena F, Mezzatesta G, Cannilla C, Spadaro L, Frusteri F (2011) Role of the ceria promoter and carrier on the functionality of Cu-based catalysts in the CO$_2$-to-methanol hydrogenation reaction. Catal Today 171(1):251–256. doi:10.1016/j.cattod.2011.04.038

23. Zhang L, Zhang Y, Chen S (2012) Effect of promoter SiO$_2$, TiO$_2$ or SiO$_2$-TiO$_2$ on the performance of CuO-ZnO-Al$_2$O$_3$ catalyst for methanol synthesis from CO$_2$ hydrogenation. Appl Catal A Gen 415–416:118–123. doi:10.1016/j.apcata.2011.12.013

24. Karelovic A, Bargibant A, Fernández C, Ruiz P (2012) Effect of the structural and morphological properties of Cu/ZnO catalysts prepared by citrate method on their activity toward methanol synthesis from CO$_2$ and H$_2$ under mild reaction conditions. Catal Today 197 (1):109–118. doi:10.1016/j.cattod.2012.07.029

25. Gao P, Li F, Zhao N, Xiao F, Wei W, Zhong L, Sun Y (2013) Influence of modifier (Mn, La, Ce, Zr and Y) on the performance of Cu/Zn/Al catalysts via hydrotalcite-like precursors for CO$_2$ hydrogenation to methanol. Appl Catal A Gen 468:442–452. doi:10.1016/j.apcata.2013. 09.026

26. Arena F, Mezzatesta G, Zafarana G, Trunfio G, Frusteri F, Spadaro L (2013) Effects of oxide carriers on surface functionality and process performance of the Cu–ZnO system in the synthesis of methanol via CO$_2$ hydrogenation. J Catal 300:141–151. doi:10.1016/j.jcat.2012. 12.019

27. Ladera R, Pérez-Alonso FJ, González-Carballo JM, Ojeda M, Rojas S, Fierro JLG (2013) Catalytic valorization of CO$_2$ via methanol synthesis with Ga-promoted Cu–ZnO–ZrO$_2$ catalysts. Appl Catal B Environ 142–143:241–248. doi:10.1016/j.apcatb.2013.05.019

28. Bansode A, Urakawa A (2014) Towards full one-pass conversion of carbon dioxide to methanol and methanol-derived products. J Catal 309:66–70. doi:10.1016/j.jcat.2013.09.005

29. Din IU, Shaharun MS, Subbarao D, Naeem A (2014) Synthesis, characterization and activity pattern of carbon nanofibres based Cu-ZrO$_2$ catalyst in the hydrogenation of carbon dioxide to methanol. Adv Mater Res 925:349–353. doi:10.4028/www.scientific.net/AMR.925.349

30. Gao P, Zhong L, Zhang L, Wang H, Zhao N, Wei W, Sun Y (2015) Yttrium oxide modified Cu/ZnO/Al$_2$O$_3$ catalysts via hydrotalcite-like precursors for CO$_2$ hydrogenation to methanol. Catal Sci Technol 5(9):4365–4377. doi:10.1039/c5cy00372e

31. Chen Y, Choi S, Thompson LT (2015) Low-temperature CO$_2$ hydrogenation to liquid products via a heterogeneous cascade catalytic system. ACS Catal 5(3):1717–1725. doi:10. 1021/cs501656x

32. Ren H, Xu C-H, Zhao H-Y, Wang Y-X, Liu J, Liu J-Y (2015) Methanol synthesis from CO$_2$ hydrogenation over Cu/γ-Al$_2$O$_3$ catalysts modified by ZnO, ZrO$_2$ and MgO. J Ind Eng Chem 28:261–267. doi:10.1016/j.jiec.2015.03.001

33. Lei H, Nie R, Wu G, Hou Z (2015) Hydrogenation of CO$_2$ to CH$_3$OH over Cu/ZnO catalysts with different ZnO morphology. Fuel 154:161–166. doi:10.1016/j.fuel.2015.03.052

34. Xiao J, Mao D, Guo X, Yu J (2015) Effect of TiO$_2$, ZrO$_2$, and TiO$_2$–ZrO$_2$ on the performance of CuO–ZnO catalyst for CO$_2$ hydrogenation to methanol. Appl Surf Sci 338:146–153. doi:10.1016/j.apsusc.2015.02.122

35. Witoon T, Bumrungsalee S, Chareonpanich M, Limtrakul J (2015) Effect of hierarchical meso–macroporous alumina-supported copper catalyst for methanol synthesis from CO$_2$ hydrogenation. Energy Convers Manage 103:886–894. doi:10.1016/j.enconman.2015.07.033

36. Li L, Mao D, Yu J, Guo X (2015) Highly selective hydrogenation of CO$_2$ to methanol over CuO–ZnO–ZrO$_2$ catalysts prepared by a surfactant-assisted co-precipitation method. J Power Sources 279:394–404. doi:10.1016/j.jpowsour.2014.12.142

37. Cai W, de la Piscina PR, Toyir J, Homs N (2015) CO$_2$ hydrogenation to methanol over CuZnGa catalysts prepared using microwave-assisted methods. Catal Today 242:193–199. doi:10.1016/j.cattod.2014.06.012

38. Gao P, Xie R, Wang H, Zhong L, Xia L, Zhang Z, Wei W, Sun Y (2015) Cu/Zn/Al/Zr catalysts via phase-pure hydrotalcite-like compounds for methanol synthesis from carbon dioxide. J CO_2 Util 11:41–48. doi:10.1016/j.jcou.2014.12.008

39. Kunkes EL, Studt F, Abild-Pedersen F, Schlögl R, Behrens M (2015) Hydrogenation of CO_2 to methanol and CO on Cu/ZnO/Al_2O_3: Is there a common intermediate or not? J Catal 328:43–48. doi:10.1016/j.jcat.2014.12.016

40. Tisseraud C, Comminges C, Belin T, Ahouari H, Soualah A, Pouilloux Y, Le Valant A (2015) The Cu–ZnO synergy in methanol synthesis from CO_2, part 2: origin of the methanol and CO selectivities explained by experimental studies and a sphere contact quantification model in randomly packed binary mixtures on Cu–ZnO coprecipitate catalysts. J Catal 330:533–544. doi:10.1016/j.jcat.2015.04.035

41. Yang H, Gao P, Zhang C, Zhong L, Li X, Wang S, Wang H, Wei W, Sun Y (2016) Core–shell structured Cu@m-SiO_2 and Cu/ZnO@m-SiO_2 catalysts for methanol synthesis from CO_2 hydrogenation. Catal Commun 84:56–60. doi:10.1016/j.catcom.2016.06.010

42. Posada-Pérez S, Ramírez PJ, Gutiérrez RA, Stacchiola DJ, Viñes F, Liu P, Illas F, Rodriguez JA (2016) The conversion of CO_2 to methanol on orthorhombic β-Mo_2C and Cu/β-Mo_2C catalysts: mechanism for admetal induced change in the selectivity and activity. Catal Sci Technol 6(18):6766–6777. doi:10.1039/c5cy02143j

43. Chen Y, Choi S, Thompson LT (2016) Low temperature CO_2 hydrogenation to alcohols and hydrocarbons over Mo_2C supported metal catalysts. J Catal 343:147–156. doi:10.1016/j.jcat.2016.01.016

44. Ro I, Liu Y, Ball MR, Jackson DHK, Chada JP, Sener C, Kuech TF, Madon RJ, Huber GW, Dumesic JA (2016) Role of the Cu-ZrO_2 interfacial sites for conversion of ethanol to ethyl acetate and synthesis of methanol from CO_2 and H_2. ACS Catal 6(10):7040–7050. doi:10.1021/acscatal.6b01805

45. da Silva RJ, Pimentel AF, Monteiro RS, Mota CJA (2016) Synthesis of methanol and dimethyl ether from the CO_2 hydrogenation over Cu·ZnO supported on Al_2O_3 and Nb_2O_5. J CO_2 Util 15:83–88. doi:10.1016/j.jcou.2016.01.006

46. Kiss AA, Pragt JJ, Vos HJ, Bargeman G, de Groot MT (2016) Novel efficient process for methanol synthesis by CO_2 hydrogenation. Chem Eng J 284:260–269. doi:10.1016/j.cej.2015.08.101

47. Dong X, Li F, Zhao N, Xiao F, Wang J, Tan Y (2016) CO_2 hydrogenation to methanol over Cu/ZnO/ZrO_2 catalysts prepared by precipitation-reduction method. Appl Catal B Environ 191:8–17. doi:10.1016/j.apcatb.2016.03.014

48. Deerattrakul V, Dittanet P, Sawangphruk M, Kongkachuichay P (2016) CO_2 hydrogenation to methanol using Cu-Zn catalyst supported on reduced graphene oxide nanosheets. J CO_2 Util 16:104–113. doi:10.1016/j.jcou.2016.07.002

49. Witoon T, Kachaban N, Donphai W, Kidkhunthod P, Faungnawakij K, Chareonpanich M, Limtrakul J (2016) Tuning of catalytic CO_2 hydrogenation by changing composition of CuO–ZnO–ZrO_2 catalysts. Energy Convers Manage 118:21–31. doi:10.1016/j.enconman.2016.03.075

50. Gaikwad R, Bansode A, Urakawa A (2016) High-pressure advantages in stoichiometric hydrogenation of carbon dioxide to methanol. J Catal 343:127–132. doi:10.1016/j.jcat.2016.02.005

51. Tisseraud C, Comminges C, Pronier S, Pouilloux Y, Le Valant A (2016) The Cu–ZnO synergy in methanol synthesis part 3: impact of the composition of a selective Cu@ZnOx core–shell catalyst on methanol rate explained by experimental studies and a concentric spheres model. J Catal 343:106–114. doi:10.1016/j.jcat.2015.12.005

52. Liang X-L, Dong X, Lin G-D, Zhang H-B (2009) Carbon nanotube-supported Pd–ZnO catalyst for hydrogenation of CO_2 to methanol. Appl Catal B Environ 88(3–4):315–322. doi:10.1016/j.apcatb.2008.11.018

53. Kong H, Li H-Y, Lin G-D, Zhang H-B (2011) Pd-decorated CNT-promoted Pd-Ga_2O_3 catalyst for hydrogenation of CO_2 to methanol. Catal Lett 141(6):886–894. doi:10.1007/s10562-011-0584-4

54. Liang X-L, Xie J-R, Liu Z-M (2015) A novel Pd-decorated carbon nanotubes-promoted Pd-ZnO catalyst for CO_2 hydrogenation to methanol. Catal Lett 145(5):1138–1147. doi:10.1007/s10562-015-1505-8

55. Oyola-Rivera O, Baltanás MA, Cardona-Martínez N (2015) CO_2 hydrogenation to methanol and dimethyl ether by Pd–Pd_2Ga catalysts supported over Ga_2O_3 polymorphs. J CO_2 Util 9: 8–15. doi:10.1016/j.jcou.2014.11.003

56. Jiang X, Koizumi N, Guo X, Song C (2015) Bimetallic Pd–Cu catalysts for selective CO_2 hydrogenation to methanol. Appl Catal B Environ 170–171:173–185. doi:10.1016/j.apcatb.2015.01.010

57. Liao F, Wu X-P, Zheng J, Li M-J, Zeng Z, Hong X, Kroner A, Yuan Y, Gong X-Q, Tsang SCE (2016) Pd@Zn core–shell nanoparticles of controllable shell thickness for catalytic methanol production. Catal Sci Technol 6(21):7698–7702. doi:10.1039/c6cy01832g

58. Díez-Ramírez J, Valverde JL, Sánchez P, Dorado F (2015) CO_2 hydrogenation to methanol at atmospheric pressure: influence of the preparation method of Pd/ZnO catalysts. Catal Lett 146 (2):373–382. doi:10.1007/s10562-015-1627-z

59. Vesselli E, Schweicher J, Bundhoo A, Frennet A, Kruse N (2011) Catalytic CO_2 hydrogenation on nickel: novel insight by chemical transient kinetics. J Phys Chem C 115 (4):1255–1260. doi:10.1021/jp106551r

60. Sharafutdinov I, Elkjær CF, Pereira de Carvalho HW, Gardini D, Chiarello GL, Damsgaard CD, Wagner JB, Grunwaldt J-D, Dahl S, Chorkendorff I (2014) Intermetallic compounds of Ni and Ga as catalysts for the synthesis of methanol. J Catal 320:77–88. doi:10.1016/j.jcat.2014.09.025

61. Grabowski R, Słoczyński J, Śliwa M, Mucha D, Socha RP, Lachowska M, Skrzypek J (2011) Influence of polymorphic ZrO_2 phases and the silver electronic state on the activity of Ag/ZrO_2 catalysts in the hydrogenation of CO_2 to methanol. ACS Catal 1(4):266–278. doi:10.1021/cs100033v

62. Pasupulety N, Driss H, Alhamed YA, Alzahrani AA, Daous MA, Petrov L (2015) Studies on Au/Cu–Zn–Al catalyst for methanol synthesis from CO_2. Appl Catal A Gen 504:308–318. doi:10.1016/j.apcata.2015.01.036

63. Martin O, Martin AJ, Mondelli C, Mitchell S, Segawa TF, Hauert R, Drouilly C, Curulla-Ferre D, Perez-Ramirez J (2016) Indium oxide as a superior catalyst for methanol synthesis by CO_2 hydrogenation. Angew Chem Int Ed 55(21):6261–6265. doi:10.1002/anie.201600943

64. Jia L, Gao J, Fang W, Li Q (2009) Carbon dioxide hydrogenation to methanol over the pre-reduced $LaCr_{0.5}Cu_{0.5}O_3$ catalyst. Catal Commun 10(15):2000–2003. doi:10.1016/j.catcom.2009.07.017

65. Jia L, Gao J, Fang W, Li Q (2010) Influence of copper content on structural features and performance of pre-reduced $LaMn_{1-x}Cu_xO_3$ ($0 \leq x<1$) catalysts for methanol synthesis from CO_2/H_2. J Rare Earth 28(5):747–751. doi:10.1016/s1002-0721(09)60193-9

Chapter 6
Conclusions and Outlook

Abstract In this chapter, we summarize all the homogeneous and heterogeneous transformation of CO_2 to formate/formic acid and methanol. The important factors such as solvent, additive, metal, ligand, and hydrogen source that influence the reaction performance are discussed.

In this book, we describe the recent progress in CO_2 hydrogenation to energy-related products, specifically formate/FA and methanol with homogeneous and heterogeneous catalysts. The remarkable achievements contribute significantly to understanding the mechanism of CO_2 transformation and realizing the possibility of a methanol or hydrogen economy.

To activate the most stable CO_2 molecule, chemists have employed various strategies, including optimization of hydrogen sources, solvents, and additives and the design of sophisticated catalysts.

Various hydrogen sources have been utilized in CO_2 reduction to formate/FA or methanol. Boranes and hydrosilanes are considerably used especially in homogeneous catalysis. They have gained considerable interest in academic research due to their high contribution to CO_2 reduction and in understanding the mechanism of CO_2 activation. However, sensitivity and expensive cost limit their industrial application. Highly robust, cheap, and renewable boranes and hydrosilanes are therefore required to overcome these shortcomings. By contrast, H_2 remains to be the most favorable and easily available hydrogen source. Nevertheless, most H_2 are currently generated from the industrial reforming of natural gas. H_2 must be produced in a green approach, such as electrolysis of water with excess electricity or water photolysis.

Polar solvents, such as DMSO, DMF, water, and ionic liquid, are found to be effective for CO_2 reduction. Water is particularly attractive because it is uniquely cheap and eco-friendly. However, water-soluble or water-compatible catalysts are required. In addition, application of ionic liquids with high boiling point as solvents facilitates FA evaporation.

Basic additives including carbonate, bicarbonate, and organic amines promote CO_2 reduction to formate. Although stoichiometric strong base, such as Verkade's base, is favorable in elaborating the reaction rate, high cost prevents its practical application. When inorganic base is used, additional acid must be added to neutralize formate. Separation of FA from FA–amine salt and recycling of amine is a problem that requires solution.

For the development of efficient homogeneous catalysts, various phosphine ligands, *C,C*-chelated ligands, *N,N*-chelated ligands, and pincer ligands have been explored. The non-innocent ligand effects of pincer ligands endow the pincer complexes with high efficiency of H_2 or CO_2 activation via unique aromatization/ de-aromatization and/or hydrogen-bonding interactions. The hydroxy-substituted aromatic *N*-heterocyclic ligands construct bio-inspired proton-responsive complexes, which exhibit extraordinary activity for CO_2 hydrogenation in aqueous solutions under mild conditions. The synergistic electronic effects and pendant base effects of such ligands substantially improve catalytic activities. The unique property of facilitating proton transfer through the second coordination sphere similar to those of hydrogenase demonstrates the remarkable success of enzyme mimicking.

Homogeneous catalysts are more effective for CO_2 reduction to FA than CO_2 reduction to methanol. Nevertheless, important progress has been made in CO_2 transformation to methanol with various homogeneous catalysts through indirect approaches, such as disproportionation of FA, multistep synthesis, and most recently reported direct CO_2 hydrogenation, hydroboration, and hydrosilylation.

Although precious metals exhibit high efficiency, catalysts with earth-abundant metals, such as Fe, Co, and Ni, were also developed with considerable success. Boron-containing metal complexes, even metal-free organocatalysts, such as FLPs are highly efficient for CO_2 activation and/or reduction with appropriate hydrogen sources under mild conditions. The developments of bio-inspired catalysts with earth-abundant metals and organocatalysts are important subjects for future research.

Contrary to homogeneous catalysts, controlling the selectivity of heterogeneous catalysts in CO_2 reduction is rather difficult. A number of heterogeneous catalysts were prepared by immobilizing homogeneous catalysts, which are efficient for CO_2 hydrogenation to formate or FA. In addition, various heterogeneous catalysts based on Ni, Pd, Ru, Ir, and Au were also prepared by sintering with an appropriate support and used to reduce CO_2 to FA. The Ni nanoporous catalyst has recently been reported to be highly effective and selective for the hydrogenation of carbonate to FA. Nanoporous metal catalysts are promising for practical FA production from CO_2 and deserve more investigation.

Heterogeneous catalysts have been extensively investigated, and several excellent catalysts have been developed for CO_2 hydrogenation to methanol. Among the studied catalysts, Cu-based catalysts are considered to be the optimal choice for methanol synthesis due to their high activity. Furthermore, catalysts based on Pd, Ni, Ag, Au, In, and $AB_{1−x}B_xO_3$ perovskite are also effective for CO_2 reduction to methanol. A large surface area is crucial for high catalytic activity because it is favorable for better dispersion of active metal, thereby enhancing catalyst performance. In comparison with homogeneous catalysts, heterogeneous catalysts remain

less active and selective. Therefore, the development of highly efficient, selective, and stable heterogeneous catalysts based on earth-abundant elements is desired.

Although important advancement has been recently achieved by CO_2 transformation to liquid fuels, such as FA and methanol, several problems, as above-mentioned, need to be solved before its industrial application. Nevertheless, given that numerous scientists are devoted in researching CO_2 transformations, significant progress could be expected in the near future.